University of Sheffield

Olfactory rod cells: a putative mechanosensory and ionoregulatory rare cell type in the zebrafish olfactory epithelium that expresses the adhesion G-protein-coupled receptor *adgrg6*

King Yee Cheung

A thesis submitted in partial fulfilment of the requirements for the degree of Doctor of Philosophy

School of Biosciences

September 2023

Table of Contents

Acknowledgements

The work in this thesis was funded by an A*STAR Research Attachment Programme PhD studentship (ARAP-2019-01-0014).

This project has been the product of many people's hard work and teamwork. Firstly, I would like to thank my supervisors, Tanya Whitfield and Suresh Jesuthasan, for providing me with constant support and guidance over the past four years. I am grateful for the hours of productive and stimulating discussions, and advice given inside and outside of the lab. You have both taught me lessons that I will take with me throughout life.

I would like to thank members past and present of the Whitfield lab and the Jesuthasan lab for training me in various techniques at the bench or at the microscope, for assistance in the lab, and for useful discussions during our weekly lab meetings. I am also grateful to members of the Noël and Roehl labs in Sheffield, as well as the Carney, Ingham, and Wee labs in Singapore, for practical help or for providing reagents whenever it was needed.

I am grateful to my advisors, Andrew Lin and Henry Roehl, who both helped me keep on track and provided interesting suggestions from an outside perspective throughout the course of my project.

Without the hard work and dedication from the staff at the Bateson Centre Aquaria and Wolfson Light Microscopy Facility in Sheffield, as well as the Lee Kong Chian School of Medicine Animal Research Facility and the NTU Optical Bio-Imaging Centre in Singapore, this work would not have been possible, so thank you all.

I would also like to thank Mert Ege, Christa Ringers, and Nathalie Jurisch-Yaksi for kindly providing me with fixed transgenic larvae all the way from Norway, and Nathalie again for notifying us of a useful scRNA-seq dataset; Karen Carmago-Sosa and Robert Kelsh for providing me with fixed *sox10* mutant larvae from Bath; Emily Noël for providing me with *flna*

mutant larvae; and Julia Peloggia and Tatjana Piotrowski for their time and assistance with the initial analysis of scRNA-seq data.

Finally, to my family and friends who are all scattered across the world, thank you for your endless support and for showing interest in my work, even when you may not have understood it. I am especially appreciative of everyone who went out of their way to ensure that my time away from home was a special experience, even when I felt homesick, and who helped make Singapore feel like my second home.

Declaration

I, King Yee Cheung, confirm that the thesis is my own work. I am aware of the University's Guidance on the Use of Unfair Means (www.sheffield.ac.uk/ssid/unfair-means). This work has not previously been presented for an award at this, or any other, university.

Experimental work during the first year and a half of my PhD was disrupted by the COVID-19 pandemic, but during lockdown I was able to analyse data that had been generated by others. In those instances where I have collaborated with others, this is acknowledged in the text.

A proportion of the work in this thesis was published in Cheung, K. Y., Jesuthasan, S. J., Baxendale, S., van Hateren, N. J., Marzo, M., Hill, C. J., Whitfield, T. T. (2021). Olfactory rod cells: a rare cell type in the larval zebrafish olfactory epithelium with a large actin-rich apical projection. *Front. Physiol.* 12, 626080. doi: 10.3389/fphys.2021.626080, of which I was the first author (see Appendix 2). This may result in a high similarity match in the Turnitin originality report.

Olfactory rod cells: a putative mechanosensory and ionoregulatory rare cell type in the zebrafish olfactory epithelium that expresses the adhesion G-protein-coupled receptor *adgrg6*

Abstract

Sensory systems contain a variety of specialised cell types, including receptors and non-sensory cells. Characterisation of every cell type is crucial for a full understanding of the neurophysiology behind these sensory systems. This thesis reports the presence of olfactory rod cells, a rare cell type in the zebrafish olfactory epithelium which differs from known classes of olfactory cells. Using a combination of staining, genetic, and imaging techniques, I have characterised the morphology, development, gene expression, and potential functions of these cells. Olfactory rod cells each bear a distinct actin-rich apical projection extending about 10 µm above the epithelial surface, which oscillates in live larvae, possibly as a result of ciliary beating. They have a rounded cell body positioned apically in the epithelium, and posterolaterally in the larval olfactory pit, near to multi-ciliated cells. Olfactory rod cells arise during embryogenesis and are present through to adulthood. *Adgrg6*/*gpr126*, a human disease-implicated gene which codes for an adhesion G-protein-coupled receptor with a proposed mechanosensory role, is specifically expressed in olfactory rod cells within the larval zebrafish olfactory epithelium. Transcription of *cfos* in olfactory rod cells following mechanical stimulation suggests that they are mechanosensory. Furthermore, a modulation in olfactory rod cell numbers following exposure to a low salinity environment, along with expression of a sodium-potassium ion transport protein in a subset of the cells, insinuate a potential function in ionoregulation. This work identifies a novel multimodal cell that may facilitate olfactory function by influencing ion balance and cilia beat dynamics. Given the implication of ionocytes and ciliary clearance in respiratory diseases, further work on olfactory rod cells may have clinical relevance.

List of abbreviations

aGPCR = adhesion class G-protein-coupled receptor

cAMP = cyclic adenosine monophosphate

CBF = ciliary beat frequency

CFTR = cystic fibrosis transmembrane conductance regulator protein

CI = confidence interval

CNC = cranial neural crest

CNG = cyclic nucleotide-gated

CNS = central nervous system

cP = centipoise

CSF-cN = cerebrospinal fluid-contacting neurons

CTF = C-terminal fragment

DIC = differential interference contrast

DIG = digoxigenin

DMSO = dimethyl sulfoxide

dpf = days post-fertilisation

ECM = extracellular matrix

fps = frames per second

GnRH3 = gonadotropin-releasing hormone 3

GPCR = G-protein-coupled receptor

GPS = GPCR proteolysis site

hpf = hours post-fertilisation

HCR RNA-FISH = *in situ* hybridisation chain reaction

HR ionocyte = H^+-ATPase-rich ionocyte

ISH = *in situ* hybridisation

JACoP = Just Another Co-localization Plugin

LMP = low melting point

MBP = myelin basic protein

MCC = multi-ciliated cell

MOE = (mammalian) main olfactory epithelium

MVC = microvillous cell

NaR ionocyte = Na^+,-K^+-ATPase-rich ionocyte

NCC = Na^+,-Cl^- co-transporter

Nm ionocyte = neuromast-associated ionocyte

ns = not significant

NTF = N-terminal fragment

OB = olfactory bulb

OE = olfactory epithelium

OMP = olfactory marker protein

OR = odorant receptor

OSN = olfactory sensory neuron

PCR = polymerase chain reaction

PFA = paraformaldehyde

PBS = phosphate-buffered saline

PNS = peripheral nervous system

PPE = pre-placodal ectoderm

ROI = region of interest

SCC = solitary chemosensory cell

scRNA-seq = single-cell RNA sequencing

s.d. = standard deviation

SEM = scanning electron microscopy

S.E.M. = standard error of the mean

ssEM = serial-section electron microscopy

TAAR = trace amine-associated receptor

TEM = transmission electron microscopy

TrpC2 = transient receptor potential channel C2

TrpM5 = transient receptor potential channel M5

UMAP = uniform manifold approximation and projection

VR = vomeronasal receptor

List of figures

List of tables

Chapter 1. Introduction

1.1. Introduction

The olfactory system is fundamental in behaviour; it involves the detection of myriad odorants, sending chemical information to the brain via a network of olfactory sensory neurons (OSNs), and ultimately eliciting appropriate behavioural responses (reviewed in Kermen et al., 2013). Olfaction allows for the detection of food, danger, mates, and influences emotions and memory formation (reviewed in Axel, 1995; Buchanan et al., 2003). Losing the sense of smell in disorders such as anosmia and hyposmia increases risk of undetected dangers and can be indicative of more serious underlying medical conditions such as Parkinson's and Alzheimer's Diseases (reviewed in Whitlock, 2015). OSNs in the olfactory epithelium (OE) project their axons directly into the olfactory bulbs (OBs) of the brain, thus providing an entry route for pathogens to enter the brain. Cells in the OE can themselves be damaged by viral infection, for example during SARS-CoV-2 infection, leading to a loss of the sense of smell (Brann et al., 2020; Gupta et al., 2020; reviewed in Xydakis et al., 2021; Choi et al., 2022; Kraus et al., 2022). There is therefore a clear importance to studying all aspects of the olfactory system for a better understanding of its neurophysiology and to provide an avenue for future clinical advancements. Despite the extensive progress that has been made, several major mysteries remain, such as the identity of some rare cell types.

Research in sensory systems has become increasingly popular in recent decades and has contributed to shaping current understanding of sensory signalling transduction — from characterisation of the development and transcriptome of sensory cells, to assaying their neurophysiological functions. Zebrafish (*Danio rerio*) are a key model organism for studying the olfactory system due to countless advantageous properties. Many of the genes, cell types, and brain structures involved in the human olfaction pathway are evolutionarily conserved in zebrafish (Figure 1.1; reviewed in Ache and Young, 2005; Alioto and Ngai, 2005), and the entire zebrafish olfactory system is easily accessible for *in vivo* imaging and manipulation. More broadly, zebrafish produce large batches of transparent embryos with rapid development and become free-swimming larvae by 3 days post-fertilisation (dpf). They are widely used to study

developmental biology, genetics, molecular biology, neuroscience, regenerative medicine, cancer and diseases. The zebrafish genome has a high homology to the human genome, with many mutant phenotypes resembling human clinical disorders, thus demonstrating that they make accessible and suitable models for human diseases (Howe et al., 2013). Furthermore, many experimental techniques can be applied to zebrafish, such as genome editing, transgenesis, single-cell RNA sequencing (scRNA-seq), and numerous imaging methods, to answer key research questions (Irion et al., 2014; Randlett et al., 2015; Hildebrand et al., 2017; Farnsworth et al., 2020).

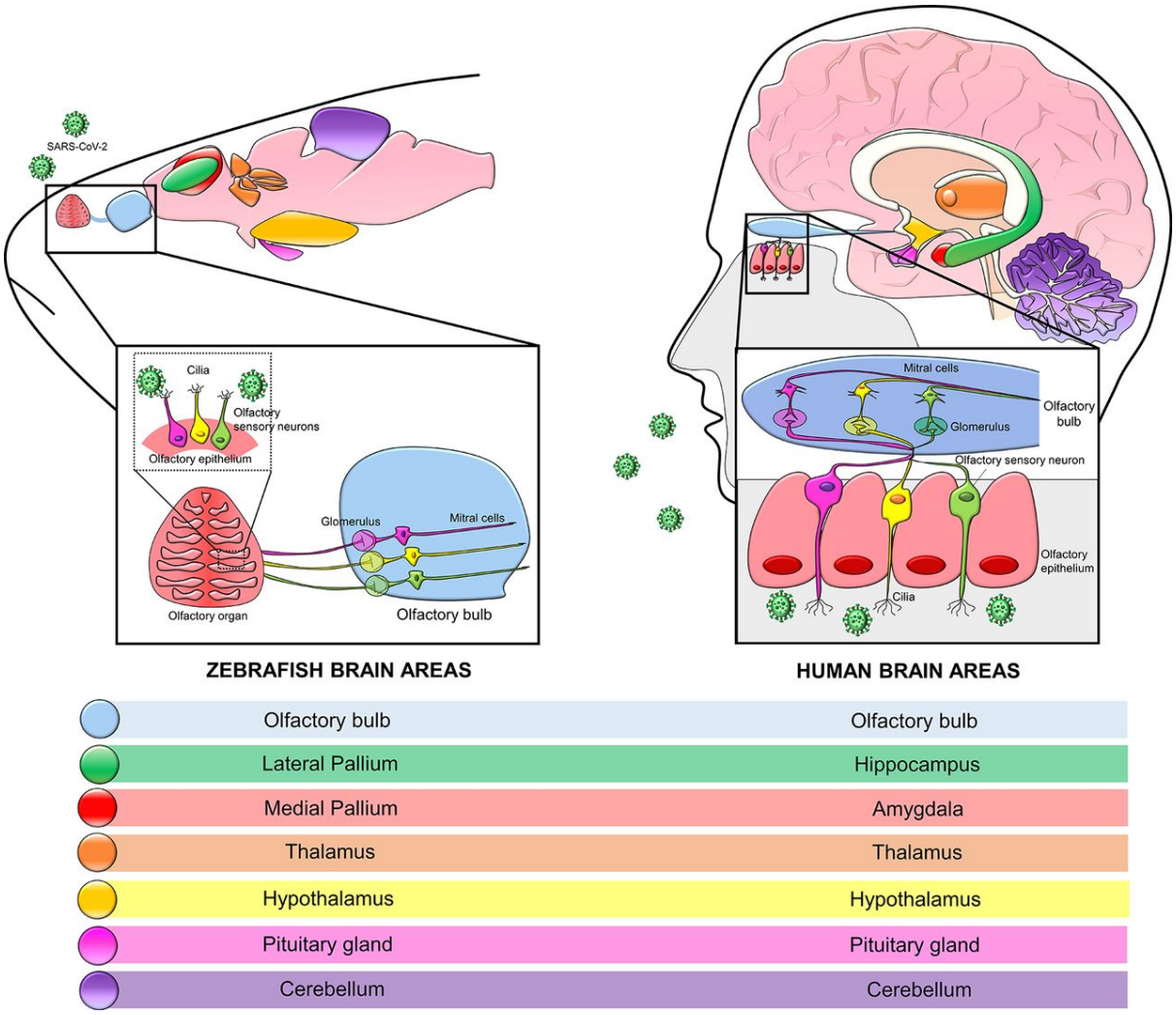

Figure 1.1. The evolutionarily conserved neuronal connections and brain structures in the zebrafish and human olfactory systems (from Costa et al., 2021).

OSNs in the OE project their axons directly to the OBs (blue) of the brain in both zebrafish and humans. Mitral cells relay these neuronal connections to higher brain areas, for example the hypothalamus (yellow), medial

pallium (red) in zebrafish, and its equivalent, the amygdala (red) in humans. Also depicted here is a possible entry route for the SARS-CoV-2 virus into the central nervous system in both zebrafish and humans.

This thesis provides a review of the current knowledge of the anatomy, development, and physiological function of the vertebrate olfactory system, in addition to a review of the human disease-implicated zebrafish gene, *adgrg6*. This thesis then examines the conundrums of olfactory rod cells, an uncharacterised rare cell type found within the zebrafish OE, and discusses the aims, hypotheses, and state-of-the-art experimental approaches for elucidating the unanswered questions set out in this project.

1.2. The vertebrate olfactory system

1.2.1. Cell types within the olfactory epithelium

The vertebrate OE is a multimodal sensor mediated by a diverse set of cells. Two broad classes of sensory receptor — ciliated and microvillous — have been identified in the OE on the basis of morphology, receptor expression, and projection pattern (reviewed in Elsaesser and Paysan, 2007). OSNs, which express G-protein-coupled odorant receptors (ORs) and give rise to the sense of smell, are bipolar neurons that extend a dendrite to the apical surface of the OE and an axon to the OB (reviewed in Axel, 1995). Other sensory cells, some of which have no detectable axon, are also present. In mammals, these include microvillous cells (MVCs) that express transient receptor potential channel M5 (TrpM5) channels and other taste components (Hansen and Finger, 2008; Lin et al., 2008a; Genovese and Tizzano, 2018). A subset of OSNs can act as mechanosensors (Grosmaitre et al., 2007; Iwata et al., 2017; reviewed in Sánchez-Alcañiz and Benton, 2017). Thus, the wide range of cell types in the OE allows for the detection of mechanical and other chemical stimuli in addition to sensing odours.

This variety of receptors is seen not only in terrestrial (air-breathing) animals, but also in aquatic vertebrates. In zebrafish, five classes of OSN have been identified so far. Each occupies a stereotyped position within the pseudostratified OE, with the dendrite bearing a distinct and characteristic specialisation projecting into the environment (Figure 1.2; Hansen and Zeiske,

1998; Hansen and Zielinski, 2005; Sato et al., 2005; reviewed in Maier et al., 2014). Ciliated neurons express olfactory marker protein (OMP), and OR and trace amine-associated receptor (TAAR) genes. They have a cell body that lies deep within the OE, an axon that projects to dorsal and medial regions of the OB, and a slender dendrite extending to the surface of the olfactory pit. Here, the dendritic knob bears a cluster of primary cilia that project into the olfactory cavity (Hansen and Zeiske, 1998; Gloriam et al., 2005; Hansen and Zielinski, 2005; Sato et al., 2005; Liberles and Buck, 2006). Microvillous OSNs, characterised by the expression of transient receptor potential channel C2 (TrpC2) and vomeronasal (VR)-type pheromone receptors, have cell bodies that lie in the intermediary layer of the OE, an axon that projects to the lateral part of the OB, and a dendrite bearing a tuft of short, actin-rich microvilli (Hansen and Zeiske, 1998; Hansen and Zielinski, 2005; Sato et al., 2005). Crypt neurons, less abundant than ciliated or microvillous OSNs, have rounded cell bodies that sit apically in the OE, with both cilia and microvilli extending from a crypt within the cell body (Hansen and Zeiske, 1998; Hansen and Zielinski, 2005; Parisi et al., 2014; Biechl et al., 2016; Bettini et al., 2017; Sepahi et al., 2019). Kappe neurons lie in the superficial layers of the adult zebrafish OE and are named for their apical actin-rich cap, presumed to be microvilli (Ahuja et al., 2014). Pear-shaped neurons are also positioned superficially in the adult OE and have short apical dendrites, but express some markers in common with ciliated neurons (Wakisaka et al., 2017). Aside from these OSNs, it is not known what other sensory cell types exist in the OE.

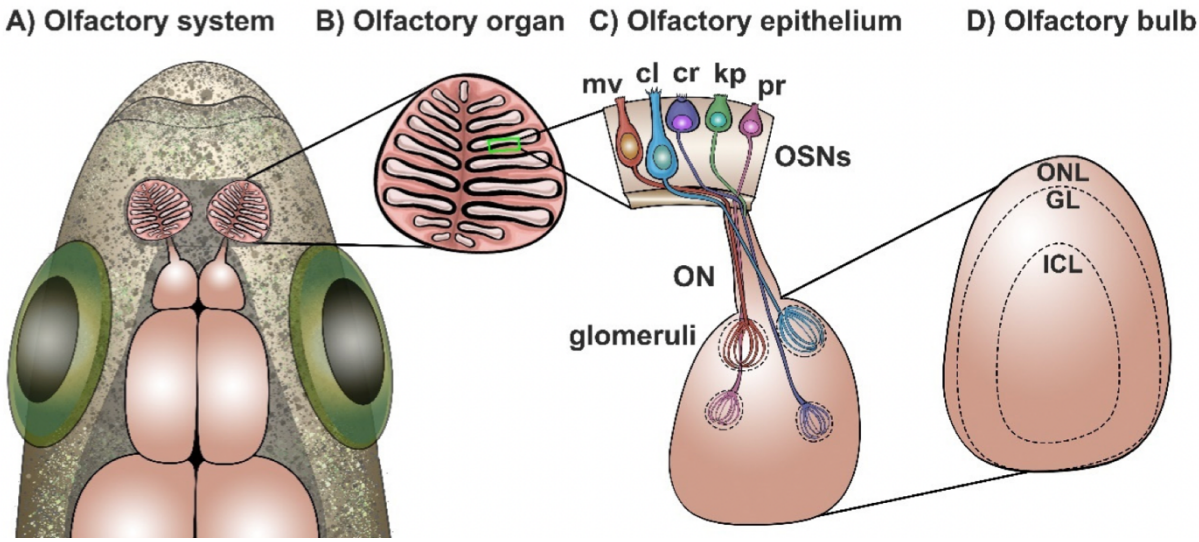

Figure 1.2. Neuronal cell types in the adult zebrafish olfactory epithelium (from Calvo-Ochoa and Byrd-Jacobs, 2019).

(A) Dorsal view of the olfactory system in the adult zebrafish, showing the rosette-shaped olfactory organ connecting to the OB in the forebrain. **(B)** The olfactory organ consists of the OE organised in lamellar structures extending from a central non-sensory raphe. **(C)** The OE contains five different known classes of OSN: microvillous neurons (mv), ciliated neurons (cl), crypt neurons (cr), kappe neurons (kp), and pear neurons (pr). The shape and target projections of each cell type, along with their relative positioning within the OE are depicted in the diagram. **(D)** The OB is organised into three different layers: the superficial olfactory nerve layer (ONL), the glomerular layer (GL) where OSNs converge onto glomeruli, and the intracellular layer (ICL).

The OE is directly exposed to the external environment, and is thus continually subject to damage and infection. Numerous mechanisms enable efficient sampling of stimuli while maintaining tissue integrity and defence. These functions are provided by non-sensory cells in the OE, which include basal (stem) cells that replenish the OSNs, sustentacular (support) cells, and goblet cells, which produce mucous containing anti-microbial peptides (Hansen and Zeiske, 1993, 1998; Byrd and Brunjes, 1995; Demirler et al., 2019; reviewed in Olivares and Schmachtenberg, 2019; reviewed in Calvo-Ochoa et al., 2021). Multi-ciliated cells (MCCs), located medially and laterally on the rim of each olfactory pit in fish, each bear multiple long motile cilia. These have a characteristic 9+2 axoneme and beat at around 24 Hz, resulting in an asymmetric flow that draws water and odorants into the olfactory cavity and flushes them out again (Reiten et al., 2017; reviewed in Ringers et al., 2019). Additional cell types with critical functions, such as immune cells, also populate the OE (Sepahi et al., 2019; Kraus et al., 2020). With many new experimental approaches being developed, there is an exciting scope for identifying and characterising novel cell types.

1.2.2. Anatomy and neurophysiology of the olfactory system

Individual organisms have a remarkable ability to process, distinguish, and recognise diverse odorants. The molecular basis of OR gene expression and the structural organisation of the olfactory system contribute to the ability to transmit odorant information with high specificity (Buck and Axel, 1991; reviewed in Axel, 1995; reviewed in Firestein, 2001).

Each OSN expresses only one type of G-protein-coupled OR on their apical dendrites which binds to a specific odorant molecule such as an amino acid or pheromone; this is known as the one neuron-one receptor rule (Buck and Axel, 1991; reviewed in Axel, 1995; Alioto and Ngai, 2005). Upon binding of odorants to ORs, an electrical response is triggered in OSNs via activation of G-protein G_{olf} and adenylyl cyclase type III, leading to an increase in intracellular cyclic adenosine monophosphate (cAMP) and Ca^{2+} levels. This in turn depolarises the cell and produces an action potential (reviewed in Firestein, 2001; reviewed in Su et al., 2009). OSN axons project through the epithelial basal layer into the OBs of the forebrain, carrying the received olfactory information directly to the brain. With aid from an array of intercellular axon guidance cues such as Robo2 or Netrin1 (Miyasaka et al., 2005; Lakhina et al., 2012), axons of neurons expressing the same OR converge onto the same target glomerulus; this is known as the one glomerulus-one receptor rule (Figures 1.2C, 1.3; reviewed in Axel, 1995; Dynes and Ngai, 1998; reviewed in Firestein, 2001; reviewed in Miyasaka et al., 2013). Different classes of OSN project to glomeruli in different areas of the OB to mediate distinct behavioural responses; for example, microvillous OSNs expressing amino acid-specific (Ala, Cys, His, Lys, Met, Phe, Trp, and Val) receptors project their axons to glomeruli in the lateral side of the OB glomerular layer to regulate appetitive feeding behaviours (reviewed in Axel, 1995; Koide et al., 2009).

The deeper layers of the OB contain mitral and granule cells. Mitral cell dendrites receive direct information via synaptic contact with OSNs, while mitral cell axons project to different higher brain areas within the telencephalon and diencephalon (Figure 1.3). On the other hand, granule cells facilitate neuron-neuron interactions within the OB (Byrd and Brunjes, 1995; reviewed in Firestein, 2001). Different OB targets in the brain mediate different responses; for example, olfactory information received in the habenula is linked to fearful behaviour. Zebrafish with loss of habenular activity show lack of avoidance responses to fear-inducing odorants such as the alarm substance 'Schreckstoff' (Agetsuma et al., 2010; Lee et al., 2010; Mathuru et al., 2012; Krishnan et al., 2014).

In conclusion, via G-protein G_{olf} and adenylyl cyclase type III-dependent activation, the olfactory system gives rise to a topographical map of neuronal activity in the brain, a phenomenon observed across multiple species including humans and zebrafish. This

demonstrates that specific OR gene expression and structural organisation are important factors for efficient olfactory signalling transduction and are evolutionarily conserved (reviewed in Axel, 1995; reviewed in Rinaldi, 2007; reviewed in Imai et al., 2010).

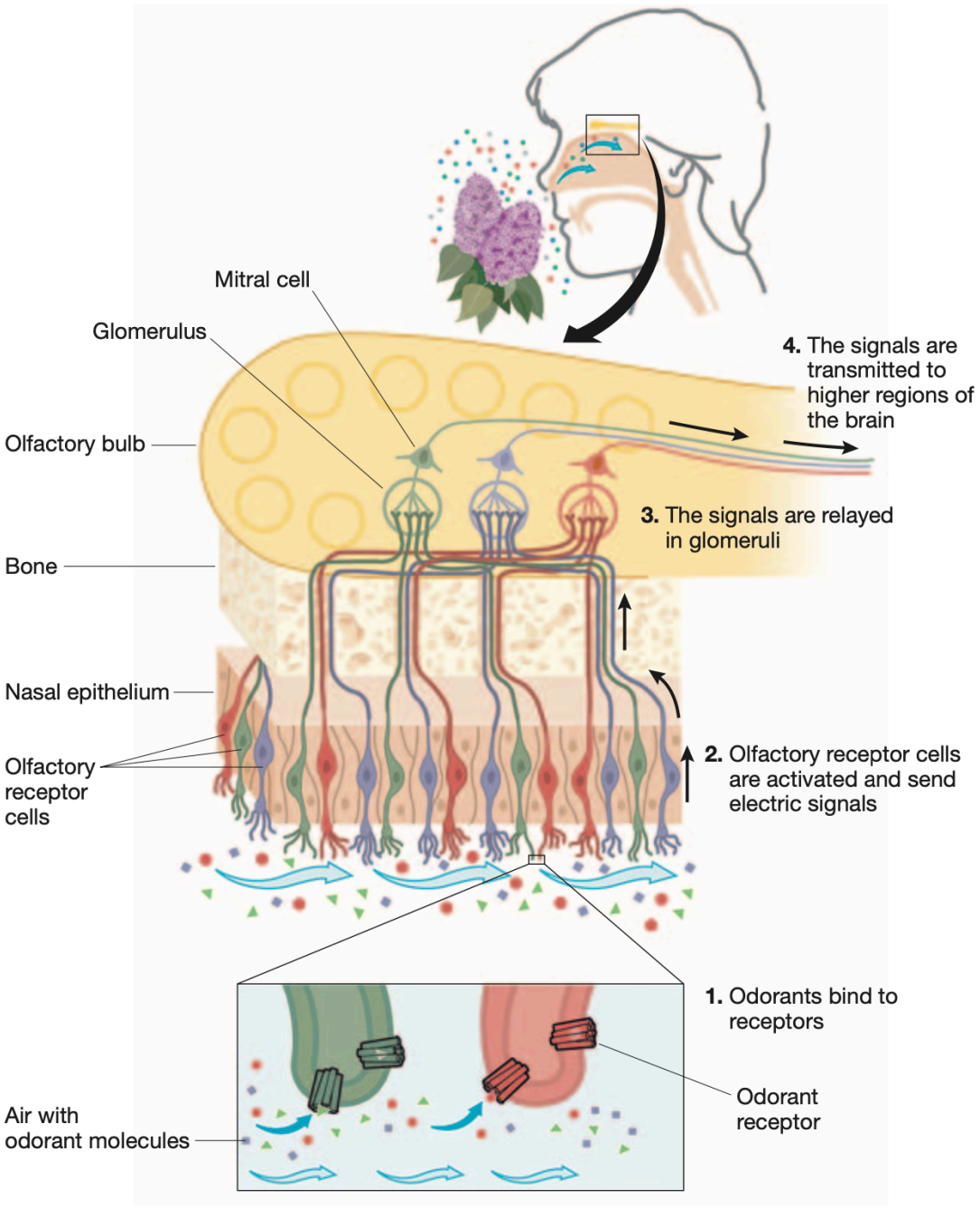

Figure 1.3. The human olfactory signalling transduction pathway (from Rinaldi, 2007).

Each OSN in the OE express one type of OR on their apical dendrites which binds to specific odorant molecules (one neuron-one receptor rule). OSNs depolarise and transmit the electrical signal to the OB via their basal axon. OSNs expressing the same ORs (here distinguished by green, blue, and red neurons) converge onto the same

target glomerulus in the OB (one glomerulus-one receptor rule). The axons form synaptic connections with mitral cells, which relay the neuronal information to higher brain regions.

1.2.3. Early development of the olfactory system

Development of a fully functional vertebrate olfactory system depends on highly specific spatiotemporal gene expression patterns during embryogenesis. The olfactory placode is generated from pre-placodal ectoderm (PPE) through cellular migration and convergence (Whitlock and Westerfield, 2000). Olfactory pits in zebrafish embryos arise at around 34 hours post-fertilisation (hpf) during the pharyngula prim-20 stage. Actomyosin contractility and mechanical forces from early olfactory neurons pulling on the overlying peridermal skin tissue allow the opening of the olfactory pit and reveal the placodal OE tissue beneath (Baraban et al., 2023). Mature ciliated and microvillous OSNs are present by 48 hpf (Hansen and Zeiske, 1993; Whitlock and Westerfield, 1998). The zebrafish OE continues to undergo epithelial folding in juvenile stages to become a rosette-shaped organ in adults (Hansen and Zeiske, 1993, 1998; Hansen and Zielinski, 2005).

A fully formed olfactory system contains many distinct cell types; however, their developmental origin is a subject of debate (reviewed in Rajan and Saxena, 2022). OSNs in the zebrafish OE were thought to originate in the PPE, whereas the closely associated gonadotropin-releasing hormone 3 (GnRH3) cells of the terminal nerve were reported to originate from the cranial neural crest (CNC; Whitlock et al., 2003). Through photoconversion-based fate mapping, live cell tracking, and laser ablation, Saxena et al. (2013) proposed a dual embryonic origin for microvillous OSNs, suggesting that they arise from both CNC and PPE. However, evidence from lineage reconstruction experiments led to a subsequent rebuttal from Aguillon et al. (2018), who contested that all olfactory neurons, including OSNs and GnRH3 cells, are derived entirely from PPE progenitors. The lineage of olfactory cells remains disputed.

Establishment of the PPE and CNC from the anterior neural plate occurs during gastrulation and are respectively regulated by pre-placodal competence transcription factors, such as *eya1*, *six1b*, *foxi1*, *gata3*, and *dlx3b* (Figure 1.4A; reviewed in Miyasaka et al., 2013; Shigetani

et al., 2016), and neural crest specifier genes, such as *sox10*, *tfap2a* and *foxd3* (Wang et al., 2011). The importance of such genes during development can be observed by their disruption through inducing loss-of-function mutations; for example, double *tfap2a* and *foxd3* mutant zebrafish embryos completely lack neural crest derivatives including olfactory-associated sensory and neurosecretory cells (Whitlock et al., 2003; Wang et al., 2011). This demonstrates that highly specific spatiotemporal gene expression surrounding the anterior neural plate is fundamental for specifying olfactory progenitors and initiating the formation of olfactory organs.

Neuronal differentiation is another highly specific and controlled developmental process occurring downstream of olfactory progenitor specification. *Foxg1*, a forkhead family transcription factor expressed in the olfactory placodes, is required for neuronal differentiation. *Foxg1* knockdown zebrafish have a significant reduction in proliferation and differentiation of OSNs from progenitor cells (Duggan et al., 2008). *Neurogenin1* and *neurod4*, two basic helix-loop-helix transcription factors that act downstream of *Foxg1*, are also implicated in olfactory development (Figure 1.4B). Madelaine et al. (2011) demonstrated that *neurogenin1* mutants with a reduced background expression of *neurod4* have a significant reduction of early-born olfactory neurons and mature OSNs. Thus, specific genes encoding transcription factors expressed within the olfactory placodes are essential for neuronal differentiation and are additionally transcriptionally coupled to morphogenesis of the olfactory organ (Aguillon et al., 2020). Overall, this ascertains that early olfactory development is a precise and complex process.

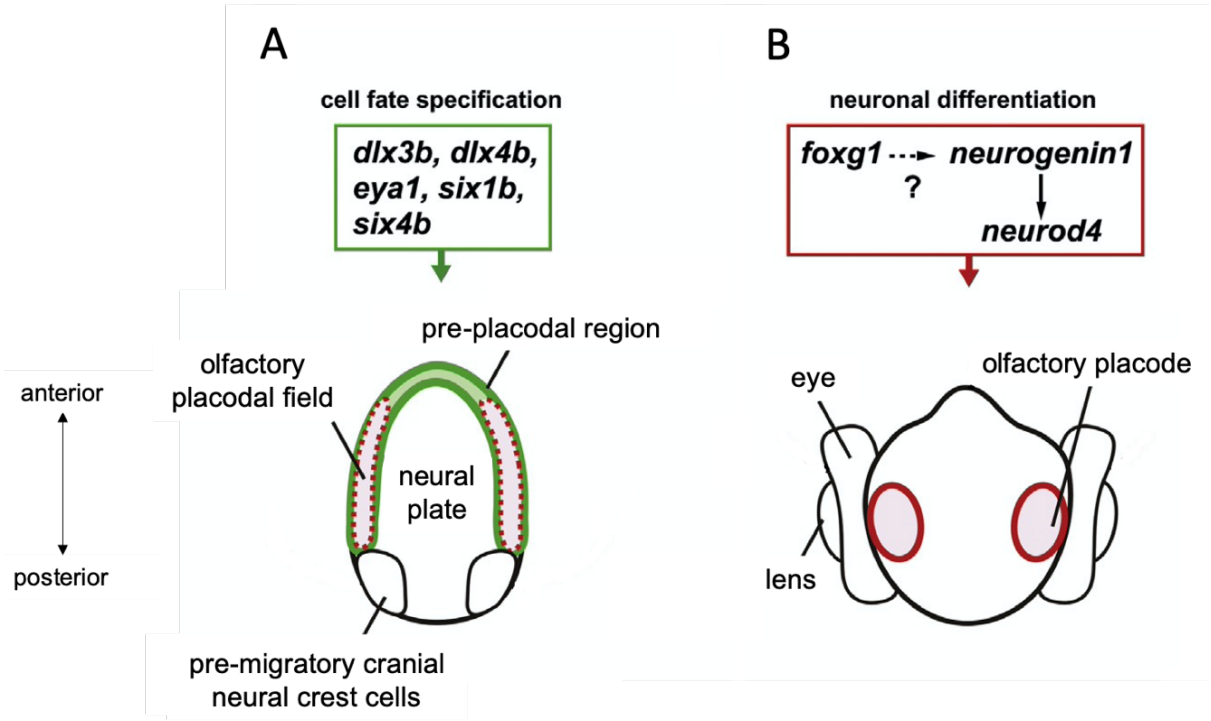

Figure 1.4. The developmental cues involved in specification of the olfactory placode and differentiation of olfactory sensory neurons in zebrafish (adapted from Miyasaka et al., 2013).

(A) Cell fate specification transcription factor genes, such as *dlx3b*, regulate the specification of the pre-placodal ectoderm (green area) at the border of the neural plate, from which the olfactory placodal field (red dotted area) and cranial sensory organs are derived. Cells of the olfactory placodal field undergo cellular migration and convergence to form the olfactory placode (not depicted). Dorsal view. **(B)** Forkhead transcription factor gene *foxg1*, and downstream basic helix-loop-helix transcription factor genes *neurogenin1* and *neurod4*, mediate OSN differentiation from the olfactory placode (red area). Frontal view.

1.2.4. Multimodality and mechanosensation in olfactory sensory neurons

Traditionally, sensory cells were thought to perform distinct functions; for example, individual OSN subtypes are specialised to detect specific odorants, rods and cones mediate vision at varying levels of light, chemoreceptors detect tastes, while hair cells only perceive mechanical stimuli. However, more recent research shows that some receptors and sensory cells can actually detect more than one sensory modality. In the case of the olfactory system, mammalian OSNs have interestingly been discovered to also act as mechanosensors (Grosmaitre et al., 2007; Iwata et al., 2017; reviewed in Sánchez-Alcañiz and Benton, 2017). In the zebrafish OE, mechanostimulation from a change in velocities of flow during the

application of odours is known to cause activation of OSNs, as measured by an increase in calcium reporter levels (Rayamajhi et al., 2023). Simultaneous processing and integration of both olfactory and mechanical stimuli have additionally been reported in a special glomerulus in the OBs of *Xenopus laevis* tadpoles (Brinkmann and Schild, 2016), and in antennal lobe neurons of male *Manduca sexta* moths (Tuckman et al., 2021) and *Apis mellifera* honey bees (Tiraboschi et al., 2021).

A voltage-clamp study in mice by Grosmaitre et al. (2007) showed that puffs of odour caused inward currents in septal organ neurons of the olfactory neuroepithelium. Similarly, the same response trend, albeit at lower amplitudes, could be induced by puffs of odourless Ringer's solution in 76.7% of the tested septal organ neurons and in 49% of OSNs in different regions of the main olfactory epithelium (MOE). The amplitudes of responses decreased when delivery of the odourless stimulus moved farther away, indicating that olfactory cells can be mechanoresponsive in a widespread and pressure-dependent manner (Grosmaitre et al., 2007). The mechanotransduction pathway in OSNs is remarkably akin to that of olfaction. Blocking the cAMP pathway with MDL12330A yielded no current change in response to neither olfactory nor mechanosensory stimuli in voltage-clamp recordings of OSNs. Additionally, inhibition of cyclic nucleotide-gated (CNG) ion channels by removal of Ca^{2+} ions in the Ringer's solution resulted in the amplitudes of both olfactory and mechanosensory responses becoming larger and longer lasting. Olfactory response adaptation in OSNs is dependent on second messenger cascades involving Ca^{2+} and inhibition of CNG channels, a phenomenon likewise observed in adaptation to mechanical stimuli. An increase in the frequency of Ringer's solution delivery resulted in dampened subsequent neuronal activity as revealed by both voltage- and current-clamp recordings. In summary, this demonstrates that both olfaction and mechanosensation in mammalian OSNs are similarly mediated by cAMP second messenger and CNG channel signalling cascades (Grosmaitre et al., 2007).

Following the breakthrough discovery of mechanosensitivity in OSNs, it was then important to explore why it is necessary for animals to integrate both modalities within a single cell and system. After hypothesising that mechanosensitivity serves to enhance olfactory transduction, Grosmaitre et al. (2007) reported that increasing the pressure of mechanical stimulation led to augmented responses to odorants in both voltage- and current-clamp

recordings. This is more evident with lower odorant concentrations, as higher odorant concentrations likely already saturated firing activity in OSNs. To put this into context *in vivo* in terrestrial mammals, airflow passing through the nasal cavity while sniffing contributes as a mechanostimulus, and so therefore improves odour perception (Grosmaitre et al., 2007). The second speculated role of such mechanosensitivity is to influence spontaneous activity (theta oscillation waves) in the OBs. In the same study, current-clamp recordings of OBs in wild-type mice showed that rhythmic activity was synchronised with the pattern of respiration. On the other hand, recordings in *Cnga2*$^{-/y}$ mice, a CNG knock-out strain with phenotypes of eliminated responses to both odorants and mechanical stimuli, showed that the two paradigms occurred independently. These findings indicate that mechanostimulation, in the form of inhalation and exhalation, can drive rhythmic activity in the OBs (Grosmaitre et al., 2007). Therefore, mechanosensation plays a surprisingly important role in facilitating the physiological function of the olfactory system.

It is widely known that force-gated ion channels are normally involved in mechanotransduction in tissues that are exposed to mechanical stimuli such as shear stress and pressure (reviewed in Douguet and Honoré, 2019); however, there is a newfound role for G-protein-coupled receptors (GPCRs) in mechanosensation. A study in mice MOE by Connelly et al. (2015) showed that ablation of a few different classes of OR, such as M71 and SR1, resulted in a loss of mechanosensitivity in OSNs. Furthermore, ectopic expression of another class of OR, I7, was sufficient to rescue both olfactory and mechanosensory responses in I7 loss-of-function mutant mice. Different classes of OR give different response profiles to mechanostimulation, but nonetheless, in conclusion, GPCRs are necessary and sufficient for mechanotransduction within the olfactory system (Connelly et al., 2015).

1.2.5. Olfactory cilia and the control of ciliary beat frequency

While fish do not actively sniff to enhance olfaction, MCCs, as described above, possess motile cilia that beat in a metachronal fashion, generating a uni-directional water flow to draw odorants into the nasal cavity and clear it of irritants, mucous, and the odorants themselves (Figure 1.5). This contributes to providing spatiotemporal resolution during olfaction, in addition to mucociliary clearance, thus facilitates odour detection (Reiten et al., 2017; Ringers

et al., 2019, 2023). Lack of ciliary beating, for example in *smh*$^{-/-}$ mutant zebrafish, leads to impaired neuronal responses to odorants (Reiten et al., 2017).

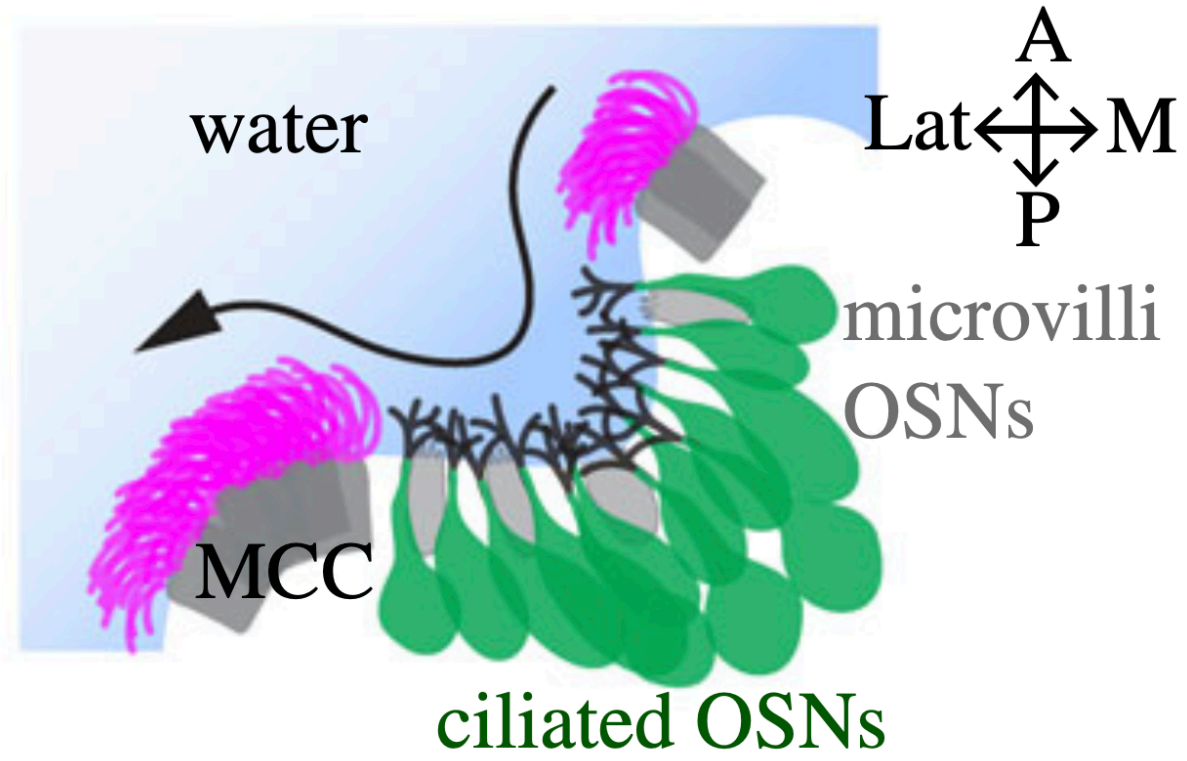

Figure 1.5. Ciliated cell types in the larval zebrafish olfactory pit (from Ringers et al., 2019).
The larval zebrafish OE contains non-sensory MCCs situated medially and laterally on the rim of the olfactory pit. Each MCC possesses multiple long motile cilia (magenta), which beat to generate an asymmetric water flow that enters the pit medially and exits laterally. Ciliated OSNs (green) are located deeper in the olfactory pit, and project OR-expressing primary cilia (black). Also depicted are microvillous OSNs (light grey).

Through computational quantification of ciliary beat frequency (CBF), Ringers et al. (2023) reported that the beating of olfactory cilia is synchronised in local domains. This feature, along with tissue-scale alignment of cilia and metachronal coordination, are proposed to aid in the physiological function of fluid pumping. Intriguingly, increasing the viscosity of the surrounding medium to up to 15 centipoise (cP) leads to a decrease in CBF and an increase in the coherence of cilia (Ringers et al., 2023). However, it is currently unclear how changes in fluid flow or viscosity may be detected by the OE or how MCCs regulate and adapt their CBF in response to these changes.

Several fluid-sensing mechanosensors exist in zebrafish. Cerebrospinal fluid-contacting neurons (CSF-cNs), for example, are mechanosensory cells in the spinal cord which contain an apical tuft of actin-rich microvilli and a motile kinocilium, and function to detect spinal cord bending to maintain the antero-posterior body axis (Böhm et al., 2016; Sternberg et al., 2018; reviewed in Ringers et al., 2019). Moreover, immotile cilia in the Kupffer's vesicle (left-right organiser) detect mechanical forces from extracellular fluid flow to instruct left-right asymmetry in the developing embryo (reviewed in Cartwright et al., 2019; Djenoune et al., 2023). There is a potential role for an olfactory mechanosensory cell type to detect changes in fluid flow and viscosity to influence CBF, but this is yet to be characterised in zebrafish.

More broadly speaking, MCCs exist in numerous regions of the human body, such as the airway, spinal cord, and reproductive tract, thus, the discovery of a mechanism to regulate CBF in the zebrafish OE would have widespread significance.

1.2.6. Clinical implications and neuroplasticity of the olfactory system

The olfactory system is implicated in ageing and in numerous neurological disorders, including Alzheimer's disease, Parkinson's disease, multiple sclerosis, and schizophrenia, where patients exhibit olfactory dysfunction (reviewed in Whitlock, 2015; Kotecha et al., 2018; reviewed in Marin et al., 2018; reviewed in Bhatia-Dey and Heinbockel, 2021; reviewed in Son et al., 2021). It is also affected in infectious diseases such as COVID-19 during SARS-CoV-2 infection (Brann et al., 2020; Gupta et al., 2020; reviewed in Xydakis et al., 2021; Choi et al., 2022; Kraus et al., 2022). Not only can an impaired sense of smell hugely impact the behaviour and survival of an animal, but it can also degrade quality of life. Fortunately, in healthy individuals, stem cells in the basal layer of the OE differentiate into new OSNs to repair this part of the nervous system throughout embryonic development and adulthood; however, regenerative capacities normally diminish with age (reviewed in Brann and Firestein, 2014).

The zebrafish olfactory system displays extraordinary dynamicity and neuroplasticity (reviewed in Calvo-Ochoa and Byrd-Jacobs, 2019). Neurotoxicants such as copper, uranium, and Triton X-100 damage the zebrafish olfactory system by degradation of OSNs and deafferentation of glomeruli in the OBs. Consequently, this produces dysfunctional olfactory

responses associated with altered behaviours and a reduction in chemotaxis (Figure 1.6; Iqbal and Byrd-Jacobs, 2010; reviewed in Calvo-Ochoa and Byrd-Jacobs, 2019). Remarkably, much like other zebrafish tissues, the olfactory system can self-repair and regenerate. The morphology and functions of the olfactory system are restored by 21 days following Triton X-100 treatment in adult zebrafish (Figure 1.6; Iqbal and Byrd-Jacobs, 2010). Such experimental approaches have clinical applications in researching methods to restore sensory function in human neurological disorders.

Zebrafish are a key model organism for studying the olfactory system, thus highlighting the importance of a complete inventory of all the cell types present and genes expressed in the OE as a resource and reference point for future studies.

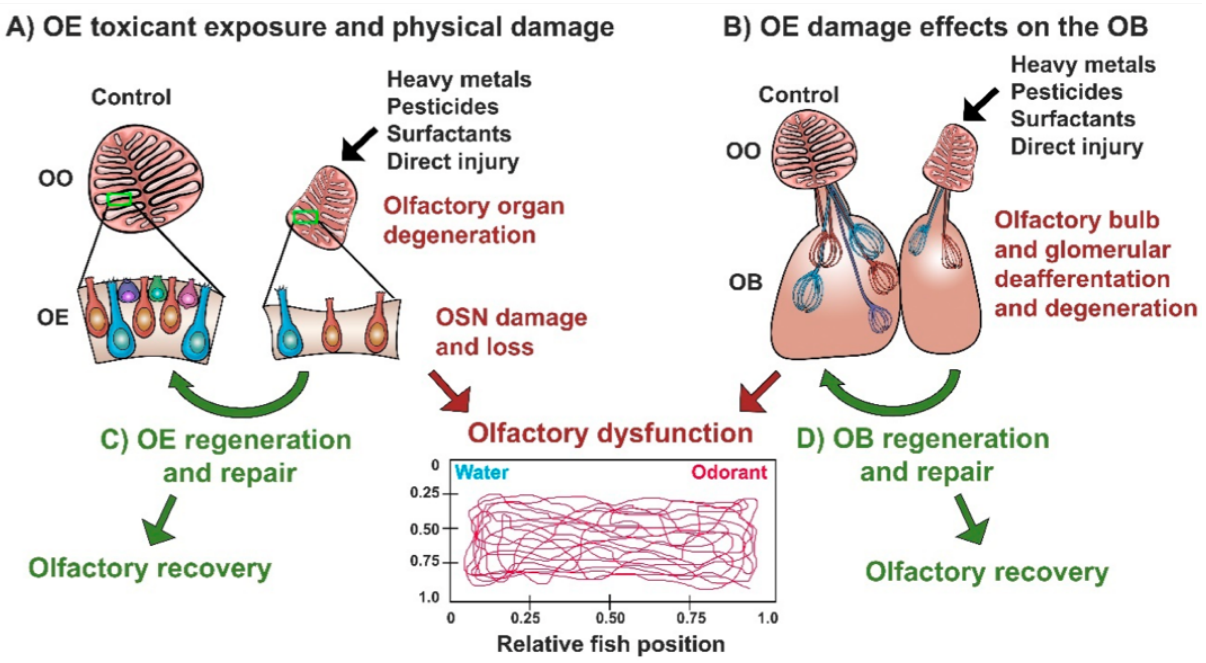

Figure 1.6. Neurotoxicity and neuroplasticity in the zebrafish olfactory system (from Calvo-Ochoa and Byrd-Jacobs, 2019).

(A) Exposure to toxic chemicals leads to degradation of the olfactory organ (OO), OE, and loss of OSNs, which cause dysfunctional responses to odorants in zebrafish. **(B)** Exposure to toxic chemicals leads to deafferentation of glomeruli in the OB, which causes olfactory dysfunction. **(C, D)** The OE and OB have reparative and regenerative abilities following damage, subsequently restoring olfactory functions.

1.3. The adhesion G-protein-coupled receptor Adgrg6 (Gpr126)

1.3.1. Adgrg6 as a proposed mechanoreceptor

Adgrg6, also known as Gpr126, is an adhesion class GPCR (aGPCR) required for various essential roles in development and diseases in humans and animal models (Figure 1.7; reviewed in Baxendale et al., 2021). Adgrg6 can be activated by cell-cell contact, as well as the binding of prion protein PrP^C (Küffer et al., 2016) and extracellular matrix (ECM) component ligands, collagen IV and laminin-211, to its large N-terminal fragment (NTF; Paavola et al., 2014; Petersen et al., 2015). Following an auto-proteolytic cleavage event at the GPCR proteolysis site (GPS) which separates the NTF and C-terminal fragment (CTF; Araç et al., 2012), one potential model of activation is by the physical removal of the NTF. This exposes a *Stachel* sequence, allowing it to bind to the CTF to auto-activate the receptor (Figure 1.7; Petersen et al., 2015). The aGPCR then signals via canonical Gα cascades ($G\alpha_s$, $G\alpha_i$, $G\alpha_{12/13}$, $G\alpha_{q/11}$), leading to adenylyl cyclase activation, cAMP production, protein kinase A activation, and expression of downstream target genes (Monk et al., 2009; Mogha et al., 2013; Lizano et al., 2021).

An investigation into the mechanism of receptor activation *in vitro* showed that binding of laminin-211 to the NTF in human ADGRG6 transfected cells did not lead to receptor activation, but instead caused a decrease in intracellular cAMP levels. In order to mimic *in vivo* receptor activity, mechanical forces were additionally required to remove the NTF during laminin-211-mediated activation of Adgrg6 (Petersen et al., 2015; reviewed in Lin et al., 2022; Mitgau et al., 2022). Mechanostimulation by increasing vibration frequency or by binding of antibodies against the NTF hemagglutinin epitope was necessary to mediate laminin-211-dependent intracellular cAMP accumulation, and only then did it promote downstream signalling (Petersen et al., 2015; Mitgau et al., 2022). This suggests a model that requires mechanosensation with ligand binding for activation of Adgrg6 *in vivo*.

Adgrg6 gene is found to be predominantly expressed in tissues exposed to shear stress and mechanical stimulation in LacZ reporter mice, such as in the vasculature and chondrocytes

(Musa et al., 2019; reviewed in Lin et al., 2022). With this in mind, researchers have therefore proposed a mechanosensory role for the Adgrg6 receptor.

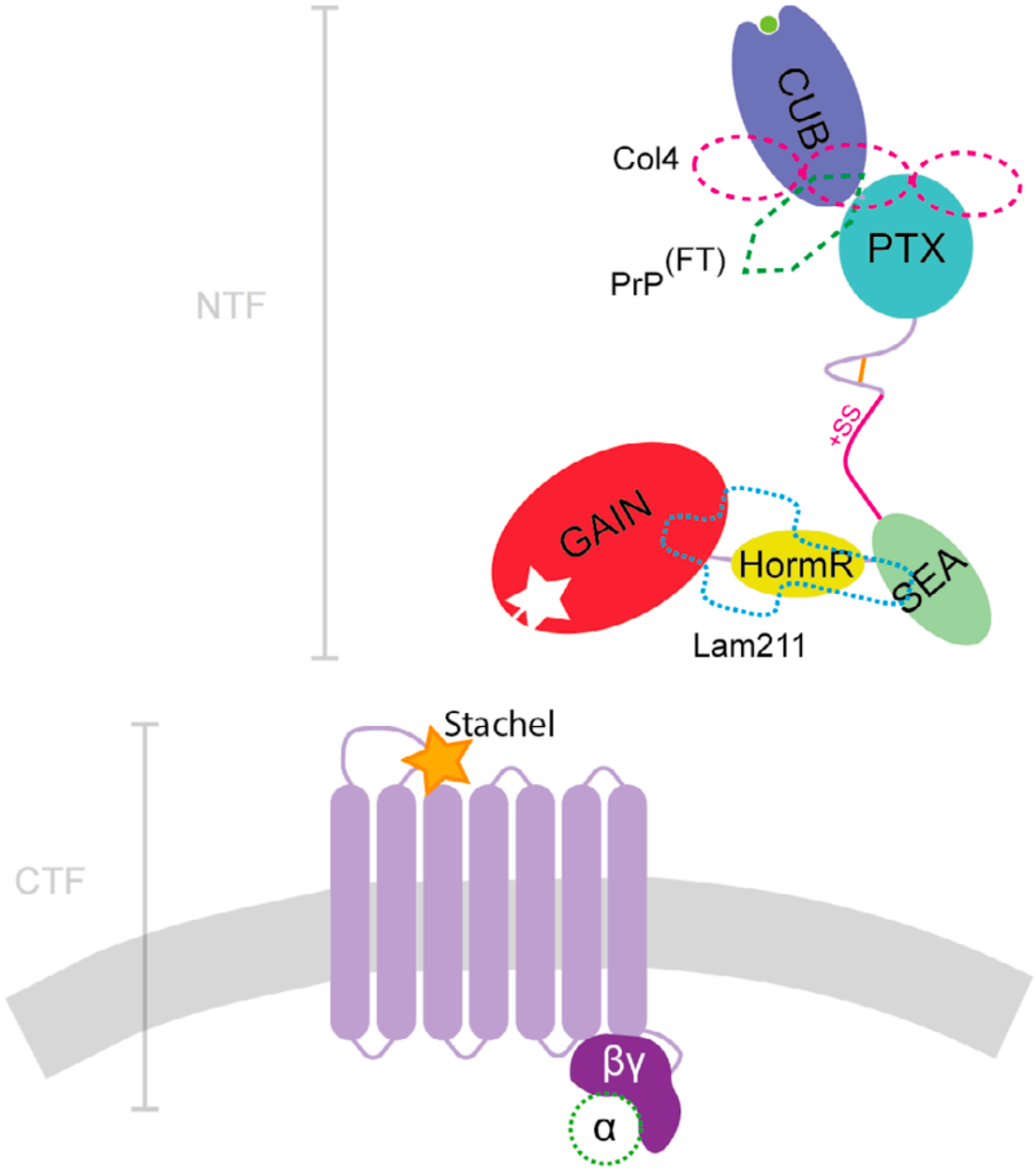

Figure 1.7. Structure of the Adgrg6 receptor (adapted from Leon et al., 2020; Baxendale et al., 2021).
Diagrammatic representation of the structure and a potential model of activation of the Adgrg6 receptor. The CTF consists of 7 transmembrane domains. The large NTF consists of a GPCR auto-proteolysis-inducing (GAIN) domain, hormone receptor (HormR) domain, Sperm protein, Enterokinase and Agrin (SEA), pentraxin (PTX), and Complement C1r/C1s, Uegf and BMP1 (CUB). Binding sites of known ligands collagen type IV (Col4; dashed pink

line), prion protein PrP^{C} flexible tail ($PrP^{(FT)}$; dashed green line), and laminin-211 (Lam211; dashed blue line) are depicted on the NTF. The binding of ligands and subsequent removal of the NTF leads to auto-activation of the receptor by the binding of the *Stachel* sequence (orange star) to the CTF. This triggers intracellular downstream signalling via Gα, adenylyl cyclase, cAMP, and protein kinase A.

1.3.2. Adgrg6 in development and disease

Adgrg6 has well defined essential roles in myelination of the peripheral nervous system (PNS) in mammals and zebrafish (Monk et al., 2009, 2011). The *adgrg6* gene is expressed in Schwann cells and is activated upon contact with neurons, leading to the maturation of the cells and subsequent myelination of the PNS (Monk et al., 2009, 2011; Mogha et al., 2013). It is further critical in maintaining the PNS in adult mice, where it is autonomously involved in remyelination following nerve injury, and non-autonomously required in recruiting macrophages to eliminate cell debris (Mogha et al., 2016). Moreover, Adgrg6 plays a role in the development of the inner ear in zebrafish embryos (Whitfield et al., 1996; Monk et al., 2009; Geng et al., 2013), a process that involves folding and fusion of epithelial tissues to form the semi-circular canal ducts (Waterman and Bell, 1984). Similarly triggered by cell-cell contact, Adgrg6 signalling is thought to act here by repressing the expression of ECM genes to control morphogenesis of this complex 3D structure (Geng et al., 2013).

Zebrafish are well established as an insightful model for studying *adgrg6*, with techniques such as genetic manipulation, mutant analysis, and drug screening being a few examples of many methods that help shed light on the gene functions, receptor signalling mechanisms, and disorder-causing mutations (reviewed in Baxendale et al., 2021). *Adgrg6* mutant zebrafish exhibit severe PNS and inner ear phenotypes; for example, homozygous mutant zebrafish larvae show a lack of or reduced expression of Schwann cell marker gene *myelin basic protein* (*mbp*) and have swollen ears (Monk et al., 2009; Geng et al., 2013). Various homozygous recessive mutations in human *ADGRG6* are likewise associated with a loss of MBP as well as contractures of major joints, likely to be a consequence of myelination defects in arthrogyrposis multiplex congenita (Ravenscroft et al., 2015). Additionally, missense mutations in a transmembrane domain of *ADGRG6* are associated with intellectual disabilities (Hosseini et al., 2019), while some *ADGRG6* variants are linked to musculoskeletal defects

(Ravenscroft et al., 2015; reviewed in Baxendale et al., 2021) and numerous human cancers (Maiga et al., 2016). Drug screening for compounds that can rescue phenotypes in *adgrg6* mutant zebrafish demonstrates how this disease model can help identify potential treatments for the corresponding human disorders, or pharmacological tools for manipulation of the signalling pathway (Diamantopoulou et al., 2019; reviewed in Baxendale et al., 2021).

1.3.3. Expression of *adgrg6* in the zebrafish olfactory system

Aside from Schwann cells and the inner ear, *adgrg6* mRNA transcripts are detected in other zebrafish tissues, such as the heart, pectoral fin, tail fin, gill cartilage, and chondrocytes (Geng et al., 2013). Intriguingly, *adgrg6* is also expressed in the OE at 24, 48, and 72 hpf (Figure 1.8; Geng et al., 2013). Although certain aspects of Adgrg6 are well researched, the olfactory cell type that expresses the gene and the functions that the gene plays within the zebrafish olfactory system have not yet been characterised. It would be of interest to researchers in both the aGPCR field and the olfactory system field to investigate this.

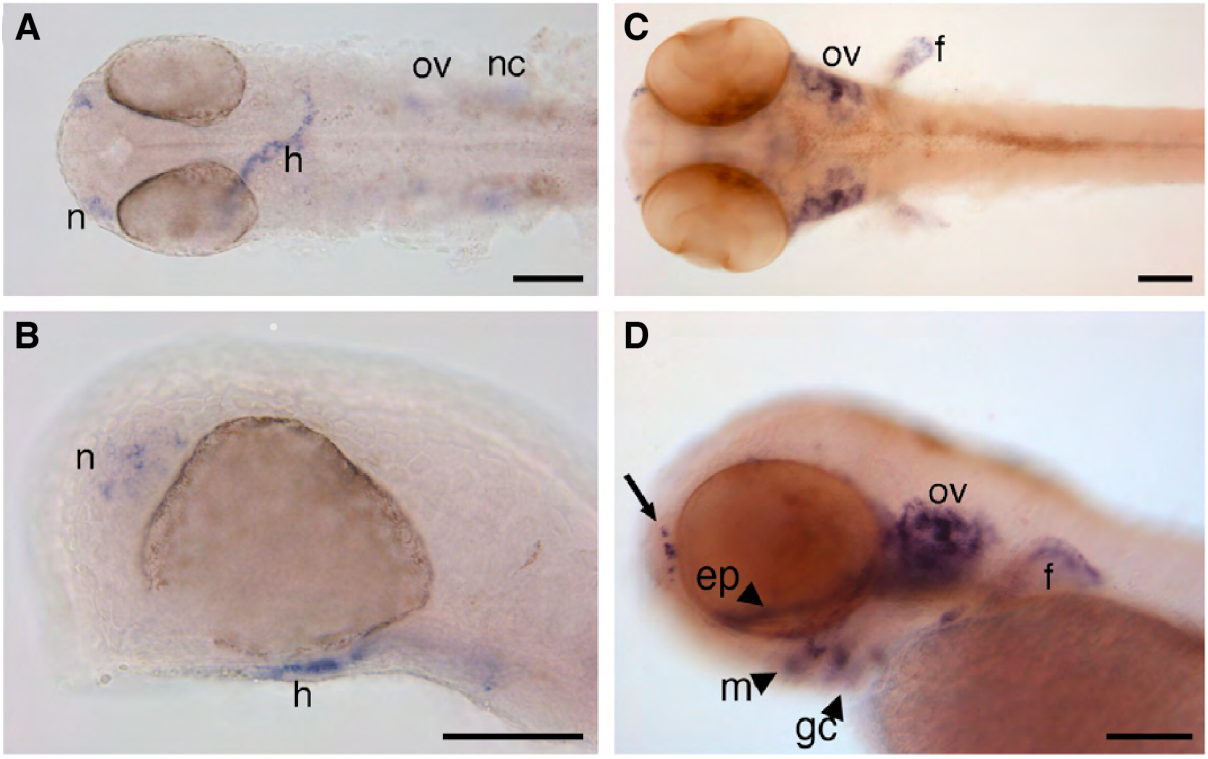

Figure 1.8. Expression of *adgrg6* mRNA in the developing zebrafish embryo (from Geng et al., 2013).

(A, B) Expression of *adgrg6* mRNA at 24 hpf in dorsal **(A)** and lateral **(B)** views. Expression is present in the neural crest (nc), heart tube (h), and OE (n, nose). **(C, D)** Expression of *adgrg6* mRNA at 48 hpf in dorsal **(C)** and lateral **(D)** views. Expression remains in the OE (arrow). Expression is also present in the otic vesicle (ov), pectoral fin (f), ethmoid plate (ep), Meckel's cartilage (m), gill cartilages (gc), and chondrocytes (arrowheads) at this stage. Note: expression of *adgrg6* mRNA in Schwann cells is not visible in these images. Scale bars = 100 µm.

1.4. Olfactory rod cells

This research project focuses on olfactory rod cells, a rare cell type in the larval zebrafish OE. Olfactory rod cells are characterised by a single actin-rich apical rod-shaped projection, hence the name 'rod' (not to be confused with photoreceptor rod cells). They were initially observed in whole-mount phalloidin stains, routinely used in the Whitfield lab to visualise actin-rich stereociliary bundles on sensory hair cells of the inner ear and lateral line, and were subsequently identified in scanning electron microscopy (SEM) images at 5 dpf (Figure 1.9). It was unclear what these olfactory cells were, as they did not resemble previously described OSNs. The morphology of the olfactory rod matched descriptions of similar structures in the OE of several other fish species (Bannister, 1965; Schulte, 1972; Breipohl et al., 1973; Ichikawa and Ueda, 1977; Yamamoto and Ueda, 1978; Rhein et al., 1981; Hernádi, 1993; Datta and Bandopadhyay, 1997), many of which were previously dismissed either as senescent forms of OSNs or as fixation artefacts (Muller and Marc, 1984; Moran et al., 1992).

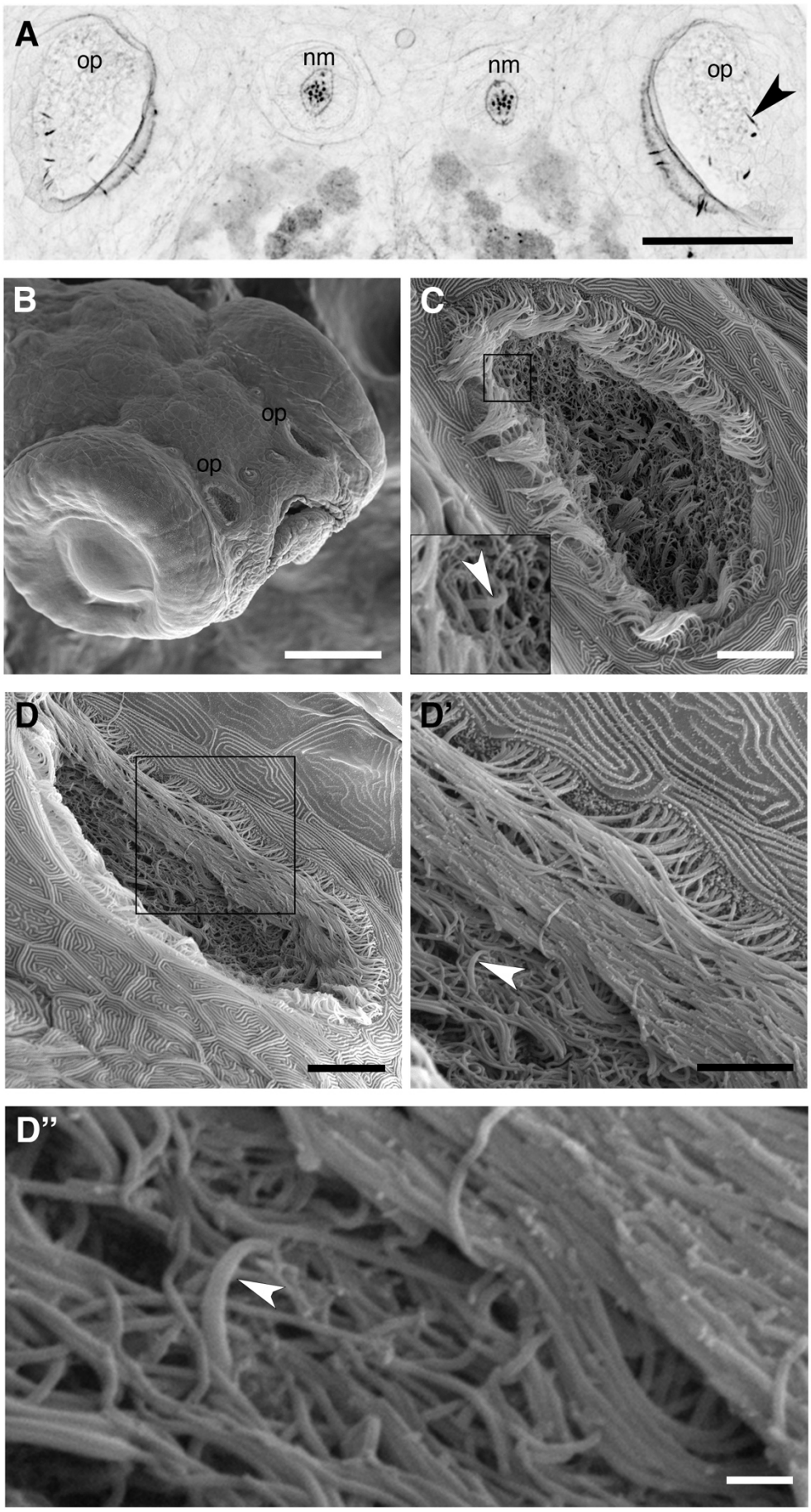
A
op
nm
nm
op
B
op
op
C
D
D'
D''

Figure 1.9. Initial phalloidin stain image and scanning electron microscopy images of olfactory rod projections in the larval zebrafish olfactory pit (images taken by T. T. Whitfield, N. J. van Hateren, and C. J. Hill; from Cheung et al., 2021).

(A) Maximum intensity projection of Airyscan confocal image of phalloidin stain of a 5 dpf wild-type larva; dorsal view, anterior to the top. Greyscale values from the original fluorescence image have been inverted. Abbreviations: nm, cranial neuromast; op, olfactory pit. Several olfactory rods (example marked by arrowhead) are visible in each olfactory pit. Scale bar = 50 µm. **(B)** SEM of the head of a 4 dpf wild-type larva. Scale bar = 100 µm. Abbreviation: op, olfactory pit. **(C, D)** SEM of 4 dpf larval wild-type olfactory pits (enlarged from panel **B**). Scale bars = 10 µm. Insert in **C** shows enlarged view of boxed area in **C**. Arrowhead marks the tip of an olfactory rod cell apical projection surrounded by olfactory cilia. **(D')** Enlarged view of boxed area in **D**. Arrowhead marks one olfactory rod. Scale bar = 5 µm. **(D'')** Enlargement of olfactory rod in **D'** (arrowhead). Scale bar = 1 µm.

1.4.1. Research aims and hypotheses

The aim of this PhD project is to characterise the properties of olfactory rod cells in zebrafish by combining techniques such as immunohistochemistry, fluorescent *in situ* RNA hybridisation chain reaction (HCR RNA-FISH), fluorescence imaging, high-resolution image analysis, mutant screens, scRNA-seq analysis, and a range of developmental and genetic tools. In particular, there is an emphasis on investigating the morphology, development, gene expression, plasticity, and function of olfactory rod cells.

As olfactory rod cells are located in a sensory organ and possess a projection that protrudes into the environment, it is hypothesised that they are a sensory cell type that detects external stimuli. The morphology of the actin-rich rod projection is suggestive of a mechanosensory function. Upon superficial observation of the initial phalloidin stain images, it appeared that the projection resembled hair cell stereocilia, thus raising the possibility that the cells could be multimodal, with potential roles in olfaction (chemosensation) and mechanosensation.

Secondly, this project also aims to identify the olfactory cell type that expresses *adgrg6* and explore the role of *adgrg6* within the olfactory system. It is hypothesised that this aGPCR recapitulates its role in mechanosensation, as this may facilitate odour perception and enhance the physiological function of the zebrafish olfactory system.

The significance of this project includes expanding knowledge on both a rare cell type and a human disease-implicated gene. This would provide further understanding of the neurophysiology behind an essential sensory system and may ultimately pave a path for future clinical advancements.

Chapter 2. Materials and methods

2.1. Animal husbandry

The animal study was reviewed and approved by ethics committees in Sheffield and Singapore. All zebrafish work in Sheffield was reviewed by the Project Applications and Amendments Committee of the Animal Welfare and Ethical Review Body (AWERB), and undertaken under licence from the UK Home Office, according to recommended standard husbandry conditions (Aleström et al., 2019). All experiments in Singapore were performed under guidelines approved by the Institutional Animal Care and Use Committee (IACUC) of Biopolis (#181408) and Lee Kong Chian School of Medicine (#A18103).

Adult zebrafish were housed in a Tecniplast system, kept in a 10 hours dark/14 hours light cycle at 28.5°C, fed twice daily, and spawned by pair-mating or marbling (Aleström et al., 2019). Embryos were collected, bleached, and staged according to standard protocols (Kimmel et al., 1995; Nüsslein-Volhard and Dahm, 2002), and raised in E3 medium (5 mM NaCl, 0.17 mM KCl, 0.33 mM $CaCl_2$, 0.33 mM $MgSO_4$, with 0.0001% methylene blue) at 28.5°C at a density of around 50 embryos per 90 mm x 15 mm Petri dish (Biomedia). For controlling the developmental rate to obtain embryos at stages 34–46 hours post-fertilisation (hpf), embryos were incubated at 25°C or 34°C and staged in accordance with Kimmel's formula, $H_T = h \div (0.055T - 0.57)$ (Kimmel et al., 1995). For live imaging, zebrafish larvae were anaesthetised with 0.5 mM tricaine mesylate (MS222) in E3 or immobilised in 1.25 mg/ml mivacurium chloride in E3.

2.1.1. List of zebrafish strains

Various wild-type, transgenic, and mutant zebrafish strains were used in this project (Table 2.1).

Table 2.1. A list of zebrafish strains used in this project.

Zebrafish strain	Reference
AB wild type	ZFIN
nacre (*mitfa*$^{-/-}$; used as wild type)	(Lister et al., 1999)
Tg(actb2:Lifeact-RFP)^{e115e}	(Behrndt et al., 2012)
Tg(sox10:Lifeact-mRFPruby)^{sh630}	(Cheung et al., 2021)
Tg(-4.9sox10:GFP)^{ba2}	(Carney et al., 2006)
Tg(elavl3:GCaMP6f)^{jf1}	(Dunn et al., 2016)
Tg(elavl3:H2B-GCaMP6s)^{jf5}	(Dunn et al., 2016)
Tg(Xla.Tubb:jGCaMP7f)^{sq214}	(Chia et al., 2019)
Tg(foxj1a:GFP)^{nw1Tg}	(Reiten et al., 2017)
Tg(foxj1b:GFP) (*T2BGSZ10*)	(Tian et al., 2009)
Tg(OMP:Gal4;UAS:ChR-YFP)^{rw034a}	(Sato et al., 2005)
Tg(19B:Gal4;UAS:GFP) (*Et(hspGGFF19B:Gal4)Tg(UAS:gfp)*)	(Reiten et al., 2017)
Tg(TRPC2:ntr-mCherry)^{rw037a}	(Sato et al., 2005)
Tg(27A:ntr-mCherry) (*SAGFF(LF)27A*)	(Kawakami et al., 2010)
Tg(pou4f3:GAP-GFP)^{s356t}	(Xiao et al., 2005)
Tg(cldnh:eGFP) (*hkz021Tg*)	(Lin et al., 2019)
Tg(cldnb:lyn-GFP)^{zf106}	(Haas and Gilmour, 2006)
sox10^{m618}	(Dutton et al., 2001)
flna^{sh531}	(Unpublished; Dr. Aylin Metzner, Albert Ong and Fredericus van Eeden labs)
adgrg6^{fr24} (strong protein-truncating allele)	(Geng et al., 2013)
adgrg6^{tk256a} (hypomorphic missense allele)	(Whitfield et al., 1996; Geng et al., 2013)

Homozygous *sox10*^{m618} mutant larvae were identified from their wild-type siblings by their lack of body pigmentation at 5 dpf. Homozygous *adgrg6*^{fr24} mutant larvae were identified by their swollen ear phenotype at 4 dpf. Homozygous *adgrg6*^{tk256a} mutant larvae were spawned

from homozygous in-crosses, thus all progenies were homozygous. Heterozygous and homozygous *flna*^{sh531} mutants were genotyped by extraction of DNA, amplification of DNA in a polymerase chain reaction (PCR), and then separation of the PCR products on an agarose gel. Forward primer: ATGCACTTCTGGTTGGCTTG. Reverse primer: AGGCAAGACAGACCTTACGT. Annealing temperature: 58°C (unpublished; protocol and primers provided by Dr. Philippa Carr, Emily Noël lab). Mutations caused a fusion of 3' end of exon 4 with 5' end of exon 5, introducing a deletion of intron 4 (approximately 400 bp) in *flna*. Homozygous *flna* mutants yielded ~300 bp amplicons, wild-type siblings yielded ~700 bp amplicons, while heterozygous *flna* larvae yielded both ~300 and ~700 bp amplicons (see Figure 3.9B). The genotyping results showed that 45% of larvae from the in-cross were heterozygous (*N* of larvae = 9), 45% were homozygous (*N* = 9), and 10% were wild-type siblings (*N* = 2), deviating from the expected Mendelian ratio.

2.2. Dissection of adult olfactory organs

For staining, adult zebrafish of either AB wild type or *Tg(actb2:Lifeact-RFP)* strains were culled on ice and fixed in 4% paraformaldehyde (PFA) in 1× phosphate-buffered saline (PBS) overnight at 4°C. Adult zebrafish were transferred to a SYLGARD 184-coated (Dow Corning) Petri dish containing PBS, and olfactory organs were dissected out using Dumont #5SF forceps (Fine Science Tools). Olfactory organs were washed in PBS before proceeding with staining protocols.

2.3. Staining and immunohistochemistry

Zebrafish larvae were fixed in 4% PFA in PBS for either two hours at room temperature or overnight at 4°C. Larvae or olfactory organs were washed three or more times with PBS, and permeabilised by incubation in PBS-Triton X-100 (0.2% Triton for 36–48 hpf embryos, 1% Triton for later stages unless stated otherwise) for several hours at 4°C until staining.

2.3.1. Phalloidin stain protocol

To visualise F-actin, samples were stained with either Alexa Fluor 488 phalloidin (Cell Signaling Technology; 1:150), Alexa Fluor 568 phalloidin (Invitrogen, Thermo Fisher Scientific; 1:50), or Alexa Fluor 647 phalloidin (Invitrogen, Thermo Fisher Scientific; 1:50) in PBS overnight at 4°C. After staining, samples were washed four times in PBS over two or more hours and stored at 4°C before imaging.

2.3.2. Antibody stain protocol

For antibody staining, after fixation and washing, larvae were permeabilised in PBS-0.2% Triton and incubated in blocking solution (10% sheep serum [Sigma-Aldrich] in PBS-0.2% Triton) for 60 minutes at room temperature. The primary antibodies used were mouse IgG1 anti-acetylated α-tubulin monoclonal antibody (Sigma-Aldrich, T5168; 1:100), rabbit IgG anti-zebrafish GPR126 polyclonal antibody (Invitrogen, Thermo Fisher Scientific, PA5-72210; 1:300), and mouse IgG1 anti-chicken Na^+,-K^+-ATPase monoclonal antibody (clone α5, Developmental Studies Hybridoma Bank; 1:200). Staining was carried out in blocking solution containing 1% dimethyl sulfoxide (DMSO; Sigma-Aldrich) overnight at 4°C. Larvae were washed three times in PBS-0.2% Triton, and then a further four times over two or more hours. The secondary antibodies used were Alexa Fluor 647-conjugated goat anti-mouse IgG1 (Invitrogen, Thermo Fisher Scientific; 1:200), Alexa Fluor 488-conjugated goat anti-rabbit IgG (Invitrogen, Thermo Fisher Scientific; 1:1000), and Alexa 568-conjugated goat anti-mouse IgG (Invitrogen, Thermo Fisher Scientific; 1:200). For double stains with phalloidin, Alexa Fluor 488 phalloidin (1:150) or Alexa Fluor 568 phalloidin (1:50) were added together with the secondary antibody and 1% DMSO in blocking solution overnight at 4°C. Larvae were then washed four times in PBS-0.2% Triton and stored at 4°C until imaging. Controls with no primary antibody against acetylated α-tubulin or Na^+,-K^+-ATPase yielded no staining (not shown).

2.3.3. GFP-boost protocol

A GFP-boost was used for screening of expression in transgenic lines such as *Tg(foxj1a:GFP)*. After fixation and washing in PBS-0.2% Triton, larvae were incubated in blocking serum (10% sheep serum in PBS-0.2% Triton) at room temperature for two hours to allow recovery of GFP fluorescence signal. A staining solution containing Alexa Fluor 488 GFP-Booster (ChromoTek; 1:400) and Alexa Fluor 647 phalloidin (1:50) in blocking solution was added to the larvae and incubated at 4°C overnight. Larvae were washed four times in PBS-0.2% Triton over two or more hours and stored in PBS at 4°C before imaging.

2.4. Whole-mount *in situ* hybridisation (ISH)

2.4.1. Synthesis of digoxigenin-labelled anti-sense RNA probe

Digoxigenin (DIG)-labelled anti-sense RNA probe was synthesised using standard restriction digest and transcription reaction protocols (Thisse and Thisse, 2008). The probe used in this project was *adgrg6*/*gpr126* (ZFIN gene ID: ZDB-GENE-041014-357), first cloned and synthesised by Geng et al. (2013).

2.4.2. ISH protocol

Whole-mount ISH was performed using standard protocol on AB wild type larvae (Thisse and Thisse, 2008). Larvae were bleached post-ISH with 10% H_2O_2, 5% formamide, and 0.5× SSC in PBS-0.1% Tween 20 for 30 minutes to remove pigmentation. Larvae were transferred to 25%, 50%, and then 75% glycerol in MilliQ water for long-term storage at 4°C.

2.4.3. Imaging of ISH samples

Anterior sections of larval heads were dissected and mounted flat in 100% glycerol on glass microscope slides for imaging. Samples were imaged on an Olympus BX51 compound

microscope equipped with differential interference contrast (DIC) optics and a C3030ZOOM camera and CELL B software, or a Micropublisher 6 camera and Ocular software.

2.5. *In situ* hybridisation chain reaction (HCR RNA-FISH)

2.5.1. HCR RNA-FISH protocol for zebrafish larvae

HCR RNA-FISH was performed on *Tg(actb2:Lifeact-RFP)* transgenic larvae following the "HCR RNA-FISH protocol for whole-mount zebrafish embryos and larvae (*Danio rerio*)" provided by Molecular Instruments (Choi et al., 2018). The probe sets used in this project were *adgrg6*-B4 (accession #: NM_001163291.1), *cldn3c*-B5 (accession #: NM_131767.1), and *cfos*-B5 (accession #: NM-205569.1). The amplifiers used were B4-488 and B5-647 (Molecular Instruments). For the *cfos*-B5 probe, 4 µl of 1 µM probe stock was used instead of 2 µl in a 500 µl hybridisation reaction, as done by Shainer et al. (2023). All samples were stored in PBS at 4°C before imaging.

2.5.2. HCR RNA-FISH protocol for dissected adult olfactory organs

The above standard HCR RNA-FISH protocol for larvae was modified for staining on olfactory organs of adult *Tg(actb2:Lifeact-RFP)* transgenic fish. After dissection, the protocol was followed for stopping the fixation reaction, dehydration, and rehydration of the samples. The proteinase K treatment step was adjusted, where the samples were treated in proteinase K (30 µg/ml) for 90 seconds instead of 45 minutes. The remainder of the protocol remained the same.

2.6. Retrograde neuronal tracing

Neurons in the OE were retrogradely labelled by injection of DiD ($DiIC_{18}(5)$; 1,1'-dioctadecyl-3,3,3',3'- tetramethylindodicarbocyanine, 4-chlorobenzenesulfonate salt; Invitrogen, Thermo Fisher Scientific) into the OB. DiD crystal was dissolved in 50 µl ethanol to make a saturated solution. Live and fixed wild-type larvae were mounted dorsally in 2% low melting point (LMP)

agarose in E3 or PBS respectively in a glass-bottomed dish (50 mm dish, no. 1.5 coverslip, 14 mm glass diameter, Poly-D-Lysine coated; MatTek). The dish was filled with the corresponding medium. Samples were viewed under Plan N 4×/0.10 and LUMPlanFL N 40×/0.80 W objectives on a fixed stage Olympus microscope, part of the Scientifica SliceScope Pro 6000 system, connected to a Hamamatsu C13440 ORCA-Flash 4.0 camera. Microinjection pipettes were pulled from 10 cm-length thin-wall borosilicate glass capillaries (outer diameter: 1.00 mm; inner diameter: 0.78 mm; Sutter Instrument) using the DMZ Zeitz-Puller with the parameters in Table 2.2. Microinjection pipettes were filled with 2 µl of DiD solution and secured to a motorised Scientifica manipulator connected to a Narishige IM-30 microinjector. DiD was injected into several areas of the OB until it had been visibly filled with blue dye. The gas pressure and balance were optimised for each experiment. Live larvae were then fixed immediately and washed following standard fixation protocols. Fixed larvae were stained with Alexa Fluor 488 as described above.

Table 2.2. Parameters to pull DiD microinjection pipettes using the P00 programme in the DMZ Zeitz-Puller.

P(A)00	**H**	300	**t(F1)**	320
	F(TH)	020	**F1**	300
	s(TH)	025	**s(F2)**	100
	t(H)	040	**F2**	200
	s(H)	000	**AD**	000

2.7. Chemical and small compound treatments

2.7.1. Neomycin treatment

A concentration of 500 µM neomycin was chosen as it was an effective concentration used by Harris et al. (2003) for minimum lateral line hair cell survival, as measured by DASPEI staining. A 5 mM solution was made by adding neomycin trisulfate salt hydrate (Sigma-Aldrich) to MilliQ water and used at a 1:10 dilution in E3 fish medium. 3 dpf *Tg(pou4f3:GFP)* transgenic larvae were treated for 60 minutes at 28.5°C. An equivalent volume of MilliQ water in E3 was

used for the control group. Larvae were washed three times in fresh E3 and left at 28.5°C for two hours. GFP signal was screened using widefield fluorescence microscopy to analyse hair cell damage. Larvae were fixed and stained with Alexa Fluor 647 phalloidin as described above.

2.7.2. Collagen type IV treatment

A concentration of 3 µg/ml collagen type IV was chosen as it was the concentration used by Paavola et al. (2014) for experiments in rat Schwann cells. Another concentration of 0.6 µg/ml was tested as this was the concentration shown to produce near-maximal fold increase in cAMP activation in Adgrg6-expressing cells (Paavola et al., 2014). A stock of 0.3 mg/ml collagen type IV from human cell culture (Sigma-Aldrich) was diluted 1:100 and 1:500 in 1.5 ml E3 to make the above working concentrations respectively. 6 dpf *Tg(actb2:Lifeact-RFP)* larvae were treated for 45 minutes in the solutions in a 4-well plate (Thermo Scientific, Thermo Fisher Scientific) at room temperature before fixation and performing HCR RNA-FISH as described above. A group of untreated larvae was used for the control group.

2.7.3. Treatment with candidate compounds for modulation of Adgrg6 receptor signalling

Adgrg6 receptor pathway candidate agonist compounds were identified by Diamantopoulou et al. (2019) (carapin-8(9)-ene, deoxygedunin, ivermectin, colforsin) or Bradley et al. (2019) (apomorphine hydrochloride) based on their ability to rescue otic and myelination defects (Diamantopoulou et al., 2019) or myelination defects alone (Bradley et al., 2019) in hypomorphic *adgrg6* zebrafish mutants. Compounds (Table 2.3; MicroSource Discovery Systems) were dissolved in DMSO to make 10 mM stock solutions. The stock solutions were diluted 1:400 in 1.5 ml E3 to make a working concentration of 25 µM. 6 dpf *Tg(actb2:Lifeact-RFP)* larvae were treated for 45 minutes in the solutions in a 4-well plate at room temperature before fixation and performing HCR RNA-FISH as described above. A group of untreated larvae was used for the control group.

Table 2.3. A list of compounds used in this project that can rescue otic and/or myelination defects in hypomorphic *adgrg6* zebrafish mutants (adapted from Bradley et al., 2019; Diamantopoulou et al., 2019).

Compound	Known for
Carapin-8(9)-ene	Undetermined
Deoxygedunin	Neuroprotective, neurotrophic
Ivermectin	Antiparasitic
Apomorphine hydrochloride	Morphine derivative, emetic, Parkinson's disease treatment
Colforsin	Adenylate cyclase activator, antiglaucoma, hypotensive, vasodilator

2.8. Delivery of mechanical stimulation

Tg(actb2:Lifeact-RFP) larvae were immobilised with 1.25 mg/ml mivacurium and mounted dorsally in 1.5% LMP agarose in E3 in a glass-bottomed dish. Once the agarose was set, the dish was filled with E3 and a portion of agarose was cut out from in front of the head, exposing the olfactory epithelia. Samples were viewed under Plan N 4×/0.10 and LUMPlanFL N 40×/0.80 W objectives on a fixed stage Olympus microscope, part of the Scientifica SliceScope Pro 6000 system, connected to a Hamamatsu C13440 ORCA-Flash 4.0 camera. Brightfield images and videos were captured with MetaMorph software version 7.8.13.0. Pipettes were pulled from 10 cm-length thin-wall borosilicate glass capillaries using the DMZ Zeitz-Puller with the parameters in Table 2.4. Microinjection pipettes were filled with E3 and secured to a motorised Scientifica manipulator connected to a Narishige IM-30 microinjector. The pipette tip was positioned anterior to the left OE, and puffs of E3 were delivered for 60 seconds, leaving the right OE as a contralateral control (see Figure 5.9A, B, Movie 5.2). The gas pressure and balance were optimised for each experiment. Larvae were left for 45 minutes before fixation and performing HCR RNA-FISH as described above.

Table 2.4. Parameters to pull mechanostimulation delivery pipettes using the P13 programme in the DMZ Zeitz-Puller.

P(A)13	**H**	350	**t(F1)**	-
	F(TH)	016	**F1**	-
	s(TH)	022	**s(F2)**	-
	t(H)	012	**F2**	-
	s(H)	050	**AD**	121
P(B)13	**H**	200	**t(F1)**	050
	F(TH)	020	**F1**	020
	s(TH)	045	**s(F2)**	055
	t(H)	006	**F2**	030
	s(H)	000	**AD**	499

2.9. Cilia beat frequency assay in normal and high viscosities

The CBF assay method was adapted from Ringers et al. (2023). A 30-cP viscous medium was made by dissolving methyl cellulose (Sigma-Aldrich, M7140) at 4% in E3. 4–5 dpf larvae (*adgrg6*$^{fr24-/-}$ homozygous mutants or wild-type siblings; Geng et al., 2013) were mounted in 2% LMP agarose in E3 with 4% tricaine in a Willco glass-bottomed dish, with the OE positioned close to the glass. Once the agarose was set, a portion of agarose was cut out to expose the OE. Imaging was carried out on a Nikon spinning disk system attached to an inverted microscope, with a 100× silicone immersion lens. Images were captured at a rate of 137–150 Hz (see Movies 5.3–5.6; imaging and playback speeds are stated in the figure legends). 60-second recordings were acquired with the larvae first immersed in E3 (1 cP), and then with the medium switched to 4% methyl cellulose (30 cP). Computational analysis of CBF was carried out on the first 10 seconds of each recording.

2.10. Assay for acclimation to different salinity environments

Adapted from the protocol published by Peloggia et al. (2021), *Tg(actb2:Lifeact-RFP)* larvae were raised in standard 1× E3 medium as described above. Larvae were then incubated in either MilliQ water (as a low salinity medium), 5× E3 (25 mM NaCl, 0.85 mM KCl, 1.65 mM $CaCl_2$, 1.65 mM $MgSO_4$; as a high salinity medium), or continued to be incubated in 1× E3 (as a control) from 3 to 5 dpf for 48 hours. There were no differences observed in the survival of larvae between the different conditions. Larvae were then fixed at 5 dpf and imaged as described below.

2.11. Fluorescence microscopy

2.11.1. Confocal imaging

Fixed zebrafish larvae and olfactory organs were mounted in 1.5–2% LMP agarose in PBS, and live larvae were mounted in 1.5–2% LMP agarose in E3 with 4% tricaine in WillCo glass-bottomed dishes (mounted in frontal view for 36–48 hpf stages, dorsal view for later stages). Samples were imaged on a Zeiss LSM880 Airyscan confocal microscope equipped with a Plan-Apochromat 20×/0.8 M27 air objective, LD LCI Plan-Apochromat 40×/1.2 Imm Korr DIC M27 water immersion objective, or Plan-Apochromat 63×/1.4 oil DIC M27 objective (Wolfson Light Microscopy Facility, The University of Sheffield). Images were acquired in Airyscan SR mode, Airyscan Fast scan mode with SR sampling, or Airyscan Fast scan mode with Opt sampling. Samples were also imaged on a Zeiss LSM800 attached to an upright microscope with a W Plan-Apochromat 40×/1.0 DIC M27 or 63×/1.0 M27 water dipping objective (NTU Optical Bio-Imaging Centre, Lee Kong Chian School of Medicine, Nanyang Technological University). The laser lines used were 488, 561, 568, 633, and 647 nm.

2.11.2. Light-sheet imaging

Live zebrafish larvae were mounted in 0.9% LMP agarose in E3 and imaged on a Zeiss Z1 Light-sheet microscope, with 4% tricaine in E3 in the sample chamber. Time series imaging was

performed with a W Plan-Apochromat 20× objective using brightfield illumination and the 561 nm laser line. For timelapse imaging of the development of olfactory rod cells, imaging was set to intervals of 10–15 minutes for the duration of the period of interest (developmental stages of the larvae are stated in the figure legends). For fast capture imaging of olfactory rod projection movement, imaging was set to continuous (imaging and playback speeds are stated in the figure legends).

2.11.3. Stereoscope widefield imaging

Widefield imaging was performed on a Zeiss Axio Zoom.V16 fluorescence stereo zoom microscope equipped with a Zeiss 60N-C 1" 1.0× C-mount and AxioCam MRm camera.

2.12. Image processing, data visualisation, quantifications, and statistical analyses

2.12.1. Processing of raw image files

Zeiss LSM880 Airyscan confocal images were first subjected to Airyscan processing on Zen Black 2.3 software (Zeiss) using "Auto" Airyscan processing parameters. Zeiss LSM800 confocal images were first subjected to Gaussian Blur 3D processing (X:0, Y:0, Z:2) in Fiji. Further processing (for example, gamma correction and maximum intensity projections) was performed in Fiji (Schindelin et al., 2012).

3D rendering was performed using the 3D Viewer plugin (Schmid et al., 2010) in Fiji.

Figures were prepared using Adobe Photoshop version 24.6.0.

2.12.2. Mapping the spatial distributions of olfactory rod cells

2D maximum intensity projection images were imported into the Desmos Graphing Calculator (desmos.com). The positions and sizes of the images were adjusted to align the rims of olfactory pits with an ellipse defined by $\frac{(x-35)^2}{5}+\frac{(y-33)^2}{10}=7.6^2$. The positions of the base of

each olfactory rod projection, relative to the ellipse, were plotted as coordinates onto the graph, where one dot represented one olfactory rod projection and different coloured dots represented different larvae. The resulting graphs were exported as .png image files.

2.12.3. Quantification of olfactory rod cell numbers and projection lengths

The number of olfactory rod cells per olfactory pit was quantified by manual counting. Olfactory rod projection lengths were measured in 3D from confocal images using Fiji, and calculated in Microsoft Excel using the PyT method (based on the Pythagorean theorem) from Dummer et al. (2016). Quantifications were exported into GraphPad Prism 8, 9, and 10 for performing statistical analyses and making graphs.

2.12.4. Quantification of *cfos* RNA expression

Left and right-side olfactory epithelia were separately segmented using the Segmentation Editor plugin in Fiji (Schindelin et al., 2012), and the resulting 3D regions of interest (ROIs) were saved as binary masks. The level of fluorescence within the ROI was quantified using the 3D Objects Counter v2.0 function in Fiji (Bolte and Cordelières, 2006), by selecting the Mean Gray Value parameter and redirecting to the raw *cfos* HCR RNA-FISH confocal stack in 3D OC Options. Quantifications were exported into Estimation Statistics for performing statistical analyses and making graphs.

2.12.5. Quantification of colocalising *adgrg6* and *cfos* RNA expression

Raw confocal images of HCR RNA-FISH were spatially averaged with a radius of 3.0 pixels (Choi et al., 2018). Manders' colocalisation coefficients were calculated using the Just Another Co-localization Plugin (JACoP; Bolte and Cordelières, 2006) on Fiji, by selecting the M1 & M2 coefficients analysis option in the plugin window. Thresholds for both *adgrg6* and *cfos* channels were manually adjusted so that all positive cells were selected. The resulting M1 coefficient showed the proportion of *cfos* signal pixels overlapping with *adgrg6* signal pixels (data not shown), while the resulting M2 coefficient showed the proportion of *adgrg6* signal

pixels overlapping with *cfos* signal pixels. Quantifications were exported into Estimation Statistics for performing statistical analyses and making graphs.

2.12.6. Quantification of cilia beat frequency

Raw .nd2 files were converted to .tif files in NIS-Elements Viewer software version 5.21. Only the first 10 seconds of each 60-second recording were analysed. CBFs were quantified in Fiji using the FreQ analysis v0.3.0 plugin (Jeong et al., 2022). The analysis parameters are as follows; recording frequency was set to 137–150 Hz (dependent on each recording), and sliding window to smooth power spectrum was set to 2 Hz. The minimum and maximum accepted frequencies were set to 10 and 40 Hz respectively. The ROI for analysis was manually drawn around the rim of the olfactory pit for each sample. The bin size for histograms was set to 2 Hz. The resulting frequency 1 of signal pixels in the ROIs were discussed in my results.

2.12.7. Statistical analyses

Statistical analyses were carried out in GraphPad Prism 8, 9, and 10. Datasets were considered normally distributed if they passed at least one of four normality tests (Anderson-Darling, D'Agostino & Pearson, Shapiro-Wilk, and Kolmogorov-Smirnov tests). Subsequent statistical tests used are stated in the figure legends. Bars on graphs indicate mean ± standard error of the mean (S.E.M.), unless stated otherwise. *P* values are indicated as follows: $P > 0.05$ (not significant, ns), $P < 0.05$ (*), $P < 0.01$ (**), $P < 0.001$ (***), $P < 0.0001$ (****).

The effect sizes (Hedges' g) of some datasets were analysed in Estimation Statistics (estimationstats.com) with a confidence interval (CI) of 95% (Ho et al., 2019).

2.13. Single-cell RNA sequencing (scRNA-seq) data analysis

A scRNA-seq dataset generated from dissected adult zebrafish olfactory organs, published by Kraus et al. (2022), was analysed in this project. The dataset was initially processed and normalised by our collaborator J. Peloggia (T. Piotrowski lab). The dataset was subsequently

analysed using Seurat packages (Satija et al., 2015; Butler et al., 2018; Stuart et al., 2019; Hao et al., 2021, 2023) in R version 3.2.4 and RStudio version 2023.0.1.494. See Appendix 3 for the scripts for the analyses.

Chapter 3. Descriptive and morphological characteristics of olfactory rod cells in the developing larval zebrafish olfactory epithelium

3.1. Introduction

Actin-rich rod-shaped projections were initially observed by T. T. Whitfield on the apical surface of the larval zebrafish OE in a series of phalloidin stains and SEM images (see Figure 1.9). It was unclear what these projections were, thus there became a scope for characterising these mystery cells.

Firstly, I aimed to elucidate the descriptive characteristics of olfactory rod cells, such as their size, shape, distribution, development, and cytoskeletal composition of the projection by phalloidin staining, antibody staining, and retrograde labelling. Secondly, I aimed to identify actin-reporter transgenes that are expressed in the olfactory rod projection or in the cell body, as these would become useful markers for the cells in live larvae. Lastly, I aimed to explore the potential involvement of candidate genes in the formation of olfactory rod cells by screening mutant zebrafish lines.

3.2. Results

3.2.1. Actin-rich rod-shaped apical projections, distinct from OSN microvilli and cilia, are present in the olfactory epithelium of larval and juvenile zebrafish

Staining of the wild-type larval and juvenile zebrafish OE with fluorescently-conjugated phalloidin, which binds to F-actin, reveals the presence of several actin-rich rod-like projections (‘olfactory rods’) in each olfactory pit (Figure 3.1A–B’). These projections differ in number, distribution, size and morphology from any of the described apical projections of zebrafish OSNs. The projections extend from below the apical surface of the OE and project about 5–10 µm above it, tapering to a point. This is an order of magnitude longer than OSN microvilli, which are typically 0.5–0.8 µm in length (Hansen and Zeiske, 1998). Olfactory rods

are shorter than the surrounding phalloidin-negative olfactory cilia (Figure 3.1C–D'), and do not label with an anti-acetylated α-tubulin antibody (Figure 3.1C–C'''). Olfactory rods are not evenly distributed across the OE, but are mostly clustered posterolaterally in each olfactory pit near the lateral patch of multi-ciliated cells (MCCs), although there is variation between individuals (Figure 3.1E). At low magnification, the olfactory rods appear similar to the actin-rich stereociliary bundle of mechanosensory hair cells of the inner ear and lateral line. However, higher magnification images reveal that the olfactory rod is not oligovillous, but appears to be a single structure (Figure 3.1B', C''', D'). This contrasts with the stepped array of multiple stereocilia present on the apical surface of mechanosensory hair cells (Figure 3.1F).

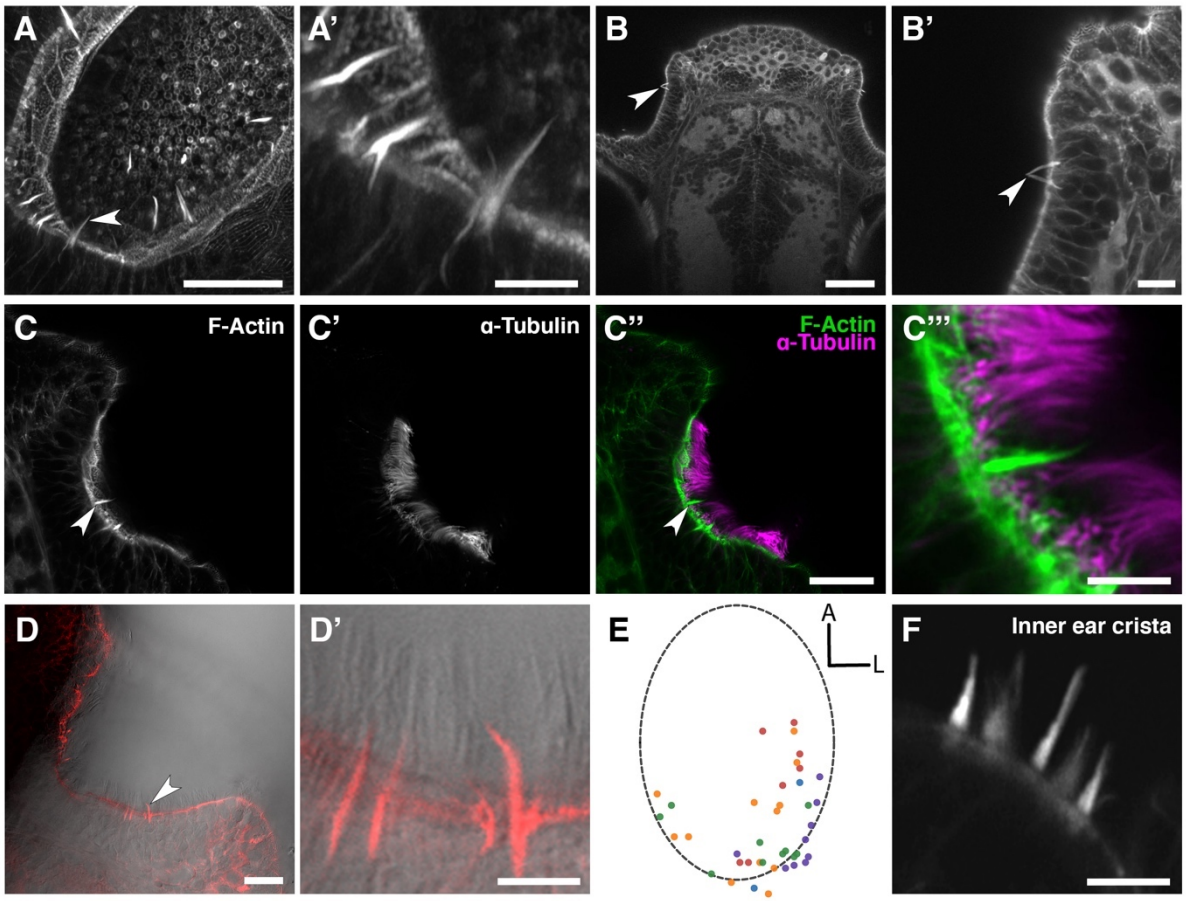

Figure 3.1. Phalloidin and antibody staining reveals the presence of actin-rich rod-shaped projections, distinct from OSN microvilli and cilia, in the zebrafish larval and juvenile olfactory epithelium (images taken by T. T. Whitfield, N. J. van Hateren, S. J. Jesuthasan, and K. Y. Cheung; published in Cheung et al., 2021).

(A) Maximum intensity projection of an Airyscan confocal image of phalloidin stain in an olfactory pit of a 5 dpf wild-type larva; anterior to the top right, lateral to the bottom right. Arrowhead marks one example olfactory rod. Scale bar = 20 µm. **(A')** Enlargement of olfactory rods in **A**. Scale bar = 5 µm. **(B)** Dorsal view low power image

of phalloidin stain in the head of an 18 dpf (5 mm) wild-type juvenile zebrafish; anterior to the top. Arrowhead marks the position of two olfactory rods in an olfactory pit. Scale bar = 50 µm. **(B')** Enlargement of OE in **B**. Arrowhead marks two olfactory rods. Scale bar = 10 µm. **(C–C'')** Airyscan confocal image of Alexa-phalloidin signal **(C)**, acetylated α-tubulin immunohistochemistry signal **(C')**, and merged signals **(C'')** in an olfactory pit of a 4 dpf wild-type larva; anterior to the top, lateral to the right. Arrowhead marks one example olfactory rod. Scale bar = 20 µm. **(C''')** Enlargement of olfactory rod in **C''**. Scale bar = 5 µm. **(D)** DIC image and phalloidin stain (red) in an olfactory pit of a 5 dpf wild-type larva; anterior to the top, lateral to the right. Arrowhead marks one example olfactory rod. Scale bar = 20 µm. **(D')** Enlargement of olfactory rods in **D**. Surrounding olfactory cilia are visible and unlabelled by Alexa-phalloidin. Scale bar = 5 µm. **(E)** A map of the positions of olfactory rod cell projection bases in olfactory pits of 4 dpf wild-type larvae (*N* of olfactory pits = 5), based on 2D maximum intensity projections of confocal images of phalloidin stains; anterior 'A' to the top, lateral 'L' to the right. One dot represents one olfactory rod. Different coloured dots represent olfactory rods from different larvae. **(F)** Airyscan confocal image of phalloidin stain in an inner ear crista of a 5 dpf wild-type larva. Hair cell stereocilia are labelled with Alexa-phalloidin, and are arranged in a stepped array. In the stereociliary bundle on the extreme left, four different stereociliary lengths are visible (compare with **A'**). Scale bar = 5 µm.

3.2.2. Olfactory rods arise early during olfactory pit development

To characterise the timing of appearance and development of the olfactory rods during embryonic and larval stages, I stained fixed wild-type samples from 36 hpf, just after formation of the olfactory pits (Hansen and Zeiske, 1993), to 5 dpf. Occasional olfactory rods were present in olfactory pits at 36 hpf, but were only consistently present beyond 46 hpf (Figure 3.2A, B). Although the number of olfactory rods per pit varied at each stage, the average number increased over time. By 5 dpf, each pit contained 10.7 ± 2.9 (mean ± standard deviation, s.d.) olfactory rods (Figure 3.2B). After measuring the olfactory rods in 3D, I found an increase in projection length (from the base of the phalloidin-positive projection to the tip) from 36 hpf to 5 dpf, with the most significant increase occurring by 48 hpf, despite a relatively large range in length at each stage. At 5 dpf in fixed samples, the mean projection length was 10.4 ± 2.2 (s.d.) µm, with the longest measuring 17.5 µm (Figure 3.2C).

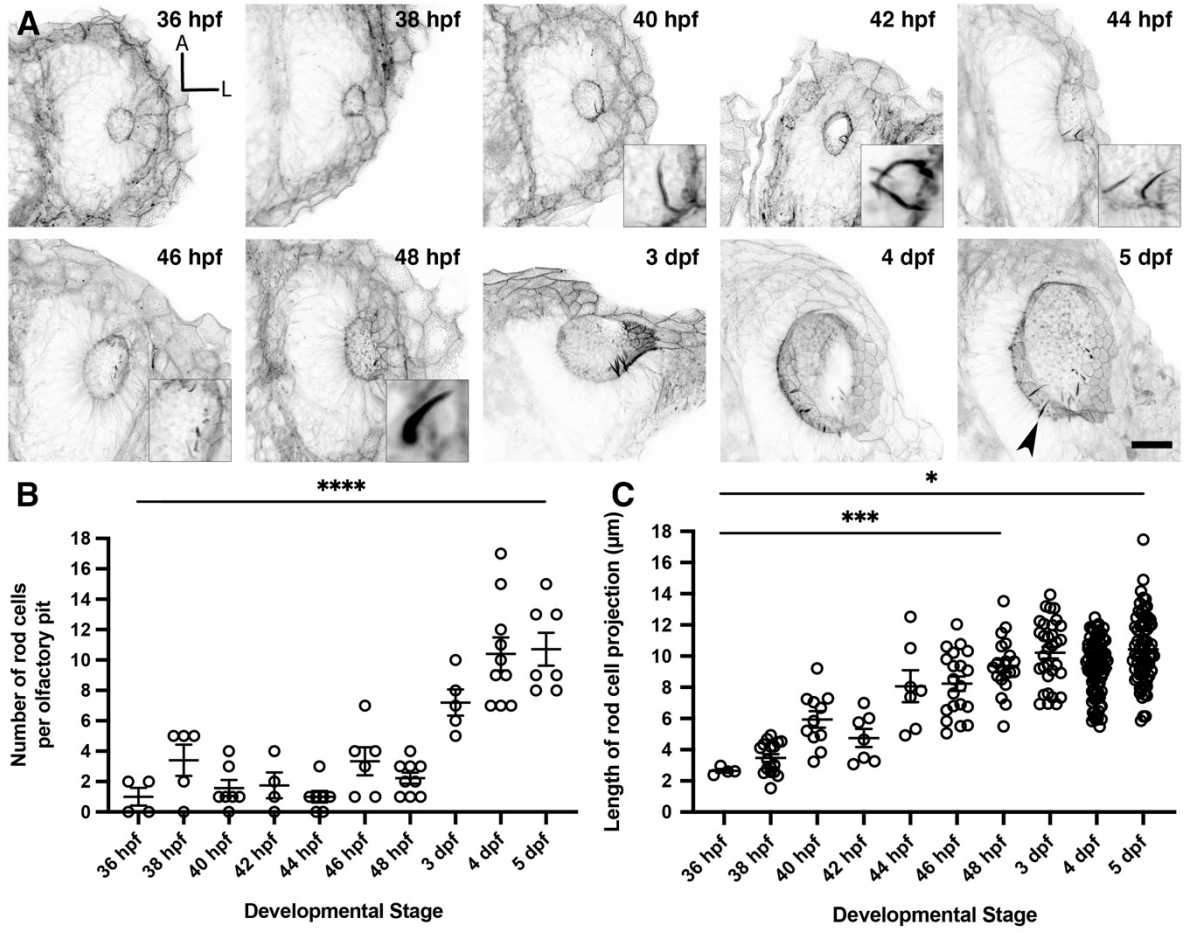

Figure 3.2. Olfactory rods arise early and continue to grow during zebrafish olfactory pit development (published in Cheung et al., 2021).

(A) Maximum intensity projections of Airyscan confocal images showing the wild-type development of olfactory pit and olfactory rod cells at various embryonic and larval stages, using Alexa-phalloidin as a marker; anterior 'A' to the top, lateral 'L' to the right. Greyscale values from the original fluorescence image have been inverted. Arrowhead marks one example olfactory rod. Scale bar = 20 µm. Selected inserts show olfactory rods at higher magnification. **(B)** The change in number of olfactory rod cells per olfactory pit during embryonic development — 36 hpf (*N* of olfactory pits = 4), 38 hpf (*N* = 5), 40 hpf (*N* = 7), 42 hpf (*N* = 4), 44 hpf (*N* = 7), 46 hpf (*N* = 6), 48 hpf (*N* = 9), 3 dpf (*N* = 5), 4 dpf (*N* = 10), and 5 dpf (*N* = 7). Bars indicate mean ± S.E.M. for each stage. Linear regression analysis; **** indicates $P < 0.0001$. **(C)** The change in lengths of olfactory rod cell projections during embryonic development — 36 hpf (*N* of olfactory pits = 2, *n* of olfactory rods = 4), 38 hpf (*N* = 4, *n* = 17), 40 hpf (*N* = 6, *n* = 11), 42 hpf (*N* = 3, *n* = 7), 44 hpf (*N* = 5, *n* = 7), 46 hpf (*N* = 6, *n* = 20), 48 hpf (*N* = 9, *n* = 20), 3 dpf (*N* = 5, *n* = 32), 4 dpf (*N* = 10, *n* = 82), and 5 dpf (*N* = 8, 71). Bars indicate mean ± S.E.M. for each stage. Linear regression analysis; * indicates $P = 0.0251$, *** indicates $P = 0.0009$.

3.2.3. Olfactory rods are labelled in live larvae by a Lifeact transgene

To visualise olfactory rods in live larvae, the *Tg(actb2:Lifeact-RFP)* transgenic line (Behrndt et al., 2012) was imaged at 4 and 6 dpf. Fluorescent apical projections in the olfactory pits of live larvae were present in all cases (*N* of fish = 4; Figure 3.3A–C, Movie 3.1). These matched the size, shape, and posterolateral distribution of olfactory rod cells present in fixed samples (Figure 3.3D, E). Despite potential shrinkage due to fixation, there was no overall difference in the lengths of projections between live and fixed samples (Figure 3.3E). The zig-zag pattern exhibited by RFP-positive olfactory rods in raster-scanned images of live larvae suggested that olfactory rods were moving during image capture (Figure 3.3B). Fast-capture time series imaging of the *Tg(actb2:Lifeact-RFP)* transgenic line showed that the projection oscillates (Movie 3.2), possibly as a result of ciliary beating.

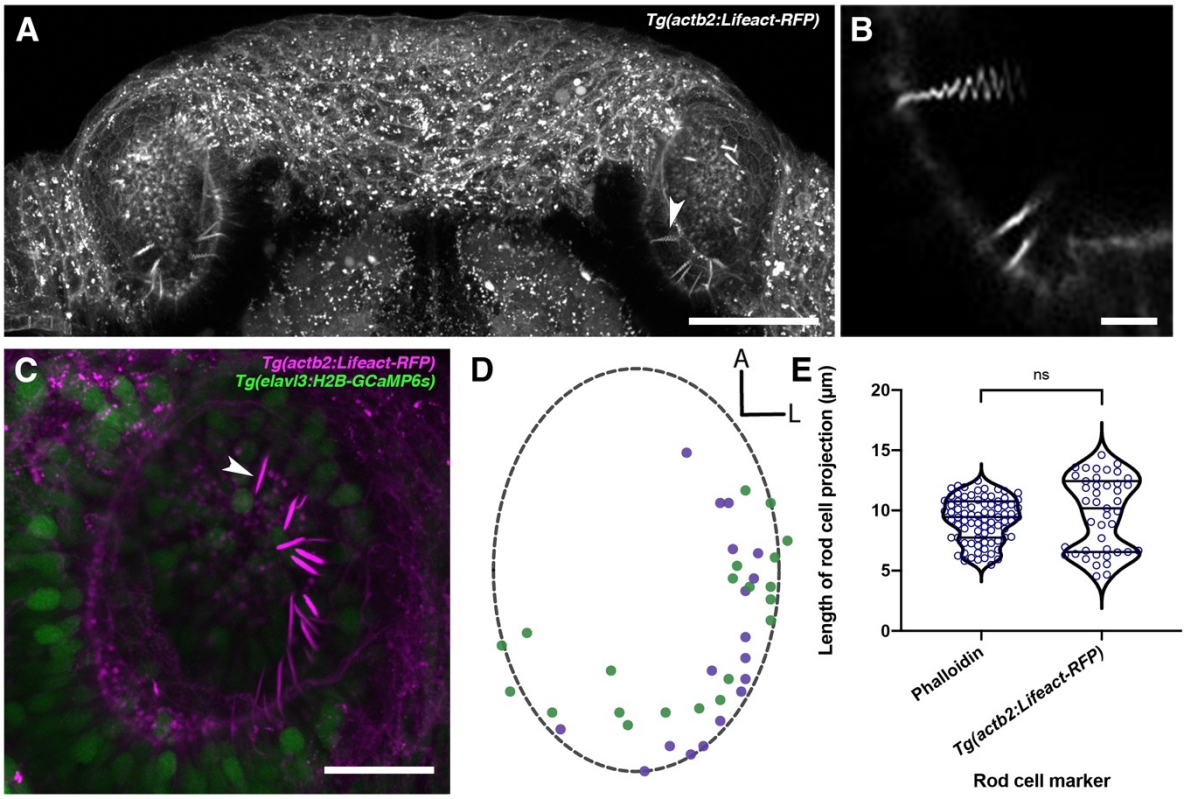

Figure 3.3. Olfactory rods are labelled in the olfactory epithelia of live zebrafish larvae by the *Tg(actb2:Lifeact-RFP)* transgene (images taken by S. J. Jesuthasan, processing and analysis by K. Y. Cheung; published in Cheung et al., 2021).

(A) Maximum intensity projection of dorsal view image of the olfactory pits of a live 6 dpf *Tg(actb2:Lifeact-RFP)* transgenic larva; anterior to the top. Arrowhead marks one example olfactory rod positive for the Lifeact-RFP transgene. Scale bar = 50 µm. **(B)** Enlargement of olfactory rods in **A** (arrowhead in **A**) oscillating during raster-scanned image capture. (Raster scanning was performed from top to bottom in the image, as it has been rotated 90° clockwise.) Scale bar = 5 µm. (See Movie 3.2.) **(C)** Maximum intensity projection image of a live 4 dpf *Tg(actb2:Lifeact-RFP);Tg(elavl3:H2B-GCaMP6s)* double-transgenic larval olfactory pit; anterior to the top, lateral to the right. Arrowhead marks one example olfactory rod positive for the Lifeact-RFP transgene (magenta). Neuronal nuclei are labelled in green. Larvae were fully mounted in agarose, so olfactory rods were not moving. Scale bar = 20 µm. (See Movie 3.1.) **(D)** A map of the positions of olfactory rod cell projection bases in olfactory pits of 4 dpf *Tg(actb2:Lifeact-RFP);Tg(elavl3:H2B-GCaMP6s)* double-transgenic larvae (*N* of olfactory pits = 2), based on 2D maximum intensity projections of confocal images; anterior 'A' to the top, lateral 'L' to the right. One dot represents one olfactory rod. Different coloured dots represent olfactory rods from different larvae, with purple corresponding to panel **C**. (Compare with Figure 3.1E.) **(E)** A quantitative comparison of the lengths of olfactory rod cell projections in fixed larvae, using Alexa-phalloidin as a marker (*N* = 10, *n* of olfactory rods = 82) versus live larvae, using Lifeact-RFP as a marker (*N* = 2, *n* = 43). Violin plot; bars indicate the median and lower and upper quartiles for each group. Mann-Whitney U test; ns, not significant (*P* = 0.232).

3.2.4. A subpopulation of olfactory rod cells express transgenes driven by *sox10* promoters

Sox10 is a known marker of both neural crest and otic epithelium (Dutton et al., 2001), but is not detectable by DIG-ISH in the OE (Whitlock et al., 2005). However, robust transgene expression driven by the *sox10* promoter has been reported in the OE and other tissues in the zebrafish (Mongera et al., 2013; Saxena et al., 2013), likely reflecting leaky expression of the transgene. A *Tg(sox10:Lifeact-mRFPruby)* transgenic line was previously generated by S. Baxendale and M. Marzo in the Whitfield lab to visualise actin localisation and dynamics in the live embryo in *sox10*-expressing tissues (Cheung et al., 2021). At 4 and 5 dpf, I observed OSNs expressing *Tg(sox10:Lifeact-mRFPruby)* in the OE; based on morphology, most of these cells were microvillous OSNs. Staining with Alexa-phalloidin on fixed samples also revealed the expression of Lifeact-mRFPruby in a subpopulation of phalloidin-positive olfactory rod cell projections (Figure 3.4A–B''). Not all olfactory rod cells expressed the transgene; an average of 64.4% of olfactory rod cells marked by phalloidin also expressed Lifeact-mRFPruby (*N* of olfactory pits = 5, *n* of olfactory rods = 59; Figure 3.4C).

The sparse expression of the *Tg(sox10:Lifeact-mRFPruby)* transgene allowed me to visualise the morphology of the cell body of olfactory rod cells and ask whether they have an axon. Lifeact-mRFPruby-expressing cell bodies were positioned apically in the OE and were relatively rounded in shape (Figure 3.4B–B'', E). They were morphologically distinct from the well-described microvillous OSNs (Figure 3.4D, E) as well as ciliated and crypt OSNs. The axons of microvillous OSNs were visible in those cells labelled by the transgene (Figure 3.4D). However, with this transgenic marker, I was unable to observe an axon extending from the cell body of olfactory rod cells (*N* of olfactory pits = 5, *n* of cells = 9; Figure 3.4E).

As for the olfactory rods labelled with Lifeact-RFP, rods labelled with Lifeact-mRFPruby oscillated in live larva (Movie 3.3). Furthermore, time-lapse imaging over a 42-hour period, from 78 hpf to 120 hpf, revealed that Lifeact-mRFPruby-expressing olfactory rods increased in numbers as expected. Once olfactory rods appeared, they remained present until the end of the time-lapse, thus indicating they are stable during larval development and are unlikely to be transient alterations of other existing cell types (Figure 3.5; Movie 3.4).

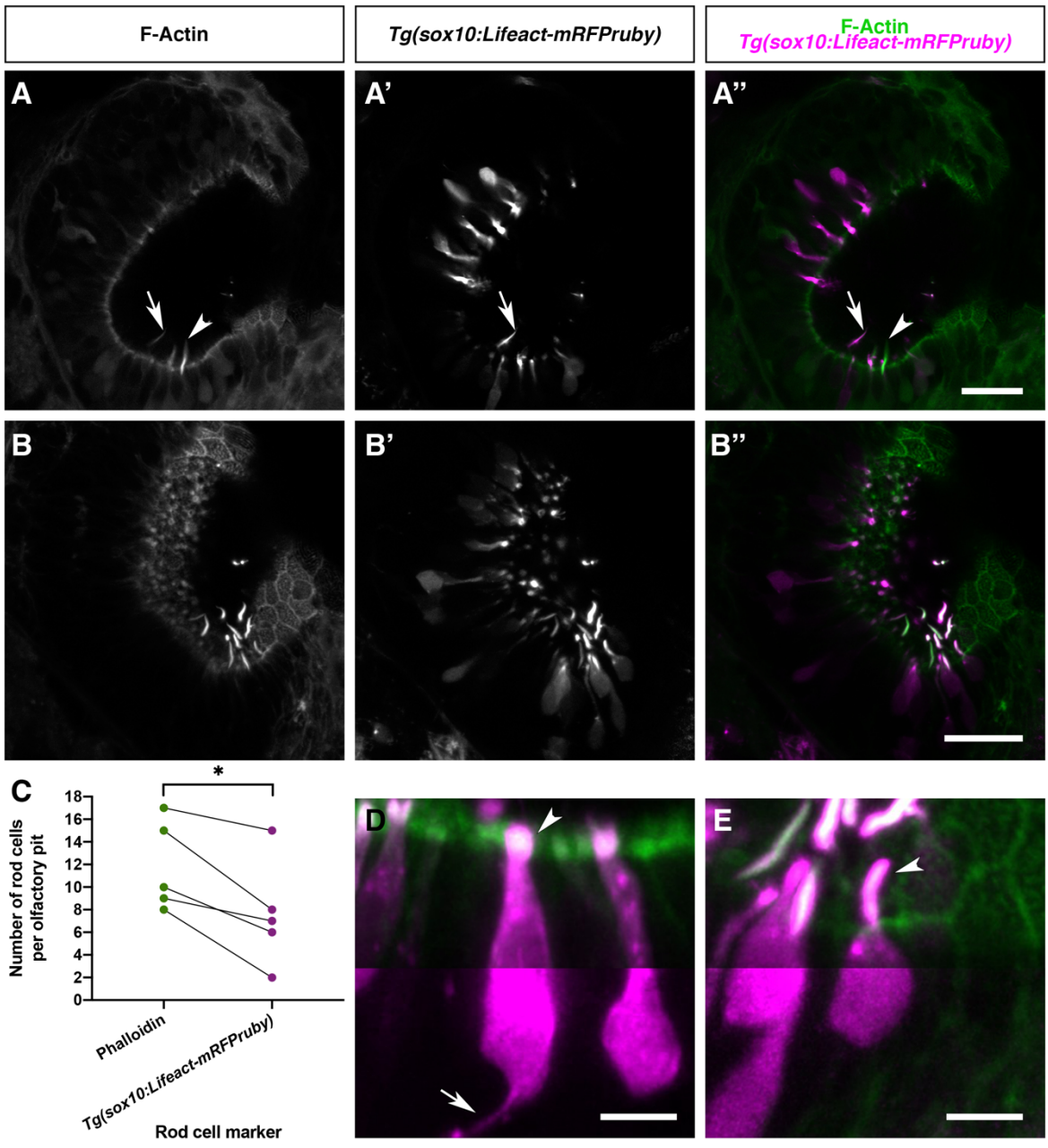

Figure 3.4. Olfactory rod cells are apically located in the zebrafish olfactory epithelium, with a rounded cell body and no detectable axon labelled by the *Tg(sox10:Lifeact-mRFPruby)* transgene (published in Cheung et al., 2021).

(A–B'') Airyscan confocal image of Alexa-phalloidin signal **(A, B)**, *Tg(sox10:Lifeact-mRFPruby)* signal **(A', B')**, and merged signals **(A'', B'')** in olfactory pits of 4–5 dpf larvae; anterior to the top, lateral to the right. Arrowhead marks one olfactory rod negative for Lifeact-mRFPruby. Arrow marks one olfactory rod positive for Lifeact-mRFPruby. Scale bars = 20 µm. **(C)** Number of olfactory rod cells positively marked by Alexa-phalloidin (*n* of olfactory rods = 59), compared with the number of those also marked by *Tg(sox10:Lifeact-mRFPruby)* (*n* = 38), in olfactory pits of 4–5 dpf larvae (*N* of olfactory pits = 5). Connecting lines indicate olfactory rods from the same

olfactory pit. Paired two-tailed *t*-test; * indicates *P* = 0.0146. **(D)** Enlargement of two microvillous OSNs, expressing Lifeact-mRFPruby, in the OE of a 4 dpf larva; Alexa-phalloidin signal (green), *Tg(sox10:Lifeact-mRFPruby)* signal (magenta). Arrowhead marks the microvillous apical projections. The gamma value for the magenta channel in the bottom half of the panel has been set to 0.5 to show the axon from one of the cells (arrow). Scale bar = 5 µm. **(E)** Enlargement of olfactory rod cells (of which both the apical actin projections and cell bodies are labelled by the *Tg(sox10:Lifeact-mRFPruby)* transgene) in the OE of a 4 dpf larva; Alexa-phalloidin signal (green), *Tg(sox10:Lifeact-mRFPruby)* signal (magenta). Arrowhead marks an olfactory rod cell apical projection, positive for both markers. The gamma value for the bottom half of the panel has been set to 0.5 as in **D**; no axon is visible. Scale bar = 5 µm. (See also Movie 3.3.)

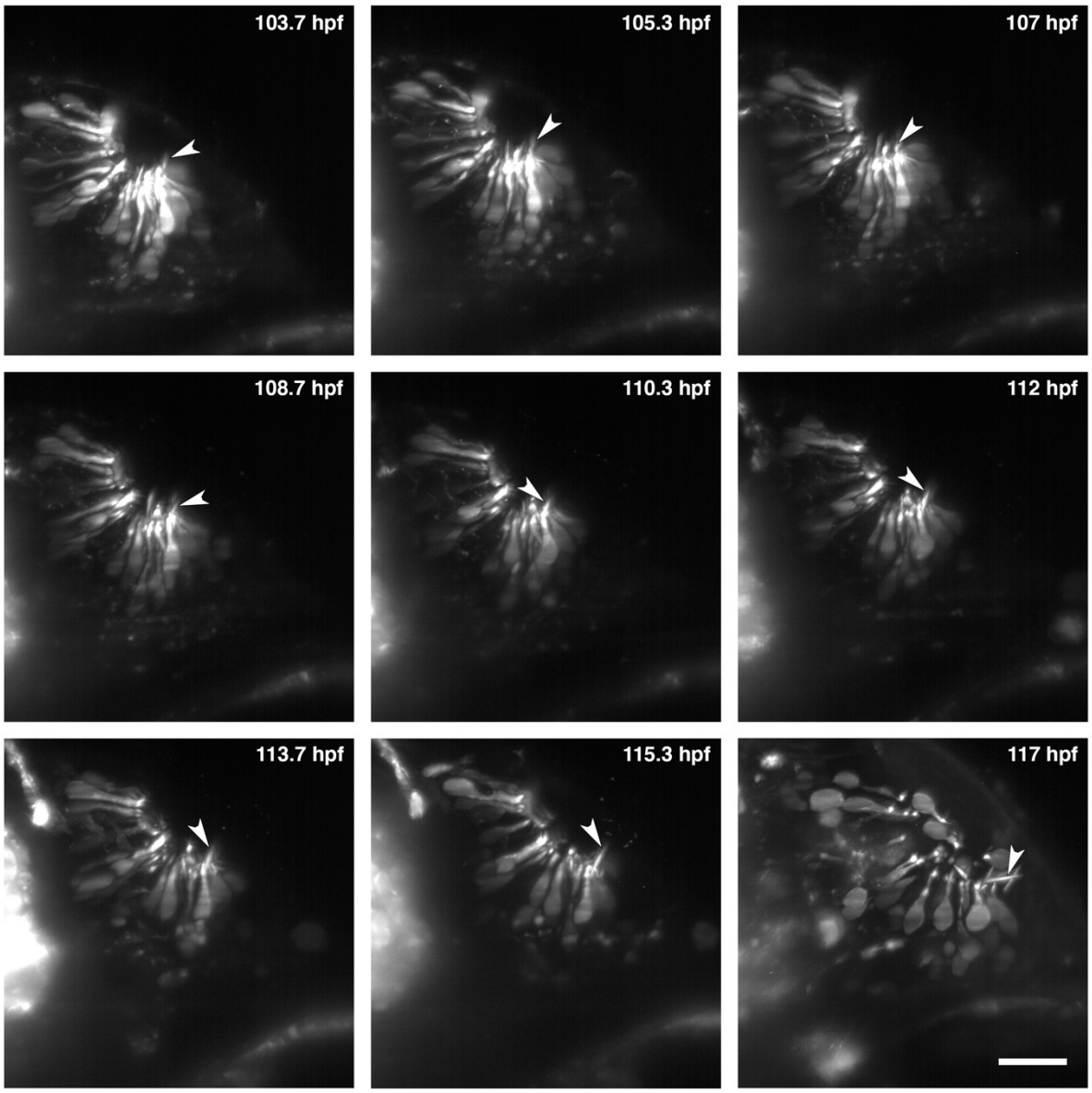

Figure 3.5. Olfactory rods are stable structures in the larval zebrafish olfactory epithelium from 78 hpf to 120 hpf.

Still images from a light-sheet time-lapse video of the developing olfactory pit of a *Tg(sox10:Lifeact-mRFPruby)* larva from 78 hpf to 120 hpf (103.7 hpf to 117 hpf shown here); anterior to the top, lateral to the right. Arrowhead marks the same olfactory rod at different timepoints. Scale bar = 20 µm. (See Movie 3.4.)

Similar to observations in the *Tg(sox10:Lifeact-mRFPruby)* transgenic line, Alexa-phalloidin staining in *Tg(sox10:GFP)* larvae (Carney et al., 2006) showed that GFP was co-expressed in the apical olfactory rod projection as well as in the olfactory rod cell body (Figure 3.6). Again, the cell body appeared to be apical in the epithelium, oval in shape with no detectable axon, and the apical projection often emerged from it at an angle. The morphology of the other cells labelled by *Tg(sox10:GFP)* matched either microvillous or ciliated OSNs, which had clearly labelled axons extending from the basal side of the cell bodies.

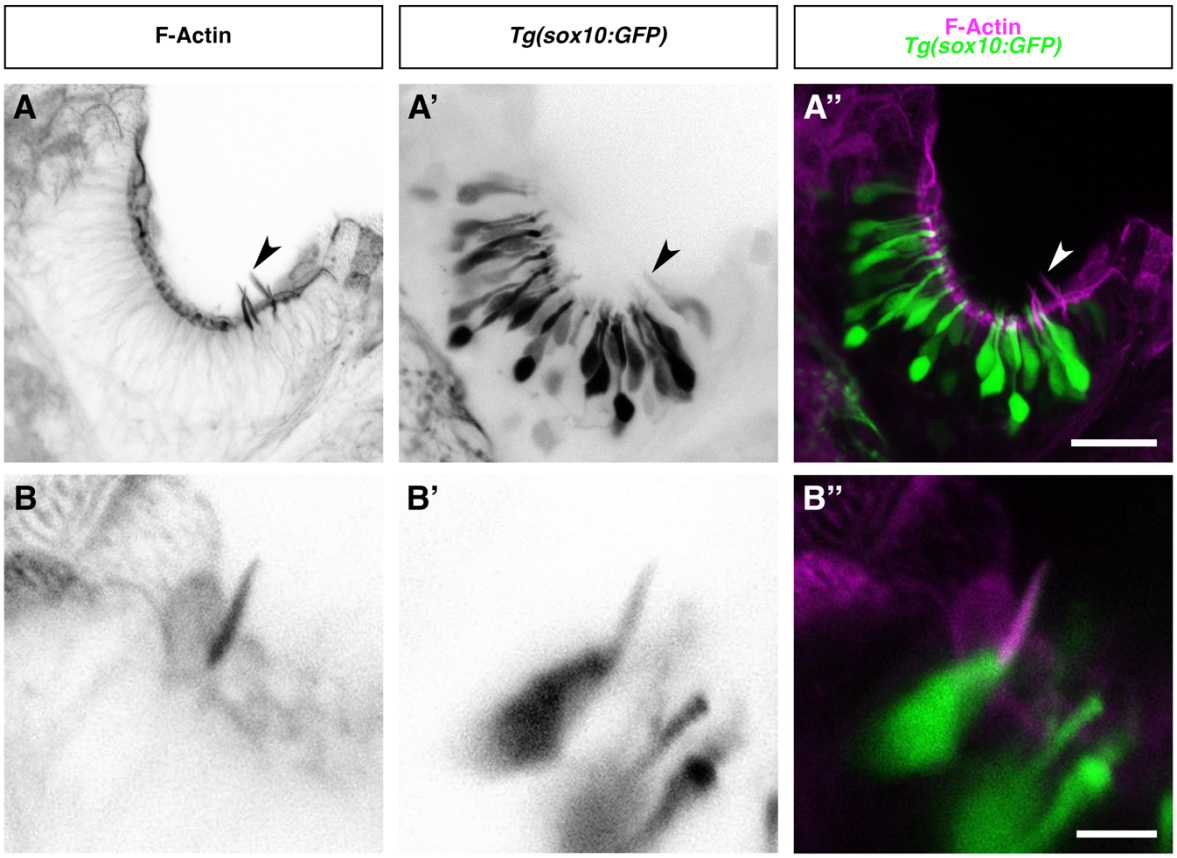

Figure 3.6. Olfactory rod cells are apically located in the zebrafish olfactory epithelium, with a rounded cell body and no detectable axon labelled by the *Tg(sox10:GFP)* transgene.

Confocal images of Alexa-phalloidin signal with greyscale values inverted **(A, B)**, *Tg(sox10:GFP)* signal with greyscale values inverted **(A', B')**, and merged signals **(A'', B'')** in olfactory pits of 5 dpf *Tg(sox10:GFP)* transgenic larvae; anterior to the top, lateral to the right. Arrowhead marks an example olfactory rod in row **A**. An olfactory

rod projection and cell body is clearly labelled by GFP in row **B**. Scale bar in row **A** = 20 µm, scale bar in row **B** = 5 µm.

3.2.5. Retrograde neuronal tracing labels a subpopulation of olfactory rod cells

Both *Tg(sox10:Lifeact-mRFPruby)* and *Tg(sox10:GFP)* transgenes mosaically labelled the rounded cell body of olfactory rod cells, but did not clearly label any axon. As an independent test of whether olfactory rod cells extend an axon into the brain, I performed retrograde tracing by injecting DiD, a lipophilic fluorescent dye, into the OB of live (*N* of larvae = 13) and fixed (*N* = 30) zebrafish at several larval and juvenile stages. Injected DiD travels down the olfactory nerve and retrogradely labels any cell in the OE that contains an axon terminating in the OB. The resulting confocal images showed that many cells, such as ciliated OSNs, were retrogradely labelled by DiD. Also labelled by DiD was a proportion of olfactory rods (Figure 3.7A–B''). The number of olfactory rods that were retrogradely labelled increased in number during development, from 5, to 7, to 20 dpf (Figure 3.7C–E). This suggests that olfactory rod cells may develop an axon as they mature. In summary, a subpopulation of larval olfactory rod cells may contain an axon on their basal side that likely terminates in the OB (Figure 3.7B'), via which signals may be sent directly to the brain.

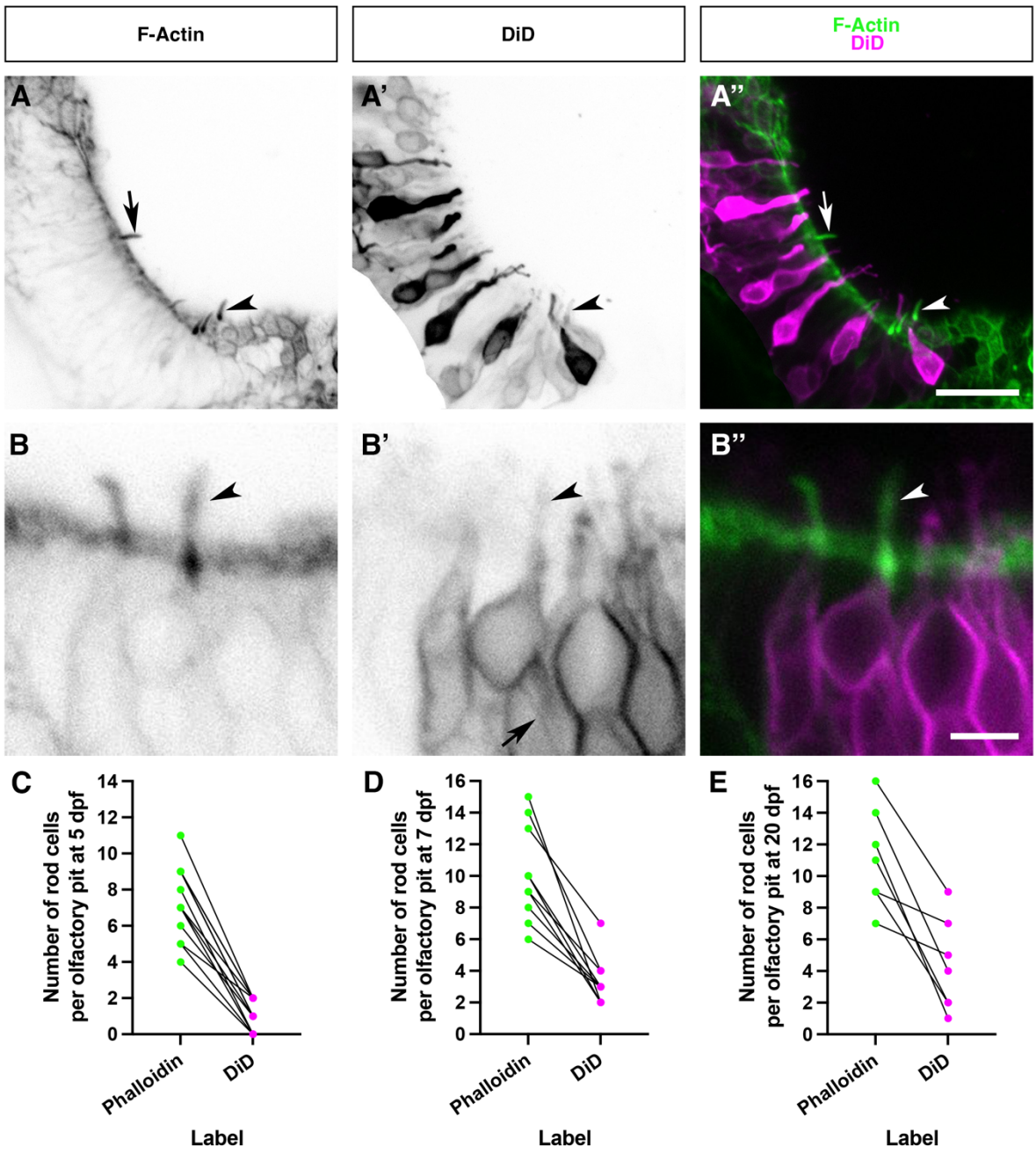

Figure 3.7. A subpopulation of olfactory rod cells is retrogradely labelled by tracer injection into the olfactory bulb.

(A–A'') Maximum intensity projection of a confocal image of Alexa-phalloidin signal with greyscale values inverted **(A)**, DiD signal with greyscale values inverted **(A')**, and merged signals **(A'')** in an olfactory pit of a 20 dpf juvenile zebrafish, where DiD was injected live and the fish was fixed post-injection; anterior to the top, lateral to the right. Arrowheads mark one example olfactory rod with retrograde DiD labelling. Arrows mark one example olfactory rod with no retrograde DiD labelling. Scale bar = 20 µm. **(B–B'')** Maximum intensity projection of confocal image of Alexa-phalloidin signal with greyscale values inverted **(B)**, DiD signal with greyscale values inverted **(B')**, and merged signals **(B'')** in a single olfactory rod cell in a 5 dpf larva, where DiD was injected into

the fixed larva. The actin-rich apical rod projection, marked by an arrowhead, is co-labelled by Alexa-phalloidin (green) and DiD (magenta). DiD also labels the whole cell body (magenta), which is apical in position and rounded in shape. Arrow marks a possible axon on the basal side of the olfactory rod cell in **B'**, which likely terminates in the OB via the olfactory nerve. Scale bar = 5 µm. Note: the olfactory rod projection on the left is not clearly retrogradely labelled by DiD. **(C–E)** Number of olfactory rod cells positively labelled by Alexa-phalloidin compared with the number of olfactory rods also retrogradely labelled by DiD in olfactory pits of fixed 5 dpf (**C**; *N* of olfactory pits = 13), 7 dpf (**D**; *N* = 10), and 20 dpf (**E**; *N* = 7) zebrafish. Connecting lines indicate the same olfactory pit.

3.2.6. Development of olfactory rod cells is not affected by a mutation in *sox10*

To test whether the development of olfactory rod cells is dependent on *sox10* function, I stained *sox10*$^{-/-}$ homozygous mutants (Dutton et al., 2001) with Alexa-phalloidin. Olfactory rods were present in *sox10*$^{-/-}$ mutants at 5 dpf (Figure 3.8), but variable in number (*N* of olfactory pits = 8, *n* of olfactory rods = 53). Taken together, mosaic expression of *sox10*-driven transgenes and presence of olfactory rods in *sox10*$^{-/-}$ mutant larvae indicate that *sox10* function is not essential for the formation of olfactory rod cells.

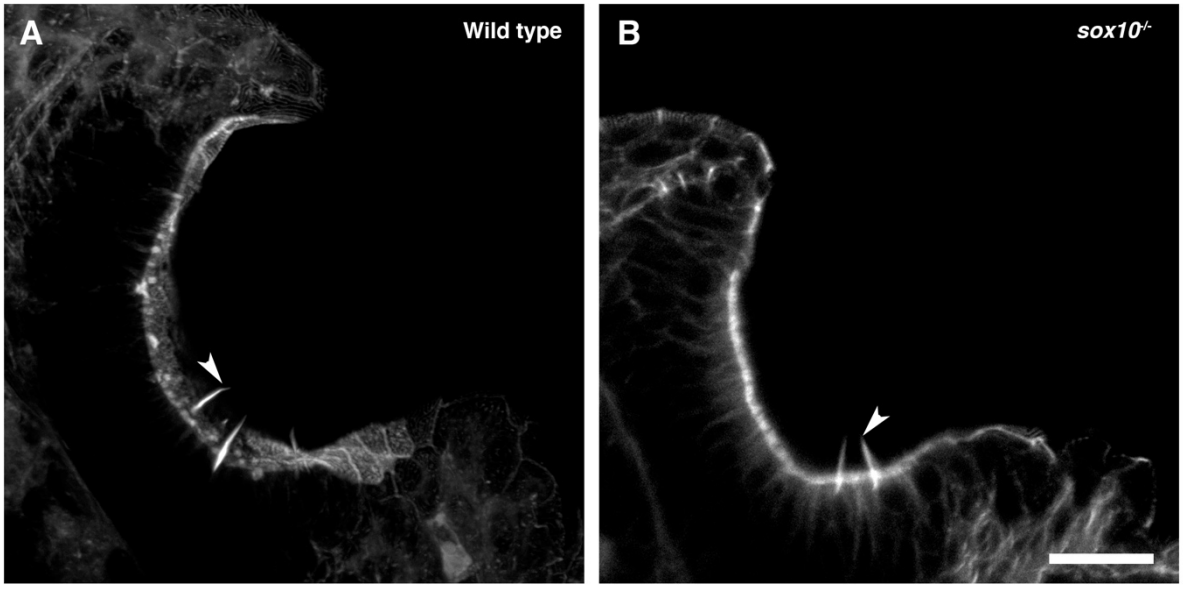

Figure 3.8. Olfactory rod cells are present in the olfactory epithelia of *sox10*$^{-/-}$ zebrafish mutants (fixed mutant larvae provided by K. Carmago-Sosa and R. Kelsh; published in Cheung et al., 2021).

(A) Maximum intensity projection of Airyscan confocal image of phalloidin stain in a 5 dpf larval wild-type olfactory pit; anterior to the top, lateral to the right. Arrowhead marks one example olfactory rod. Scale bar = 20

µm. **(B)** Airyscan confocal image of phalloidin stain in a 5 dpf larval *sox10*$^{-/-}$ mutant olfactory pit; anterior to the top, lateral to the right. Arrowhead marks one example olfactory rod. Scale bar = 20 µm.

3.2.7. Development of olfactory rod cells is not affected by a mutation in *flna*

Flna is a gene which codes for the actin-crosslinking protein filamin A (reviewed in Winder and Ayscough, 2005). Interestingly, adult heterozygous *flna* zebrafish mutants (unpublished; A. Metzner, A. Ong and F. van Eeden labs) have severe craniofacial deformations and anosmia, assessed by their lack of attraction towards food, but their phenotypes in the developing nose are unclear. Due to the function of filamin A, it was hypothesised that this protein could play a role in organising actin filaments in olfactory rod projections. To examine this, larvae from a *flna* heterozygous in-cross were stained with Alexa-phalloidin. Olfactory rod projections were present and labelled in all larvae (*N* of larvae = 20). However, severe deformations in the shape of olfactory pits were observed in 30% of larvae, where epithelia appeared invaginated (Figure 3.9A, A''). An additional 40% of larvae had mild abnormalities in the olfactory pit, where epithelia seemed kinked instead of appearing smoothly curved (Figure 3.9A, A'). I postulated that the milder phenotypes occur in heterozygous larvae, while the more severe phenotypes occur in homozygous mutants. Contrastingly, although there are some correlations, there is no clear relationship between genotype and OE phenotype (Figure 3.9C). No significant differences were observed in the number of rod projections per olfactory pit between heterozygous (9.1 ± 2.2 [mean ± s.d.]), homozygous (7.9 ± 1.2 [mean ± s.d.]), and wild-type siblings (8.5 ± 2.1 [mean ± s.d.]; Figure 3.9D). Furthermore, there were no significant differences in rod projection length between heterozygous (10.7 ± 2.0 [mean ± s.d.] µm), homozygous (11.1 ± 2.0 [mean ± s.d.] µm), and wild-type siblings (10.7 ± 1.6 [mean ± s.d] µm; Figure 3.9E). In conclusion, the *flna* mutation does not affect development of olfactory rod cells at 4 dpf.

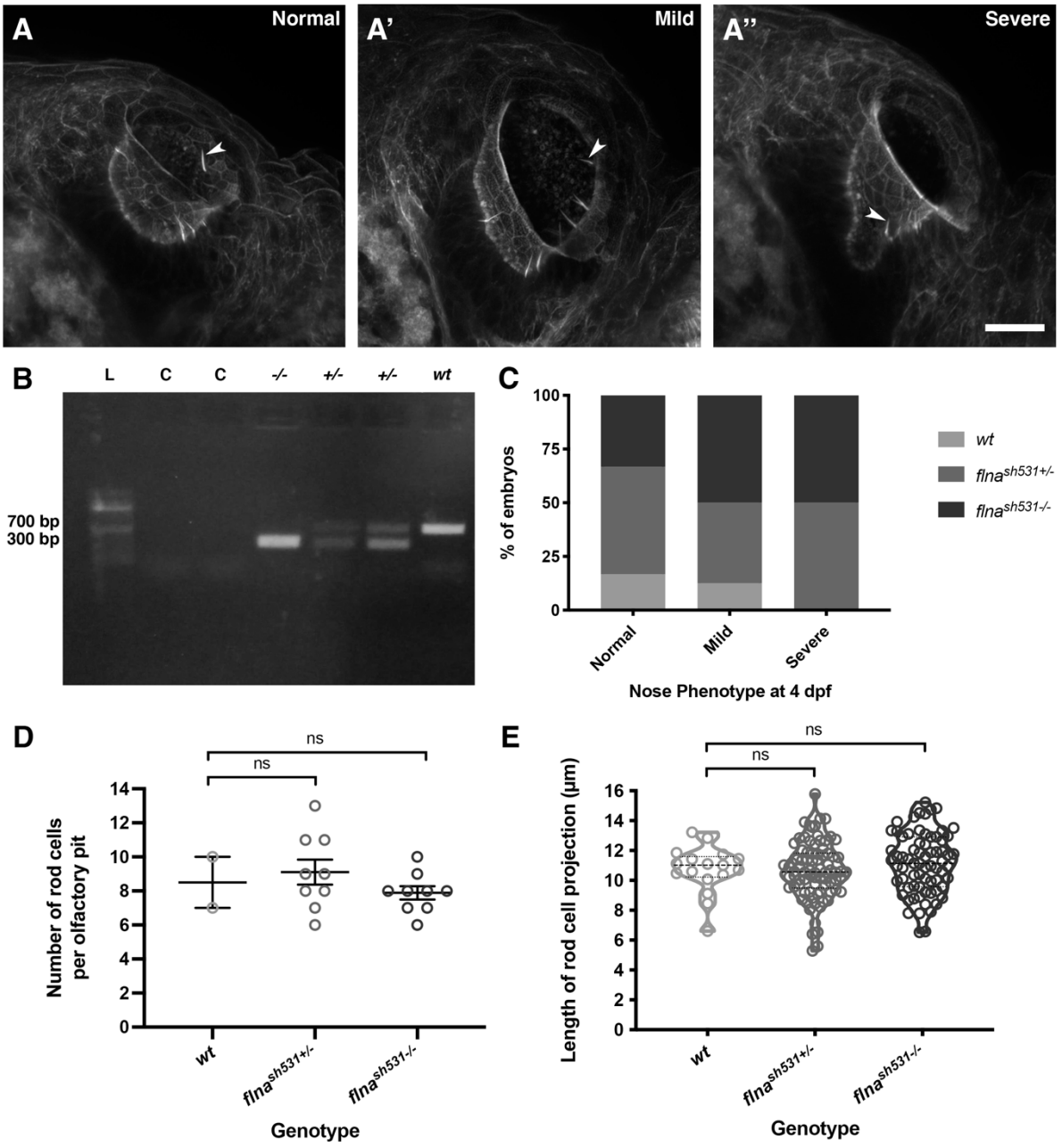

Figure 3.9. Olfactory rod cells appear normal in the olfactory epithelia of *flna*$^{-/-}$ zebrafish mutants (mutant larvae provided by E. Noël).

(A–A'') Maximum intensity projections of Airyscan confocal images of olfactory pits stained with Alexa-phalloidin in 4 dpf larvae from a *flna* heterozygous in-cross. Varying phenotypes were seen in the olfactory pits; **(A)** normal phenotype (smoothly curved epithelia), **(A')** mild deformations (kinked epithelia), and **(A'')** severe deformations (invaginated epithelia). Anterior to the top, lateral to the right. Arrowheads mark example olfactory rods. Scale bar = 20µm. **(B)** PCR gel for genotyping *flna*^{sh531} heterozygous in-cross larvae against a NEB Quick-Load 100 bp DNA ladder, L, and two water control samples, C. Mutations caused a fusion of 3' end of exon 4 with 5' end of exon 5, introducing a deletion of intron 4 (approximately 400 bp) in *flna.* Homozygous *flna*$^{-/-}$ mutants yielded approximately

300 bp amplicons, wild-type siblings yielded approximately 700 bp amplicons, while heterozygous *flna*$^{+/-}$ larvae yielded both 300 and 700 bp amplicons. (Genotyping protocol and primers provided by P. Carr, E. Noël lab.) **(C)** A quantification of the percentage of 4 dpf larvae with normal (*N* of larvae = 6), mild (*N* = 8), and severe (*N* = 6) OE phenotypes, with wild-type, heterozygous, and homozygous genotypes. **(D)** Number of olfactory rod projections per olfactory pit in 4 dpf wild-type (*N* of larvae = 2), heterozygous (*N* = 9), and homozygous (*N* = 9) larvae. Bars indicate mean ± S.E.M. for each group. Kruskal-Wallis test and Dunn's correction for multiple comparisons against the wild-type group; ns, not significant ($P > 0.05$). **(E)** Lengths of individual olfactory rod projections in 4 dpf wild-type (*n* of olfactory rods = 17), heterozygous (*n* = 82), and homozygous (*n* = 71) larvae. Violin plot; bars indicate the median and lower and upper quartiles for each group. Kruskal-Wallis test with Dunn's correction for multiple comparisons against the wild-type group; ns, not significant ($P > 0.05$).

3.3. Discussion

By using phalloidin staining, immunohistochemistry, transgenic zebrafish lines, retrograde tracing, and high-resolution fluorescence confocal imaging, I have begun to characterise a rare cell type, the olfactory rod cell, in the larval zebrafish OE. Olfactory rod cells, which had not previously been described in zebrafish, each bear a single actin-rich rod-shaped apical projection extending about 10 µm above the epithelial surface and are posterolaterally clustered in the olfactory pit. Olfactory rods arise within a few hours of the olfactory pit opening, increase in numbers and size during larval stages, and are stable structures. Live imaging with a ubiquitous Lifeact-RFP label indicates that the olfactory rods can oscillate. A subpopulation of olfactory rod cells expresses Lifeact-mRFPruby and GFP transgenes driven by the *sox10* promoter. Mosaic expression of these transgenes and retrograde tracing reveal that olfactory rod cells have rounded cell bodies located apically in the OE. Mutations in neither *sox10* nor *flna* genes cause any disruption to the formation of olfactory rods. A subset of the cells may contain an axon terminating in the OB; however, the results from the DiD injections are ambiguous. Retrograde labelling in the OE may not have completeness if the dye did not reach the whole OB. Dye injected into live larvae may travel from cell to cell via exosome transportation, thus not all labelling would be retrograde. The experiment was repeated in fixed larvae as a measure to prevent vesicular transport, but even then, it is possible that dye can be carried from cell to cell. Furthermore, any axon passing through the olfactory nerve could also be labelled by DiD injection, thus I cannot exclude the possibility of afferent innervation of olfactory rod cells from trigeminal or terminal nerve fibres, for

example. Other methods should be employed to clarify if the cells project an axon, such as creating a 3D reconstruction of the cell by tracing serial-section electron microscopy (ssEM) data (Hildebrand et al., 2017). In summary, olfactory rod cells are morphologically distinct from the well-characterised OSNs and other known cell types in terms of their apical projections, cell shape, and distribution and positioning within the OE.

3.3.1. The olfactory rod: an actin-rich apical projection

The spectacular actin-rich projection of the olfactory rod cell adds to the rich repertoire of known F-actin-based cellular specialisations, which include microvilli, stereocilia, lamellipodia, filopodia, cytonemes and microridges (reviewed in Heath and Holifield, 1991; reviewed in Theriot and Mitchison, 1991; Ramírez-Weber and Kornberg, 1999; Pinto et al., 2019; Inaba et al., 2020). Many sensory cell types, in both fish and mammals, bear actin-rich mechano- or chemosensory microvillous projections, including the stereocilia of sensory hair cells (Tilney et al., 1980; reviewed in Gillespie and Müller, 2009; reviewed in Barr-Gillespie, 2015), and the microvilli of olfactory and vomeronasal microvillous neurons, solitary chemosensory cells (SCCs) of the skin and barbel (Kotrschal et al., 1997; Finger et al., 2003; Hansen and Finger, 2008), taste bud cells (Hansen et al., 2002; Zachar and Jonz, 2012), CSF-cNs (Djenoune et al., 2014; Desban et al., 2019), Merkel cells, retinal Müller glia (Sekerková et al., 2004), and the brush and tuft cells of mammalian respiratory and intestinal epithelia, respectively (reviewed in Reid et al., 2005; reviewed in Schneider et al., 2019). As a single structure with a smoothly tapering morphology, the zebrafish olfactory rod differs from these oligovillous structures. Adult zebrafish SCCs, found distributed over the entire body surface (Kotrschal et al., 1997), and mature light cells of the zebrafish taste bud (Hansen et al., 2002) each bear a single microvillus, but at 1–3 µm in length, these are much shorter than the olfactory rods described here.

On a sub-cellular level, several classes of regulatory proteins are associated with the organisation of actin fibres in hair cell stereocilia in the ear, vomeronasal organs, and taste bud cells. Espins, for example, are involved in bundling of actin in projections mediating mechano- and chemosensory transduction, and are implicated in human deafness and vestibular disorders, thus indicating their importance within sensory systems (reviewed in

Loomis et al., 2003; Sekerková et al., 2004, 2006; reviewed in Gillespie and Müller, 2009; reviewed in Schwander et al., 2010; Chou et al., 2011; reviewed in Barr-Gillespie, 2015). Despite severe craniofacial defects and anosmia in homozygous *flna* zebrafish mutants, the actin-crosslinking protein filamin A does not appear to have a role in the formation of actin-rich olfactory rod projections. There must, however, undoubtedly be other classes of actin-binding proteins, such as espins, villins, or fascins, involved in the organisation and function of this unique projection; these remain to be investigated.

Olfactory rod cells are distinct from rodlet cells, which have been reported in many different epithelial tissues of marine and freshwater fish, including zebrafish, and contain several intracellular electron-dense rodlets within a thick cuticular-like wall (Bannister, 1966; reviewed in Morrison and Odense, 1978; Hansen and Zeiske, 1998; Dezfuli et al., 2007; DePasquale, 2020). Recently, phalloidin staining has demonstrated that the rodlets, which can be extruded from the cell, are not composed of F-actin (DePasquale, 2020). Thus, zebrafish olfactory rod cells, which are unique to the OE at larval and juvenile stages, are not related to rodlet cells.

3.3.2. Olfactory rod cells in other teleost species

Previous studies have provided descriptions of cell types similar to the olfactory rod cell in other teleost species, including the common minnow (Bannister, 1965), several eel species (Schulte, 1972; Yamamoto and Ueda, 1978), goldfish (Breipohl et al., 1973; Ichikawa and Ueda, 1977), rainbow trout (Rhein et al., 1981), common bleak (Hernádi, 1993), catfish (Datta and Bandopadhyay, 1997), and several cave fish and cave loach species (Waryani et al., 2013, 2015; Zhang et al., 2018).

Using transmission electron microscopy (TEM), Bannister (1965) reported sparsely-populated rod-shaped protrusions, approximately 4 µm in length and shorter than surrounding sensory and non-sensory olfactory cilia, in the OE of adult (3.7 cm) common minnow (*Phoxinus phoxinus*). Here, the rod-like projection consisted of several bundles of fibres, consistent with the appearance of F-actin, extending from deep within the cell (Bannister, 1965). Similarly, using TEM and SEM respectively, Schulte (1972) and Yamamoto and Ueda (1978) reported the

presence of olfactory rod cells in the OE of several adult eel species: European eel (*Anguilla anguilla*), Japanese eel (*A. japonica*), white-spotted conger (*Conger myriaster*), buffoon snake eel (*Microdonophis erabo*), and brutal moray (*Gymnothorax kikado*). In European eels, the cells were described as a receptor with a single rod-shaped appendage, measuring 0.8 µm in diameter and extending 4 µm above the apical surface of the epithelium (Schulte, 1972). Olfactory rods in the other four species measured 1 µm in diameter and 10 µm in length. Olfactory rods were either found to exist solitarily or in a group; interestingly, it was noted that olfactory cilia were sparse in areas where olfactory rods occurred in a group (Yamamoto and Ueda, 1978).

More recent reports include comparisons of the surface structures of olfactory epithelia in different adult cave fish and loaches. SEMs in *Sinocyclocheilus jii* and *S. furcodorsalis* cave fish, and in *Oreonectes polystigmus* and *O. guananensis* cave loaches revealed that olfactory rods were clustered in different regions of olfactory rosette lamellae (Waryani et al., 2013, 2015). Another SEM study on the variations in olfactory systems of adult cave fish species of different habitats reported not just one, but three different cell types all classified as 'rod cilia' in the olfactory epithelia of *S. anshuiensis* and *S. tianlinensis*. The first cell type had a long base with an oval apex, the second contained an oval base with a thin apex, while the third was rod-shaped and thin from base to tip, measuring 2.01–3.08 µm in length (Zhang et al., 2018). Despite the shorter length, this third type appeared morphologically consistent with zebrafish olfactory rod cells. Unlike other teleosts, 'rod receptor cells' were reported as the dominant cell type over ciliated and microvillous OSNs in the OE of *S. jii* (Waryani et al., 2013). This may be an example of the known compensatory enhancement of the olfactory system in blind morphs of cave fish (Bibliowicz et al., 2013; reviewed in Krishnan and Rohner, 2017).

In adult goldfish, olfactory nerve bundle transection was performed to determine which cell types are OSNs (Ichikawa and Ueda, 1977). As expected, transection caused retrograde degeneration of both ciliated and microvillous OSNs. Olfactory rod cells, however, were still identifiable by SEM in the OE 10 days after nerve transection, thus the authors concluded that goldfish olfactory rod cells are not OSNs. This is similar to the observation that OB ablation did not lead to death of a subset of MVCs in the rat OE (Carr et al., 1991). It now appears that such MVCs are a class of sensory paraneuron, as they are cholinergic and express components

of the taste transduction pathway (Genovese and Tizzano, 2018). Perhaps consistently, it is of interest that only a proportion of zebrafish olfactory rod cells appear to have an axon terminating in the OB. Whether most olfactory rod cells would similarly survive nerve transection or OB ablation remains to be explored.

Although there appear to be variations in the numbers and sizes of olfactory rod cells reported in these other teleost species, some of these cells may be homologous to the olfactory rod cells I describe in zebrafish larvae. However, all of these previous studies were limited to fixed adult samples by means of TEM and SEM, and none have tested nor confirmed the cytoskeletal composition of the olfactory rod. Following our report of the presence of olfactory rod cells in larval zebrafish (Cheung et al., 2021), the cells have also since been identified in phalloidin stains of *Danionella translucida* (unpublished; J. Veith, B. Judkewitz lab).

3.3.3. Zebrafish olfactory rod cells are not artefacts

Since the first report of olfactory rod cells, several studies have proposed that they may represent senescent forms of OSNs or fixation artefacts (Muller and Marc, 1984; Moran et al., 1992; reviewed in Hansen and Zielinski, 2005). A study in the goldfish (*Carassius auratus*) and channel catfish (*Ictalurus punctatus*), using TEM, SEM and filling with horseradish peroxidase, concluded that olfactory rods are most likely a result of fusion of olfactory cilia or microvilli — an indicator of ageing OSNs (Muller and Marc, 1984). A later study on the ultrastructure of olfactory mucosa in brown trout (*Salmo trutta*) also classified olfactory rods as products of the fusion of olfactory cilia during fixation (Moran et al., 1992). Indeed, TEM images in this study showed multiple ciliary axonemes surrounded by a single membrane (Moran et al., 1992). The presence of such fixation artefacts has led to frequent dismissal of olfactory rod cells in the literature, for example in juvenile and adult European eels (Sola et al., 1993). However, the olfactory rods I describe in the zebrafish are clearly not a fixation artefact, as they are present in the live larva and can be tracked for at least 42 hours. Moreover, they are not formed by fusion of cilia, as the olfactory rods are F-actin-positive and do not stain with an anti-acetylated α-tubulin antibody.

3.3.4. Possible origins of olfactory rod cells

Sox10 mRNA is frequently described as a neural crest marker, but is also expressed strongly in otic epithelium (Dutton et al., 2001), a placodally-derived tissue. I do not directly address the developmental origin of olfactory rod cells here, but it is of interest that they express *sox10*-driven transgenes, albeit in a mosaic fashion. Conversely, evidence from DIG-ISH data shows that *sox10* mRNA transcript expression is either lacking or undetectable in the zebrafish OE (Whitlock et al., 2005). Thus, the use of *sox10*-driven transgenic lines to identify neural crest derivatives remains controversial.

Expression of a *sox10:eGFP* transgene together with photoconversion studies has led to the conclusion that a subpopulation of microvillous OSNs in the OE is derived from neural crest (Saxena et al., 2013), and use of an inducible *sox10*:*ER^{T2}-Cre* transgenic line has identified previously 'contested' neural crest derivatives, including cells in the sensory barbels (Mongera et al., 2013). However, using lineage reconstruction through backtracking and photoconversion experiments, Aguillon et al. (2018) have argued that all olfactory neurons, including OSNs and GnRH3 cells, are derived entirely from pre-placodal progenitors. Given this controversy, it cannot be concluded whether olfactory rod cells are derived from the PPE or CNC.

Sox10-driven transgenes are expressed in a subset of both olfactory rod cells and of microvillous OSNs, with variation in the proportion of expressing cells between individuals. This could reflect true heterogeneity in the olfactory rod cell and microvillous OSN populations, or it could be a result of mosaic or leaky expression of the transgene. Mosaic expression is typical for many transgenes (Mosimann et al., 2013), while leaky expression, which can be explained through the lack of appropriate silencer elements (Jessen et al., 1999), is suspected for the *sox10* promoter fragment used in our transgenic construct (reviewed in Tang and Bronner, 2020). While I cannot conclude from these data if olfactory rod cells express *sox10* gene, the *Tg(sox10:Lifeact-mRFPruby)* and *Tg(sox10:GFP)* transgenic lines have nevertheless proved to be fortuitous tools for visualising olfactory rod cells in the live larva and can be utilised in further studies.

3.3.5. Concluding remarks

Zebrafish olfactory rod cells are a newly identified cell type, and here I characterised their size, morphology, distribution, development, and cytoskeletal composition of the apical projection. I have demonstrated that the cells are unique and not artefactual, and should be subjected to further investigation for a full understanding of the olfactory system. The current range of innovative biomedical techniques offers the exciting opportunity to characterise the properties of rare cell types. A critical next step would be to address their gene expressions and functions.

Chapter 4. Expression of candidate transgenic markers in olfactory rod cells

4.1. Introduction

Since olfactory rod cells were a newly identified cell type in zebrafish, and had not been molecularly characterised in any species, their gene expression signatures were undetermined. My next objective was to screen transgenic markers of other olfactory and sensory cell types for expression in olfactory rod cells (see Tables 2.1, 4.1). In doing so, this would not only test for molecular similarities or differences between olfactory rod cells and other cell types, but may also give a potential indication of their function.

My previous data suggested that a subset of olfactory rod cells may contain an axon, but that their morphology differed from other known classes of OSN; thus, I hypothesised that olfactory rod cells express pan-neuronal markers, but are molecularly unique and do not express markers specific to other OSNs.

4.2. Results

4.2.1. Pan-neuronal promoters drive calcium reporter expression in olfactory rod cells

To test whether olfactory rod cells have features of neuronal cells, two transgenic lines, *Tg(Xla.tubb:jGCaMP7f)* (*N* of olfactory pits = 4) (Chia et al., 2019) and *Tg(elavl3:GCaMP6f)* (*N* = 5) (Dunn et al., 2016), which have broad neuronal expression of cytoplasmic fluorescent reporters, were imaged. Dendrites and dendritic knobs of OSNs were clearly labelled by both lines. In some examples, faintly-labelled projections extending from below the surface of the OE could be observed, with a similar length and morphology to olfactory rods (Figure 4.1A–B'). Imaging of double-transgenic *Tg(elavl3:GcaMP6f);Tg(actb2:Lifeact-RFP)* larvae at 5 dpf suggested that olfactory rod cells are GcaMP6f-positive (*N* of larvae = 3; Figure 4.1C–C''). While some of the green fluorescence may have been caused by bleed-through from RFP, this

cannot account for all the signal, as rods were seen where the green fluorescence was detected even with dim red fluorescence (arrowhead, Figure 4.1C–C”; see trace of RFP and GcaMP6f levels). These observations suggest that olfactory rod cells may be a type of neuron.

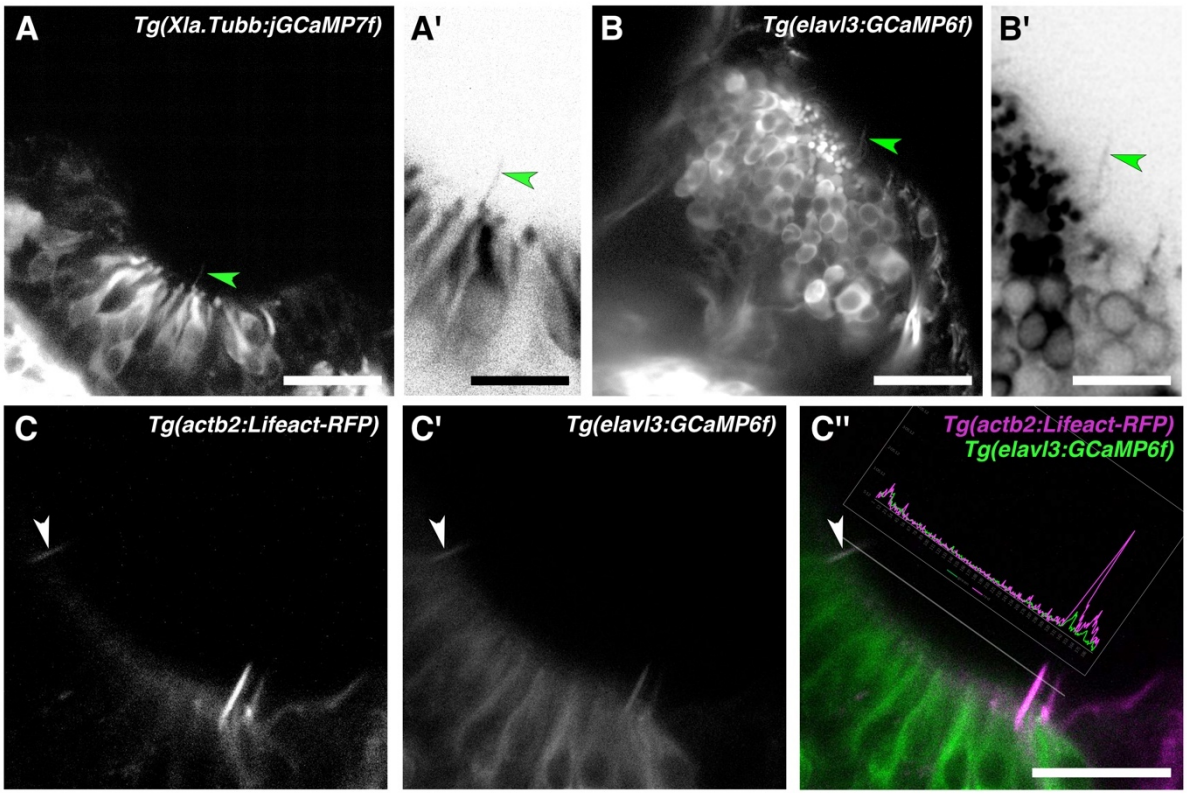

Figure 4.1. Olfactory rod cells are labelled by the cytoplasmic neuronal markers *Tg(Xla.Tubb:jGCaMP7f)* and *Tg(elavl3:GcaMP6f)* (images taken by S. J. Jesuthasan, processing and analysis by K. Y. Cheung; published in Cheung et al., 2021).

(A) Olfactory pit of a 4 dpf *Tg(Xla.Tubb:jGCaMP7f)* larva; anterior to the top, lateral to the right. Arrowhead marks one example olfactory rod, albeit faintly labelled. Scale bar = 20 µm. **(A’)** Enlargement of olfactory rod marked by arrowhead in **A** (greyscale values inverted). Scale bar = 10 µm. **(B)** Olfactory pit of a 5 dpf *Tg(elavl3:GcaMP6f)* larva; anterior to the top, lateral to the right. Arrowhead marks one example olfactory rod, albeit faintly labelled. Scale bar = 20 µm. **(B’)** Enlargement of olfactory rod marked by arrowhead in **B** (greyscale values inverted). Scale bar = 10 µm. **(C–C’’)** *Tg(actb2:Lifeact-RFP)* signal **(C)**, *Tg(elavl3:GCaMP6f)* signal **(C’)**, and merged signals **(C’’)** in an olfactory pit of a 5 dpf *Tg(elavl3:GcaMP6f);Tg(actb2:Lifeact-RFP)* double-transgenic larva; anterior to the top, lateral to the right. The trace shows levels of red and green fluorescence along the dotted line, which passes through three olfactory rods positive for both Lifeact-RFP and GcaMP6f. The olfactory rod highlighted with the arrowhead shows similar levels of fluorescence in both the red and green channels. Scale bar = 20 µm.

4.2.2. Olfactory rod cells do not express markers of ciliated cell types

The OE contains two ciliated cell types — ciliated OSNs, which comprise a major a class of OSN (Hansen and Zeiske, 1998; Hansen and Zielinski, 2005; Sato et al., 2005; Elsaesser and Paysan, 2007), and non-sensory multi-ciliated cells (MCCs; Reiten et al., 2017). To test if olfactory rod cells express any common markers of these ciliated cell types, *Tg(Foxj1a:GFP)* (marker of ciliated OSNs and MCCs; Reiten et al., 2017), *Tg(Foxj1b:GFP)* (marker of ciliated OSNs; Tian et al., 2009), *Tg(OMP:ChR2-YFP)* (marker of ciliated OSNs; Sato et al., 2005), and *Tg(19B:GFP)* (marker of MCCs; Reiten et al., 2017) transgenic larvae were stained with Alexa-phalloidin at 5 dpf. Resulting confocal images showed that in all four transgenic lines, GFP did not colocalise in the phalloidin-positive olfactory rods, nor in the cell bodies beneath the rod projections (Figure 4.2). This suggests that olfactory rod cells do not contain a cilium and are not molecularly related to the existing well-characterised ciliated cell types in the OE.

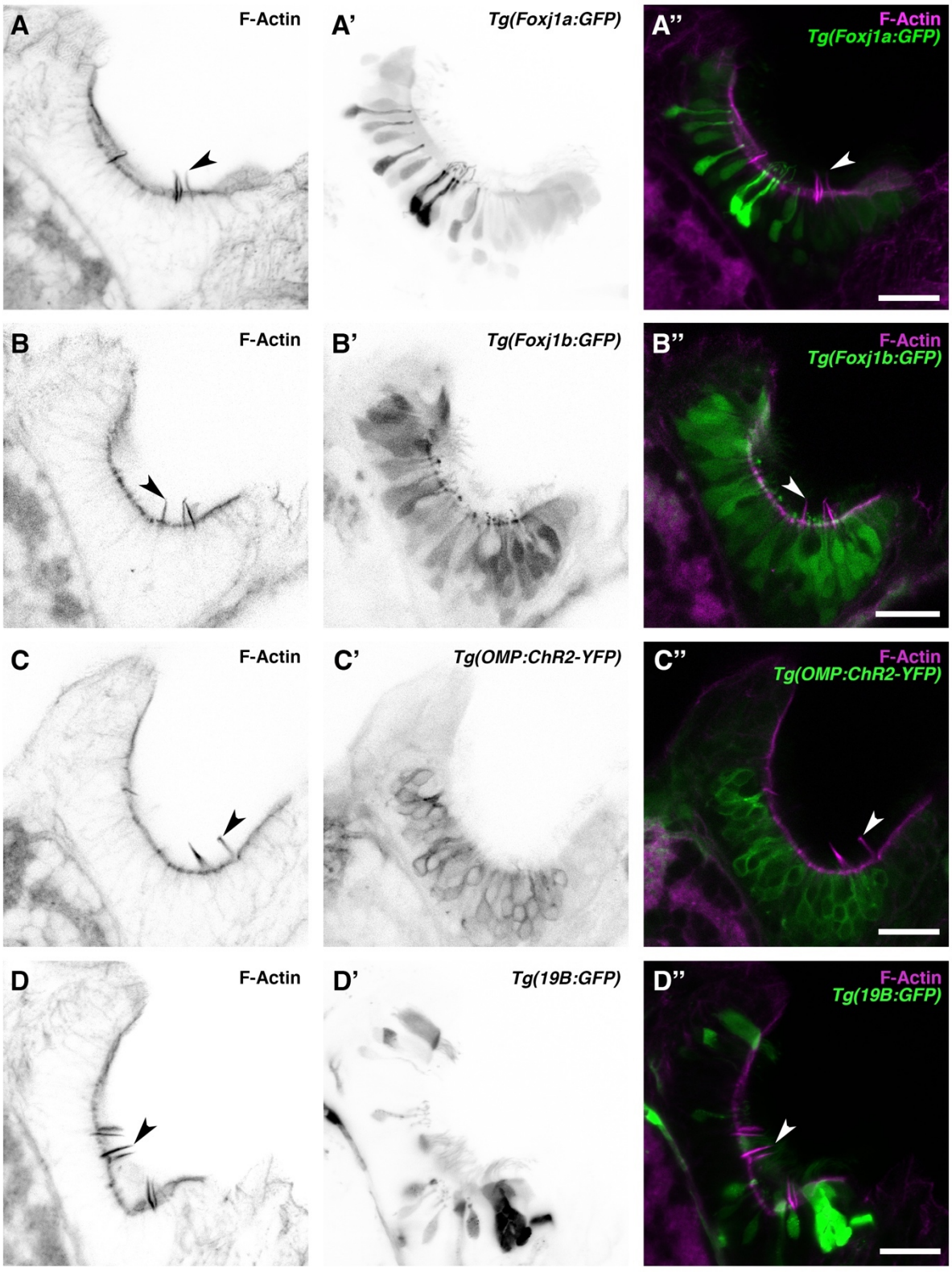

Figure 4.2. Olfactory rod cells do not express transgenic markers of ciliated olfactory sensory neurons or multi-ciliated cells (fixed transgenic larvae provided by C. Ringers and N. Jurisch-Yaksi).

Airyscan confocal images of Alexa-phalloidin signal with greyscale values inverted **(A, B, C, D)**, transgene signals with greyscale values inverted **(A', B', C', D')**, and merged signals **(A'', B'', C'', D'')** in olfactory pits of 5 dpf cilia-marker transgenic larvae; anterior to the top, lateral to the right. Arrowheads mark example olfactory rods. Scale bars = 20 μm.

4.2.3. Olfactory rod cells do not express markers of microvillous olfactory sensory neurons

The second major class of sensory cell in the OE are microvillous OSNs (Hansen and Zeiske, 1998; Hansen and Zielinski, 2005; Sato et al., 2005; Elsaesser and Paysan, 2007). *Tg(TRPC2:ntr-mCherry)* is a common transgenic marker for microvillous OSNs (Sato et al., 2005). Additionally, *Tg(27A:ntr-mCherry)* is a transgenic line that theoretically labels random subsets of OSNs (Kawakami et al., 2010); however, based on my high-resolution images of the OE, most but not all cells labelled by this line morphologically appear to be microvillous OSNs. To screen for similarities between microvillous OSNs and my cell of interest, I stained *Tg(TRPC2:ntr-mCherry)* and *Tg(27A:ntr-mCherry)* larvae with Alexa-phalloidin at 7 dpf, but mCherry expression did not colocalise in the olfactory rods in either transgenic line (Figure 4.3). Despite both cell types containing actin-rich apical projections, these results indicate that olfactory rod cells are molecularly distinct from microvillous OSNs.

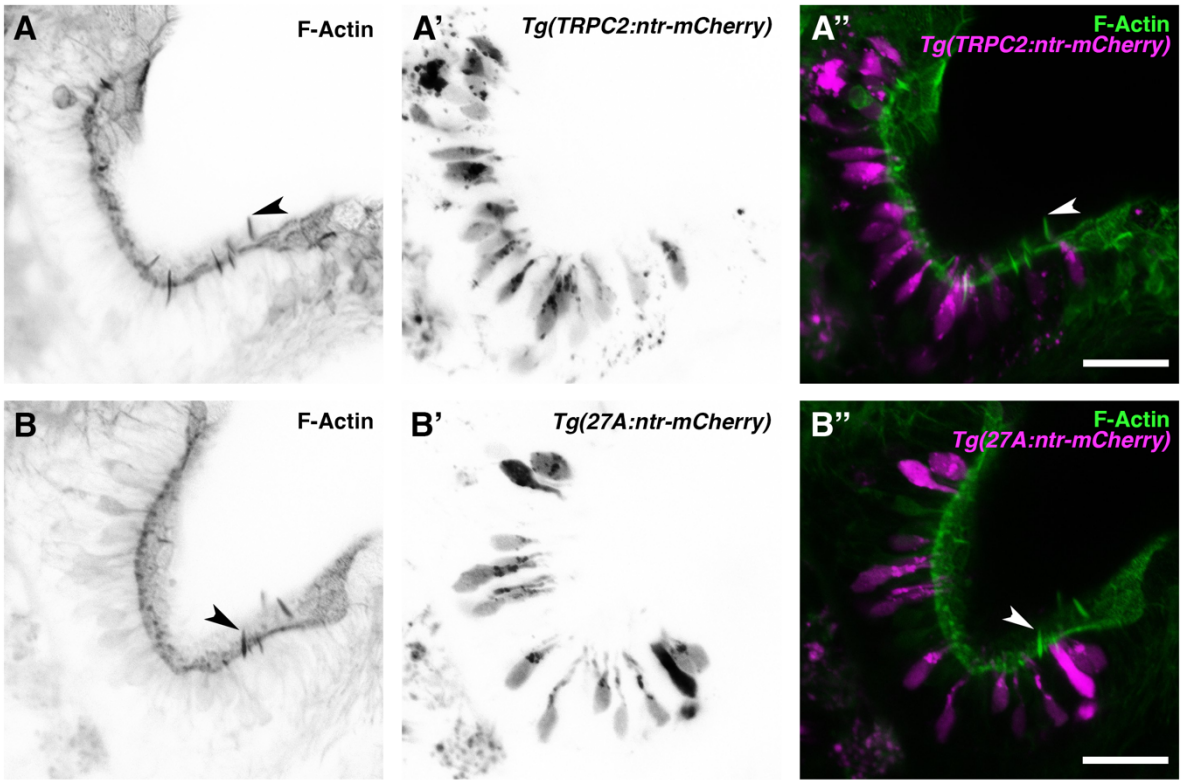

Figure 4.3. Olfactory rod cells do not express transgenic markers of microvillous olfactory sensory neurons. Maximum intensity projection of confocal images of Alexa-phalloidin signal with greyscale values inverted **(A, B)**, transgene signals with greyscale values inverted **(A', B')**, and merged signals **(A'', B'')** in olfactory pits of 7 dpf microvillous OSN-marker transgenic larvae; anterior to the top, lateral to the right. Arrowheads mark example olfactory rods. Scale bars = 20 µm.

4.2.4. Olfactory rod cells do not express a marker of mechanosensory hair cells and are not susceptible to ototoxic damage

The presence of olfactory rods was initially observed while performing whole-mount phalloidin stains for the actin-rich stereociliary bundles of sensory hair cells in the inner ear and lateral line. Given the superficial similarity in appearance of olfactory rods to hair-cell stereocilia in low-magnification phalloidin stains, and a report of a rare cell type bearing stereocilia-like microvilli in the rat OE (Menco and Jackson, 1997), I was interested to test whether there are any similarities between olfactory rod cells and mechanosensory hair cells of the inner ear and lateral line. As shown in Figures 1.9 and 3.1, the zebrafish olfactory rod appears to be a single structure rather than a collection of microvilli or stereocilia. To test

whether olfactory rod cells express sensory hair cell markers, I performed an Alexa-phalloidin stain on the *Tg(pou4f3:GFP)* transgenic line, a known marker for hair cells (Xiao et al., 2005). At 5 dpf, the stereociliary bundle of lateral line neuromast hair cells was clearly marked by both GFP and phalloidin, which acted as a positive control (Figure 4.4A–A''). However, GFP did not colocalise with the phalloidin signal in the olfactory rods, or in the cell body beneath a phalloidin-positive olfactory rod (Figure 4.4B–B'').

Mechanosensory hair cells, including those of the zebrafish lateral line, are susceptible to oxidative damage by aminoglycoside antibiotics, which can preferentially enter hair cells via mechanotransduction channels, and cause cell death following a calcium flux and release of reactive oxygen species by mitochondria (Esterberg et al., 2013, 2016; Pickett et al., 2018). To test whether olfactory rod cells are similarly sensitive, I investigated whether treatment with the aminoglycoside neomycin has the same damaging effect on olfactory rod cells as on lateral line hair cells. Following neomycin treatment at 500 µM for 60 minutes on 3 dpf *Tg(pou4f3:GFP)* larvae, lateral line hair cells were lost or severely damaged, as determined by a decrease in the number of GFP-positive cells (together with loss of their phalloidin-positive stereocilia) in both cranial and trunk neuromasts and a change in morphology of any remaining cells (Figure 4.4C, D, F, G). By contrast, olfactory rods appeared unaffected by neomycin treatment (Figure 4.4E, H), with no significant difference in the number of olfactory rods present in each olfactory pit (7.3 ± 2.9 [mean ± s.d.], *N* of olfactory pits = 4) compared with the untreated control group (7.8 ± 2.5 [mean ± s.d.] *N* = 4; Figure 4.4I). Taken together, the smooth appearance of the olfactory rods, lack of hair cell marker expression, and resistance to neomycin indicate that olfactory rod cells are not closely related to hair cells.

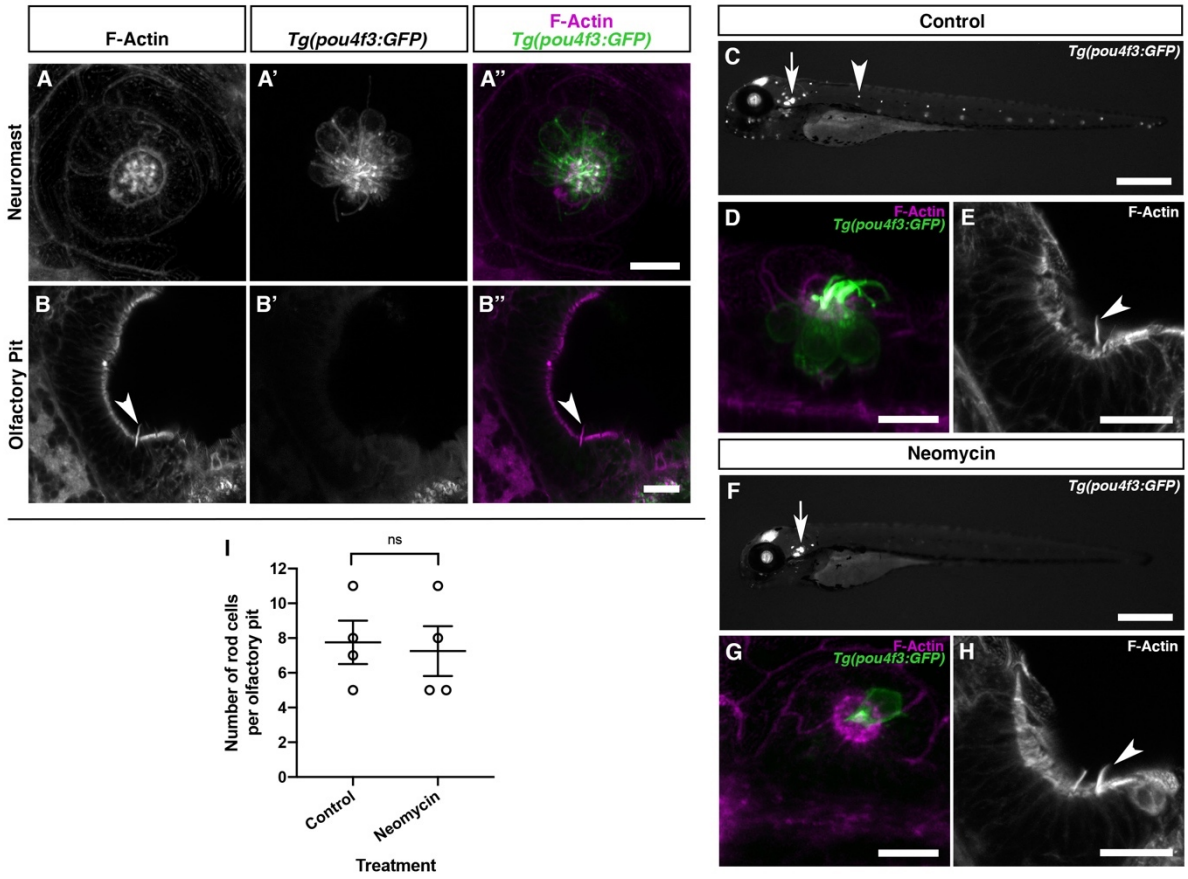

Figure 4.4. Olfactory rod cells do not express a transgenic marker of mechanosensory hair cells and are not susceptible to damage by neomycin (published in Cheung et al., 2021).

(A–A'') Maximum intensity projection of Airyscan confocal image of Alexa-phalloidin signal **(A)**, *Tg(pou4f3:GFP)* signal **(A')**, and merged signals **(A'')** in a cranial neuromast of a 5 dpf larva. Scale bar = 10 µm. **(B–B'')** Airyscan confocal image of Alexa-phalloidin signal **(B)**, *Tg(pou4f3:GFP)* signal **(B')**, and merged signals **(B'')** in an olfactory pit of a 5 dpf larva; anterior to the top, lateral to the right. Arrowhead marks one olfactory rod. Scale bar = 20 µm. **(C, F)** Widefield imaging of 3 dpf *Tg(pou4f3:GFP)* larvae showing the damaging effects of 500 µM neomycin treatment for 60 minutes on lateral line neuromast hair cells. Fluorescence is lost or greatly reduced in both trunk (arrowhead) and cranial neuromasts, whereas fluorescence in hair cells of the inner ear maculae and cristae (arrow) is unaffected. Scale bars = 500 µm. **(D, G)** Maximum intensity projections of Airyscan confocal images showing the damaging effects of 500 µM neomycin treatment for 60 minutes on hair cells in a cranial neuromast of a 3 dpf larva, using *Tg(pou4f3:GFP)* (green) and Alexa-phalloidin (magenta) as markers. Scale bars = 10 µm. **(E, H)** Maximum intensity projections of Airyscan confocal images showing no effect of 500 µM neomycin treatment for 60 minutes on olfactory rods, using Alexa-phalloidin as a marker; anterior to the top, lateral to the right. Arrowheads mark olfactory rods. Scale bars = 20 µm. **(I)** The number of olfactory rod cell projections per olfactory pit of 3 dpf *Tg(pou4f3:GFP)* larvae after 500 µM neomycin treatment for 60 minutes (*N* of olfactory pits = 4), compared with an untreated group (*N* = 4). Bars indicate mean ± S.E.M. Welch's unpaired two-tailed *t*-test; ns, not significant (*P* = 0.8018).

4.2.5. Olfactory rod cells express transgenes driven by *claudin* promoters

Finally, I investigated whether olfactory rod cells express any generic markers in common with other sensory cells. *Tg(cldnh:eGFP)* (Lin et al., 2019) and *Tg(cldnb:lyn-GFP)* (Haas and Gilmour, 2006) are transgenic lines driven by *claudin* gene promoters. Claudins are tetraspan transmembrane proteins of tight junctions (Krause et al., 2008). *Cldnh*, also known as *cldn3c*, is orthologous to human *CLDN3* and codes for a protein involved in retinal development (Lu et al., 2020). *Cldnb*, orthologous to human *CLDN4*, has roles in neuromast development, regulation of sodium ion transport, and is implicated in some cancers (Kwong and Perry, 2013). Both transgenes are known to be expressed in zebrafish sensory systems including neuromasts and the OE, but it is not specified what olfactory cell types express them. After staining 7 and 5 dpf transgenic larvae with Alexa-phalloidin, confocal images showed that *Tg(cldnh:eGFP)* was expressed at low levels in the olfactory rod cells, much lower than most other cells of the OE. This was visually apparent as there were obvious fluorescence gaps in the location of olfactory rod cell bodies (Figure 4.6A–A''). On the other hand, *Tg(cldnb:lyn-GFP)* was strongly expressed in the cell membranes of olfactory rod cells (Figure 4.6B–B''). GFP expression in the apical projection was localised to the membrane encasing the phalloidin-labelled F-actin. There was also strong expression in the neck of the cell, where the rod projection emerges from the cell body. Furthermore, there were instances of higher levels of fluorescence in olfactory rod cell membranes than the membranes of surrounding OE cells, suggesting that they have higher *cldnb* gene expression.

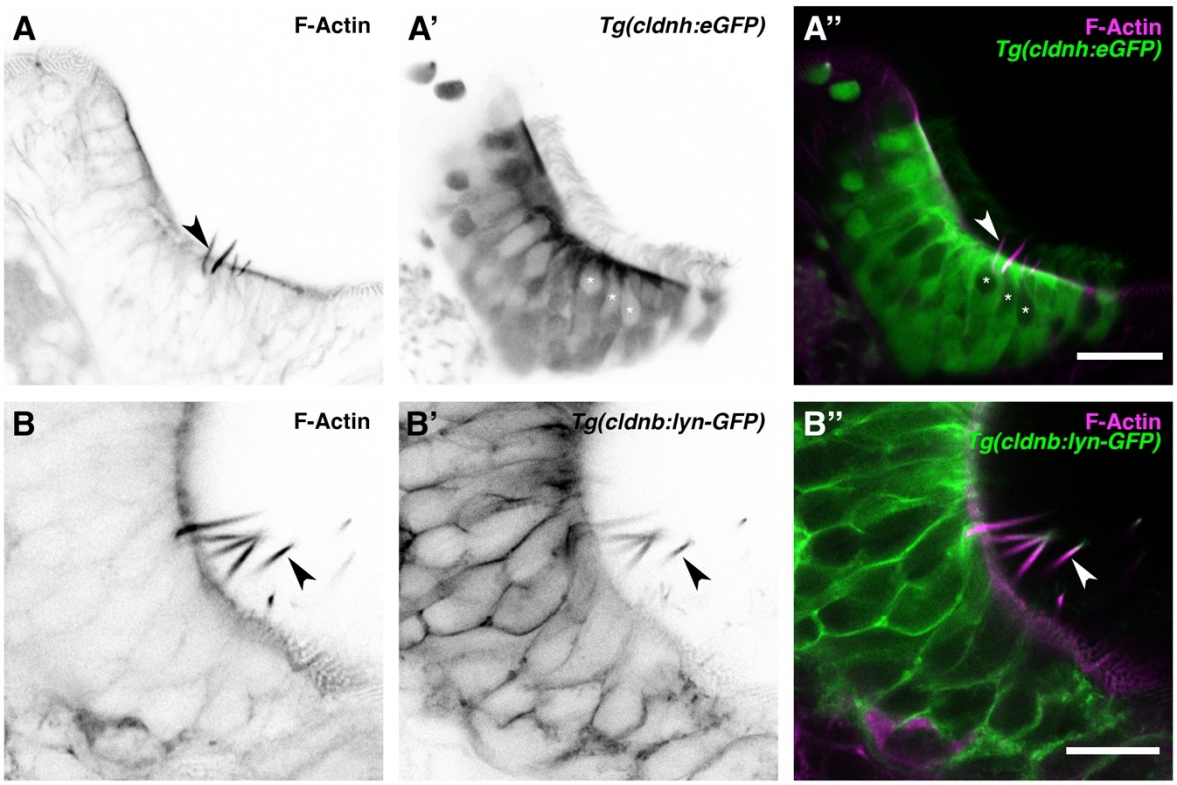

Figure 4.5. Olfactory rod cells express transgenes strongly under a *cldnb*-driven promoter, but weakly under a *cldnh*-driven promoter (images taken by K. Y. Cheung, N. J. van Hateren, and T. T. Whitfield).

Confocal images of Alexa-phalloidin signal with greyscale values inverted **(A, B)**, transgene signals with greyscale values inverted **(A', B')**, and merged signals **(A'', B'')** in olfactory pits of 7 and 5 dpf claudin-marker transgenic larvae; anterior to the top, lateral to the right. Arrowheads mark example olfactory rods. Asterisks mark fluorescence gaps in the OE. Scale bar in row **A** = 20 µm, scale bar in row **B** = 10 µm.

In conclusion, olfactory rod cells do not express specific markers of other olfactory cell types such as OSNs or MCCs, nor do they express a marker for mechanosensory hair cells. Interestingly, olfactory rod cells strongly express transgenes under a *cldnb*-driven promoter, but only very weakly under a *cldnh*-driven promoter (Table 4.1); olfactory rod cells may be one of the only cell types in the OE to have this transgene expression pattern.

Table 4.1. A list of the transgenic lines screened for expression in olfactory rod cells.

Transgenic line	Marker in the OE for	Expressed?
Tg(actb2:Lifeact-RFP)	Actin in all cells	✓
Tg(sox10:Lifeact-mRFPruby)	Actin driven by *sox10* promoter*	✓
Tg(sox10:GFP)	Microvillous OSNs*	✓
Tg(elavl3:GcaMP6f)	Cytoplasmic pan-neuronal cells	✓
Tg(Xla.Tubb:jGCaMP7f)	Neuronal beta tubulin-expressing cells	✓
Tg(Foxj1a:GFP)	Ciliated OSNs and MCCs	✗
Tg(Foxj1b:GFP)	OSNs (ciliated and other)	✗
Tg(OMP:ChR2-YFP)	Ciliated OSNs	✗
Tg(19B:GFP)	MCCs	✗
Tg(TRPC2:ntr-mCherry)	Microvillous OSNs	✗
Tg(27A:ntr-mCherry)	Microvillous OSNs†	✗
Tg(pou4f3:GFP)	Mechanosensory hair cells	✗
Tg(cldnh:eGFP)	*cldnh* (*cldn3c*)-expressing cells	✓‡
Tg(cldnb:lyn-GFP)	*cldnb*-expressing cells	✓

*Expression of transgenes under the *sox10* promoter in the OE is likely to be leaky, and appears to be mosaic in olfactory rod cells.

†Reported to be a random subset of OSNs (Kawakami et al., 2010), but most of the cells expressing the transgene in my images morphologically appeared to be microvillous OSNs.

‡Expression of transgene was much lower compared with the expression in most other cells in the OE.

4.3. Discussion

By screening a range of existing transgenic zebrafish lines known for their expression in various sensory cell types, I have identified a handful of transgenes expressed in olfactory rod cells (Table 4.1). These will become useful markers for the cells in future experiments. Although most of the transgenes screened were not expressed in the cells, negative results are

nonetheless informative as they give indication that olfactory rod cells are molecularly and possibly functionally unique from other sensory cell types.

4.3.1. Olfactory rod cells differ from known sensory cell types and multi-ciliated cells

The detection of weak expression of cytoplasmic fluorescent markers driven by pan-neuronal promoters in olfactory rod cells indicates that they may be a type of neuron. As previously shown, retrograde tracing suggested that only a subset of olfactory rod cells contains an axon; however, it is unclear from the imaging whether all or just a subset express these pan-neuronal markers. Recent unpublished imaging showed that *Tg(Xla.Tubb:jGCaMP7f)* is expressed in glial cells, and that transgenes under the *elavl3* promoter are also expressed in neuronal progenitors, thus neither are exclusively neuronal markers (unpublished; S. J. Jesuthasan lab). Nevertheless, it is likely that olfactory rod cells are a sensory cell type that detect external stimuli.

Morphologically, olfactory rod cells are indisputably distinct from other cells in the OE. Phalloidin staining on various transgenic lines demonstrated that olfactory rod cells do not express GFP driven by *omp*, *trpc2*, or *foxj1a* promoters. Therefore, they are not only morphologically, but also molecularly and likely functionally dissimilar to ciliated OSNs, microvillous OSNs, and MCCs respectively. Published data from Saxena et al. (2013) concluded that all *Tg(sox10:eGFP)*-positive cells in the OE also express *Tg(TRPC2:Venus)*, and are therefore all classed as microvillous OSNs. Contradicting this, my data showed that olfactory rod cells are a non-microvillous OSN cell type that is *Tg(sox10:GFP)*-positive but negative for *Tg(TRPC2:ntr-mCherry)*. These results do not address whether olfactory rod cells are themselves a novel class of OSN. If they express odorant GPCRs that differ from the ones expressed by other OSNs, it would be expected that they detect a distinct group of odorants. Following this, there remains a scope for screening expression of ORs and identifying a unique gene marker for further characterisation of olfactory rod cells.

Images of phalloidin stains show superficial morphological similarities between the apical projections of olfactory rod cells and mechanosensory hair cells of the inner ear and lateral line. However, a lack of expression of *pou4f3*-driven GFP in olfactory rod cells suggest that

they are molecularly distinct cell types. Additionally, resistance to an ototoxin such as neomycin suggests that olfactory rod cells do not possess the same type of mechanotransduction channels that hair cells have. Despite this result, it does not exclude the possibility that olfactory rod cells are mechanosensory and possess a different class of mechanotransduction channel. This could be examined further by techniques such as calcium imaging or patch-clamp electrophysiology.

4.3.2. Two-photon calcium imaging of olfactory rod cells

The expression of calcium reporters in olfactory rod cells was initially a promising tool for investigating their functions, as it gave the opportunity to perform two-photon calcium imaging. I tested for influxes in intracellular calcium following exposure to various potential stimuli, such as food odorants and mechanical stimuli; however, fluorescence levels in the OE were insufficient to yield quantifiable data. Furthermore, increasing the laser power for a better signal would have resulted in injuring or killing the larvae. Therefore, I was not able to use the *Tg(elavl3:GcaMP6f)* or *Tg(Xla.Tubb:GcaMP7f)* lines to gain insight into what activates olfactory rod cell activity.

Since transgenes driven by a *sox10* promoter label the whole olfactory rod cell, a possible alternative would be to create a new calcium reporter transgenic line under this promoter by using CRISPR/Cas9 technology to knock out GFP and replace with GCaMP or jRGECO1a (Dana et al., 2016) in *Tg(sox10:GFP)* embryos (Carney et al., 2006). This would hypothetically result in a strong calcium reporter expression in the cell of interest, and would be valuable for future calcium imaging experiments and functional characterisation.

4.3.3. Use of transgene expression to interpret scRNA-seq datasets

Data from this transgene screen may be used in scrutinising existing scRNA-seq datasets to transcriptomically analyse olfactory rod cells. The most relevant scRNA-seq dataset to highlight is one published by Peloggia et al. (2021), which was used to analyse the transcriptomes of neuromast-associated (Nm) ionocytes in zebrafish. The cell population that

was sequenced was FACS-sorted for GFP expression from the skin and superficial organs of *Tg(cldnb:lyn-eGFP)* transgenic larvae. Since my results revealed olfactory rod cells express GFP under a *cldnb* promoter, they would also theoretically be captured within Peloggia et al.'s (2021) sample. Thus, it may be possible to filter this dataset for cells negative for *omp*, *trpc2*, and *pou4f3*, positive for *elavl3* and *tubb* expression, and with low expression of *cldnh*, for example, to annotate an olfactory rod cell cluster. With this said, this may prove to be tricky as olfactory rod cells are extremely sparse, and as mentioned previously for the *sox10* promoter, a limitation of these experiments is that transgene expression may not reflect true gene expression. The identification of a unique gene marker by mRNA expression may instead be a more effective starting point.

4.3.4. Concluding remarks

The screening of transgenic lines reported here is by no means conclusive or exhaustive. Other candidate lines could have also been screened; for example, many transgenic lines in the Zebrafish Gene Trap and Enhancer Trap Database (zTrap; Kawakami et al., 2010), generated by the Kawakami lab, have expression in the OE, including nk2aET/hspGGFF2A (ZFIN) which curiously appears to have a strong expression in the lateral sides of the olfactory pits at 3 dpf (zTrap). However, the list I selected here makes for a solid starting point. There are limitations to the use of various gene promoters, and results may be variable with different interpretations. Nonetheless, these initial results provide candidates for the cell's potential gene expression signature which will ultimately become useful for future functional and transcriptomic analyses.

Chapter 5. Mechanosensation and expression of *adgrg6* in olfactory rod cells

5.1. Introduction

Actin-rich projections on sensory cells are known to have mechanosensory (reviewed in Gillespie and Müller, 2009), chemosensory (Höfer and Drenckhahn, 1999; Hansen et al., 2002; Zachar and Jonz, 2012), or multimodal functions (for example in CSF-cNs in zebrafish; Djenoune et al., 2014; Desban et al., 2019). Mechanosensation in the olfactory system has been reported in various model organisms, such as mice (Grosmaitre et al., 2007; Iwata et al., 2017), *Xenopus laevis* tadpoles (Brinkmann and Schild, 2016), *Manduca sexta* moths (Tuckman et al., 2021) and *Apis mellifera* honey bees (Tiraboschi et al., 2021); in these contexts, mechanosensation enhances the perception and processing of odours (Grosmaitre et al., 2007). Although responses to mechanostimulation have been reported in the zebrafish OE (Rayamajhi et al., 2023), a physiological reason for mechanosensation in the fish olfactory system is yet to be characterised. Zebrafish have motile cilia that contribute to odour detection (Reiten et al., 2017), thus there is a potential role for mechanosensation in the OE to detect changes in water flow or viscosity, for example, to feedback into the control of motile cilia beat dynamics.

Adgrg6, an adhesion class G-protein-coupled receptor (aGPCR), has a role in inner ear morphogenesis and PNS myelination (Whitfield et al., 1996; Monk et al., 2009, 2011; Geng et al., 2013), and is also proposed as a mechanosensor (reviewed in Baxendale et al., 2021). DIG-ISH data from Geng et al. (2013) showed expression of *adgrg6* mRNA in a sparse group of cells in the developing zebrafish OE at 24, 48, and 72 hpf (see Figure 1.8), but not much else is known about *adgrg6* in the olfactory system. Thus, I was keen to explore this gene further in the context of the olfactory system and mechanosensation.

Firstly, by utilising various staining methods, I aimed to analyse *adgrg6* expression at other developmental stages in the zebrafish OE, identify the olfactory cell type that expresses this gene, and check for any abnormalities in the OE of *adgrg6* mutant larvae. Secondly, I aimed

to test whether *adgrg6*-expressing cells in the OE can be activated by Adgrg6 receptor ligands or by treatment with candidate agonist compounds, identified for their rescuing ability of otic and/or myelination defects in hypomorphic *adgrg6* zebrafish mutants (see Table 2.3). I also planned to examine whether the cells can be activated in response to mechanostimulation. Finally, I hypothesised that dysfunction in the putative mechanoreceptive aGPCR would affect the dynamics of motile cilia, thus, I sought to observe whether control of cilia beat frequency (CBF) is affected in *adgrg6* zebrafish mutants.

5.2. Results

5.2.1. *Adgrg6*-expressing cells are posterolaterally located in the larval olfactory pit

To observe the mRNA transcript expression pattern of *adgrg6* in the zebrafish OE, I repeated a standard DIG-ISH in 5 dpf stage wild-type larvae using a DIG-labelled RNA probe complementary to *adgrg6* (Geng et al., 2013). The staining results showed very specific *adgrg6* expression limited to roughly 10–20 rounded-shaped cells per olfactory pit (*N* of larvae imaged = 6). The majority of these cells were posterolaterally located in the pit and apically located in the epithelium (Figure 5.1A, A'). Fascinatingly, this correlated with my previous data on the general numbers, location, and distribution of olfactory rod cells (Figure 5.1B).

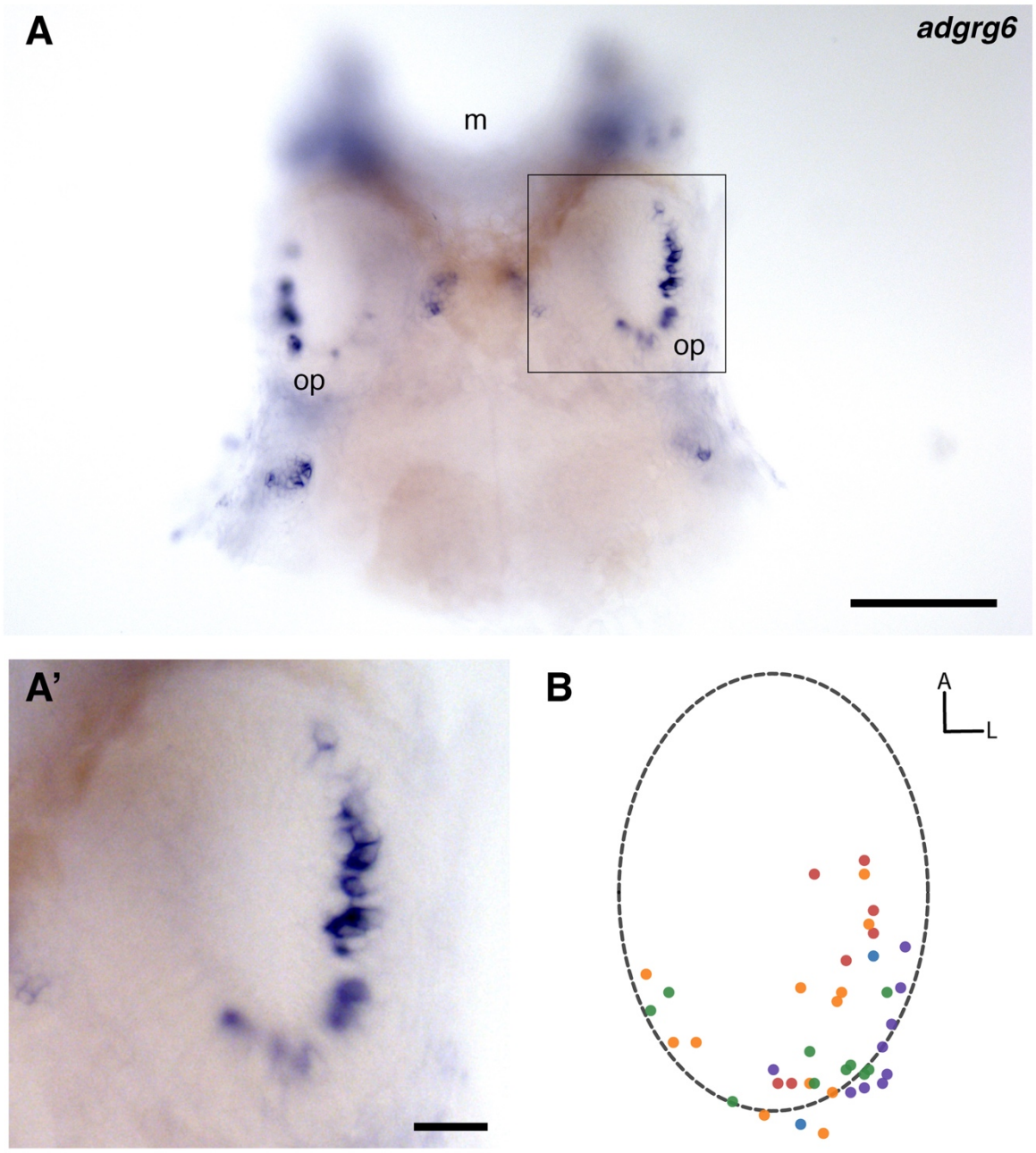

Figure 5.1. *Adgrg6*-expressing cells are apically located in the olfactory epithelium, and posterolaterally located in the olfactory pit.

(A) Expression of DIG-labelled *adgrg6* mRNA transcripts in a flat-mounted section of a 5 dpf wild-type larva head; dorsal view, anterior to the top. Abbreviations: m; mouth, op; olfactory pit. Scale bar = 100 µm. **(A')** Enlarged view of boxed area in panel **A**. Scale bar = 20 µm. **(B)** For comparison: a map of the posterolateral distribution of olfactory rod cell projections in olfactory pits of 4 dpf wild-type larvae (*N* of olfactory pits = 5), based on 2D maximum intensity projections of confocal images of phalloidin stains; anterior "A" to the top, lateral "L" to the right. One dot represents one olfactory rod. Different coloured dots represent olfactory rods from different larvae (published in Cheung et al., 2021).

5.2.2. *Adgrg6* is a unique gene marker for olfactory rod cells in the larval olfactory epithelium

Due to the remarkable correlation between *adgrg6* expression pattern in the OE and olfactory rod cell distribution, I next sought to investigate if olfactory rod cells are the cell type that expresses this gene. To do so, I performed HCR RNA-FISH (Choi et al., 2010, 2014, 2016, 2018), a fluorescence-based method that would allow me to visualise mRNA expression simultaneously with a transgenic marker for olfactory rod cells. The expression pattern from HCR RNA-FISH matched standard DIG-ISH staining; weak but specific expression in the inner ears (not shown) and cranial neuromasts, and strong posterolateral expression in the olfactory pits were consistently observed (Figure 5.2).

HCR RNA-FISH in 5 dpf *Tg(actb2:Lifeact-RFP)* larvae revealed that all *adgrg6*-expressing cells possessed an apical Lifeact-RFP-positive rod projection, and vice versa (*N* of larvae = 6, *n* of cells = 117; Figures 5.3, 5.4). Additionally, in 5 dpf *Tg(sox10:GFP)* larvae, *adgrg6* expression was colocalised in a subset of GFP-positive cells (*N* = 1, *n* = 20; Figure 5.5). It is therefore deducible that *adgrg6* is exclusively expressed in olfactory rod cells within the OE and is a unique gene marker for this cell type.

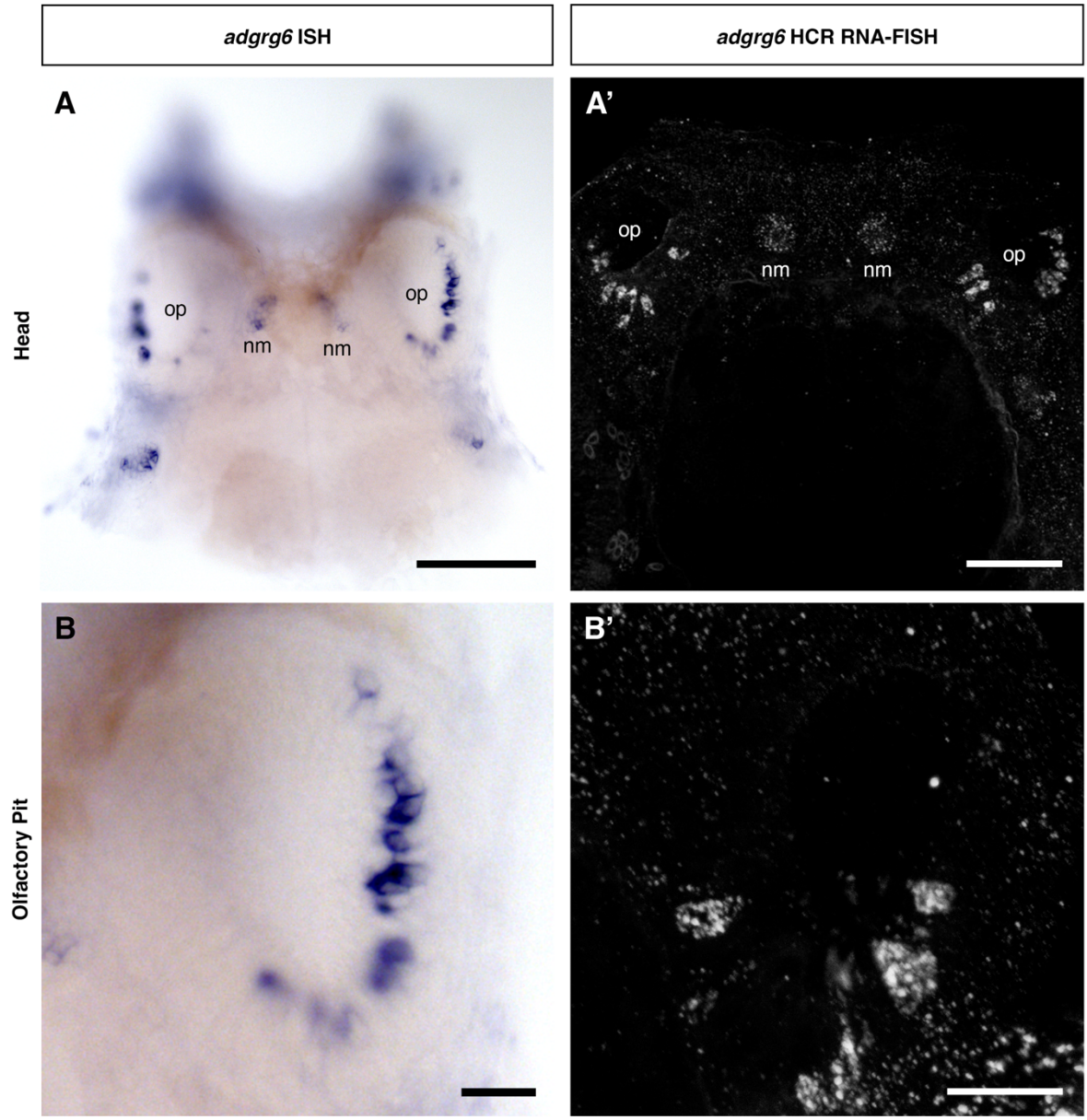

Figure 5.2. *Adgrg6* expression detected by fluorescent *in situ* RNA hybridisation chain reaction corresponds with *adgrg6* expression from *in situ* digoxigenin-labelled RNA hybridisation.

(A, B) DIG-ISH detection of *adgrg6* in a flat-mounted anterior section of the head of a 5 dpf wild-type larva; dorsal view, anterior to the top **(A)**, and olfactory pit of a 5 dpf wild-type larva; dorsal view, anterior to the top, lateral to the right **(B)**. **(A', B')** Maximum intensity projections of confocal images of *adgrg6* HCR RNA-FISH in the head of a 5 dpf wild-type larva; dorsal view, anterior to the top **(A')**, and olfactory pit of a 5 dpf wild-type larva; dorsal view, anterior to the top, lateral to the right **(B')**. Abbreviations: nm, cranial neuromast; op, olfactory pit. Scale bars = 100 µm in **A**, 50 µm in **A'**, 20 µm in **B** and **B'**.

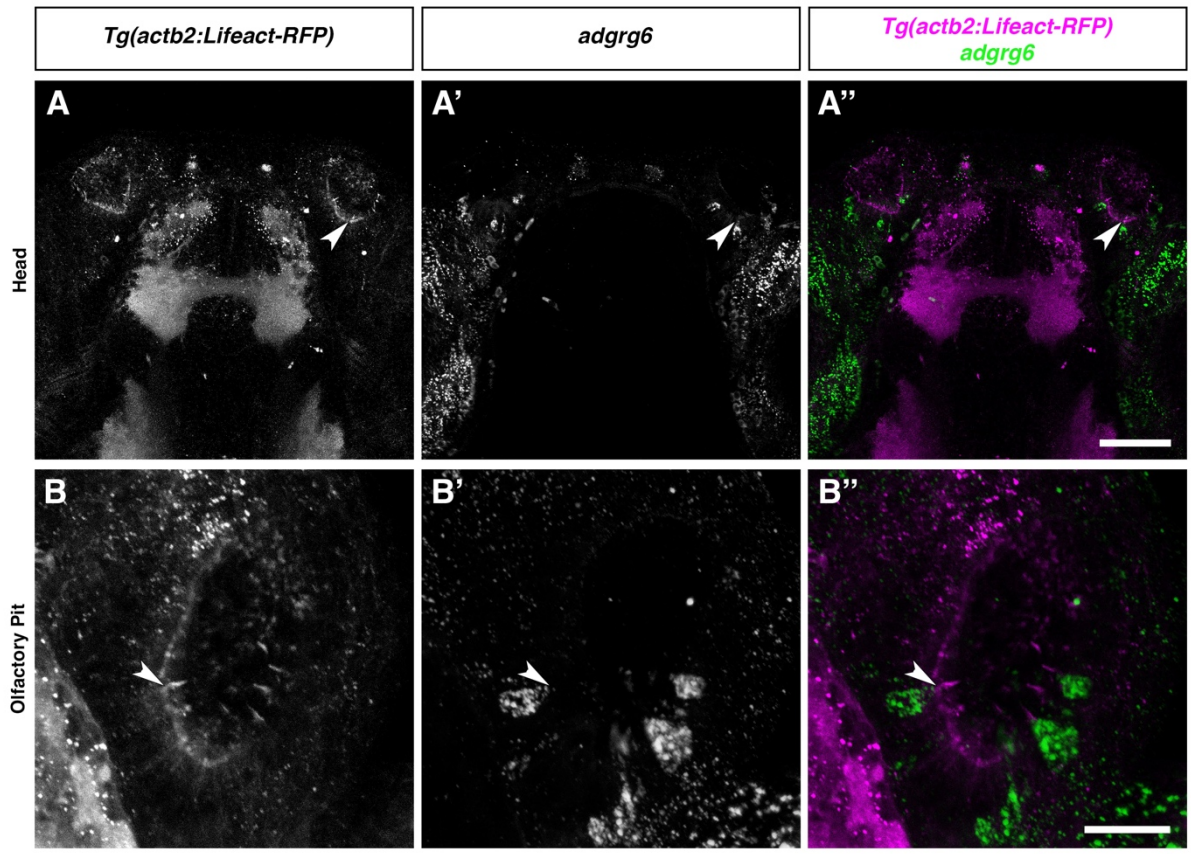

Figure 5.3. *Adgrg6*-expressing cells contain a Lifeact-RFP-labelled olfactory rod projection.

(A–A'') Maximum intensity projection of confocal image of *Tg(actb2:Lifeact-RFP)* signal **(A)**, *adgrg6* HCR RNA-FISH signal **(A')**, and merged signals **(A'')** in a 5 dpf wild-type larval head; dorsal view, anterior to the top. Scale bar = 50 µm. **(B–B'')** Maximum intensity projection of confocal image of *Tg(actb2:Lifeact-RFP)* signal **(B)**, *adgrg6* HCR RNA-FISH signal **(B')**, and merged signals **(B'')** in an olfactory pit of a 5 dpf wild-type larva; dorsal view, anterior to the top, lateral to the right. Arrowheads mark example olfactory rod cells. Scale bar = 20 µm.

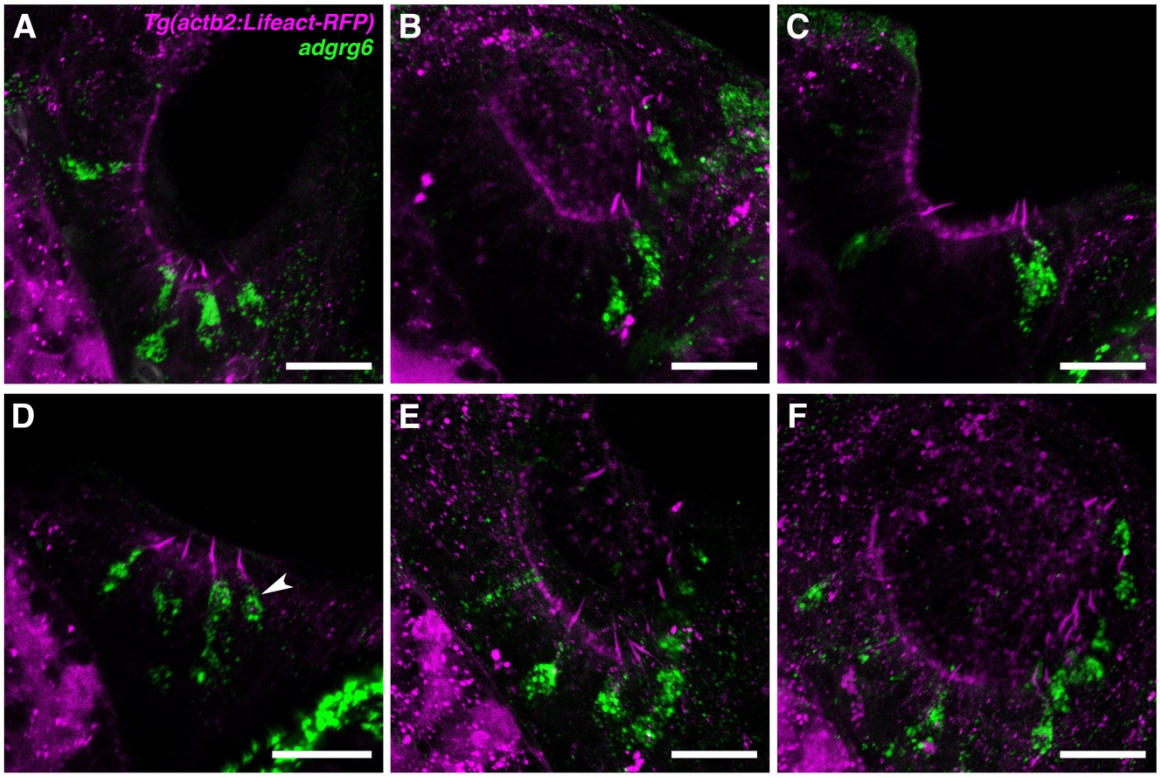

Figure 5.4. All *adgrg6*-expressing cells contain a Lifeact-RFP-labelled olfactory rod projection.

(A–F) Additional examples of maximum intensity projections of confocal images of merged *Tg(actb2:Lifeact-RFP)* (magenta) and *adgrg6* HCR RNA-FISH (green) signals in six individual olfactory pits of 5 dpf wild-type larvae (*N* of larvae = 6); dorsal view, anterior to the top, lateral to the right. Note: any *adgrg6*-expressing cell body with no visible Lifeact-RFP-positive rod projection, or any rod projection with no visible corresponding *adgrg6*-expressing cell body in these images is due to part of the cell lying outside of the *z*-slice ranges in the maximum intensity projections. Arrowhead marks an example olfactory rod cell. Scale bars = 20 µm.

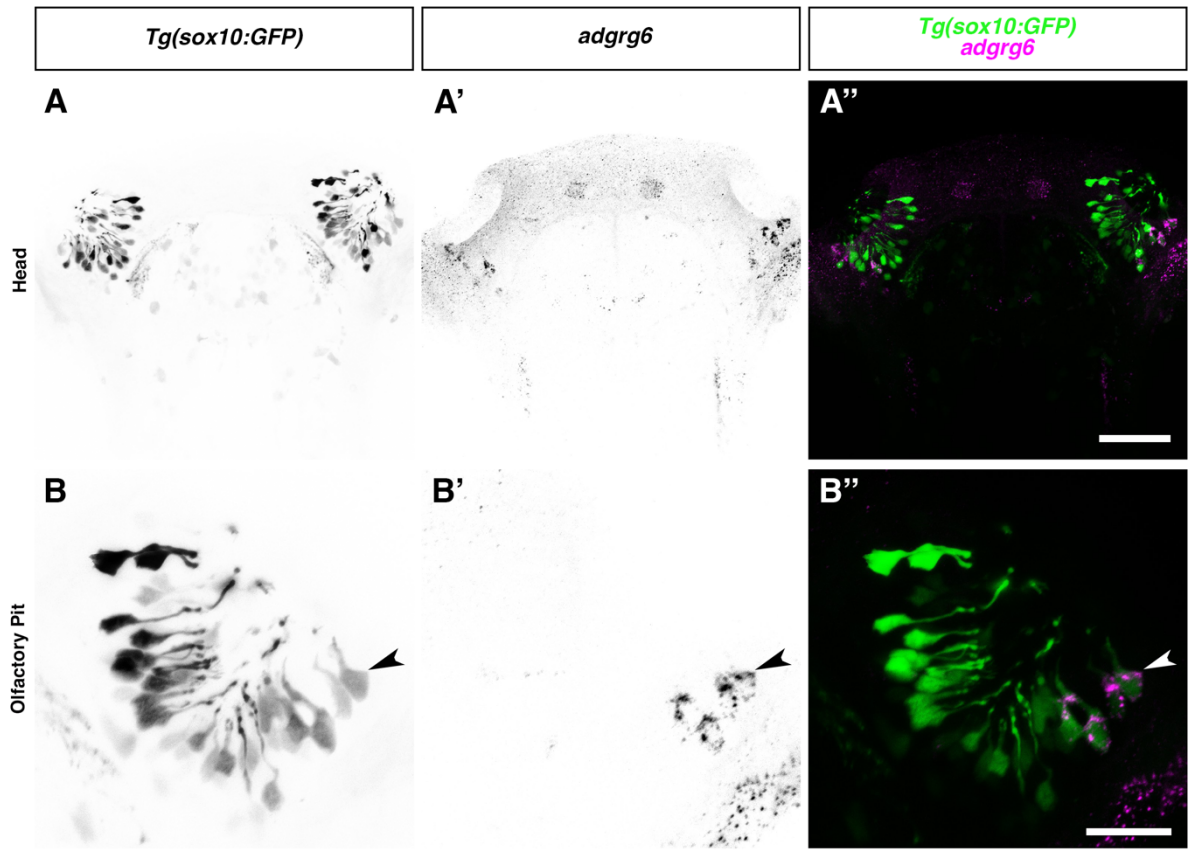

Figure 5.5. *Adgrg6* is expressed in a subset of *Tg(sox10:GFP)*-positive cells.

(A–A'') Maximum intensity projection of confocal image of *Tg(sox10:GFP)* signal with greyscale values inverted **(A)**, *adgrg6* HCR RNA-FISH signal with greyscale values inverted **(A')**, and merged signals **(A'')** in a 5 dpf wild-type larval head; dorsal view, anterior to the top. Scale bar = 50 µm. **(B–B'')** Maximum intensity projection of confocal image of *Tg(sox10:GFP)* signal with greyscale values inverted **(B)**, *adgrg6* HCR RNA-FISH signal with greyscale values inverted **(B')**, and merged signals **(B'')** in an olfactory pit of a 5 dpf wild-type larva; dorsal view, anterior to the top, lateral to the right. Arrowheads mark an example olfactory rod cell body. Scale bar = 20 µm.

5.2.3. *Adgrg6*-expressing olfactory rod cells are present in the adult zebrafish olfactory organ

My data on olfactory rod cells have so far been limited to larval and juvenile stages, as it had previously been tricky to detect the cells in the larger adult olfactory organ with no distinctive marker. The identification of a unique gene marker for the cell bodies subsequently allowed me to investigate the presence and distribution of olfactory rod cells in adults. I performed HCR RNA-FISH on dissected olfactory organs from adult *Tg(actb2:Lifeact-RFP)* fish, with probe sets for *adgrg6* alongside *cldn3c*, which is expressed in most sensory cells in the OE (used here

only to visualise the morphology of the rosette). I observed that *adgrg6* was expressed in adult olfactory organs (*N* of rosettes = 6; Figure 5.6A–A'''). *Adgrg6*-expressing cell bodies were predominantly clustered on the tips of the lamellae, with near to none in the medial portions (Figure 5.6B–B'''); this expression pattern corresponded with the non-sensory region of the OE, as reported by Bayramli et al. (2017). *Adgrg6* expression often colocalised with actin-rich puncta, labelled strongly by the Lifeact-RFP transgene, and in many instances, olfactory rod projections were also visible, extending from cell bodies (Figure 5.6C–C'''). This suggests that olfactory rod cells are present from early embryonic stages through to adulthood.

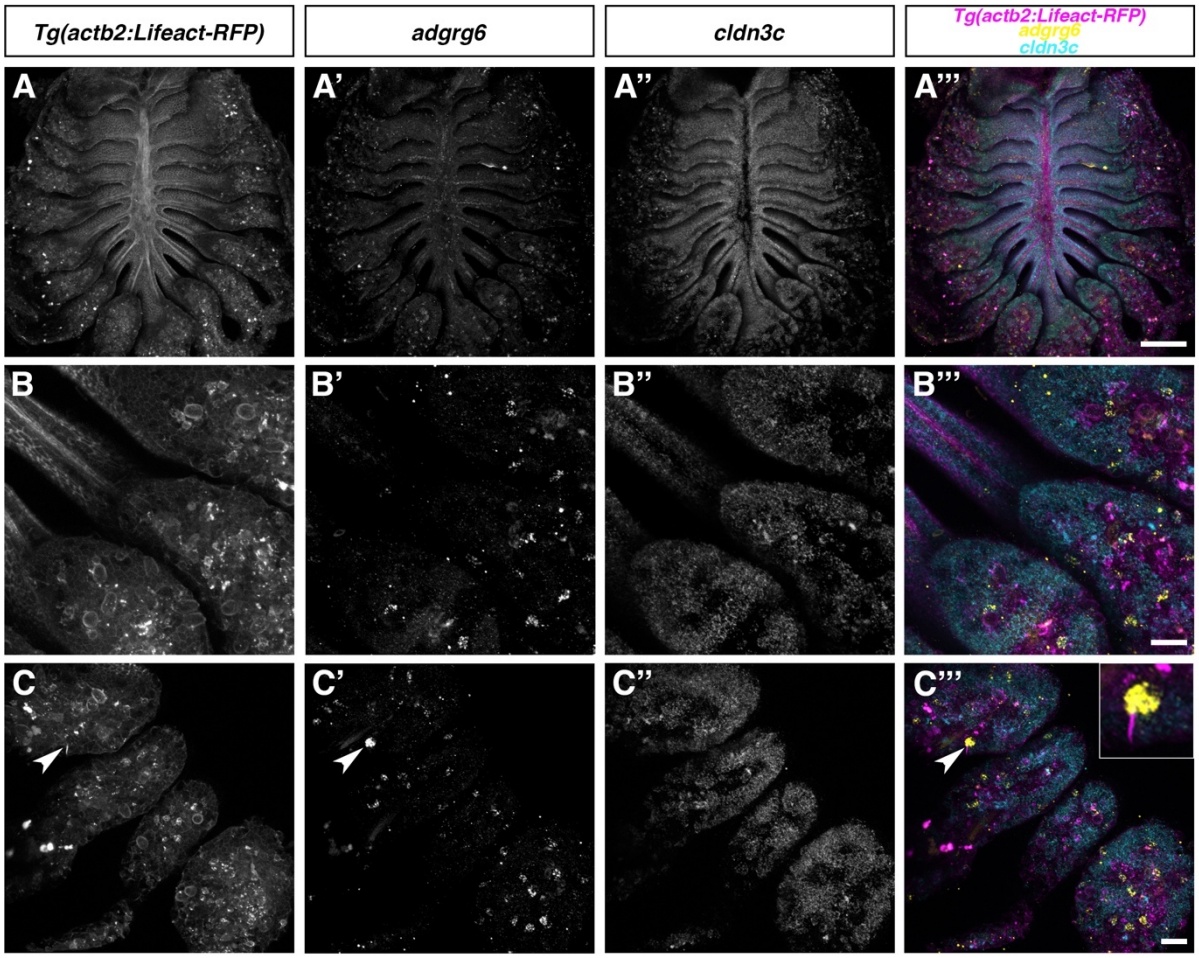

Figure 5.6. *Adgrg6*-expressing olfactory rod cells are present in the non-sensory regions of adult olfactory organs.

(A–A''') Maximum intensity projection of confocal image of *Tg(actb2:Lifeact-RFP)* signal **(A)**, *adgrg6* HCR RNA-FISH signal **(A')**, *cldn3c* HCR RNA-FISH signal **(A'')**, and merged signals **(A''')** in a dissected olfactory organ from a wild-type adult zebrafish. Scale bar = 100 µm. **(B–C''')** Maximum intensity projections of higher power confocal images of the sensory lamellae and non-sensory lamellar tips in the lower right region **(B–B''')** and lower left

region **(C–C’’’)** of the dissected olfactory organ shown in **A–A’’’**; *Tg(actb2:Lifeact-RFP)* signal **(B, C)**, *adgrg6* HCR RNA-FISH signal **(B’, C’)**, *cldn3c* HCR RNA-FISH signal **(B’’, C’’)** and merged signals **(B’’’, C’’’)**. Insert in **C’’’** shows an example olfactory rod cell (arrowhead), with *adgrg6*-expressing cell body (yellow) and a Lifeact-RFP-positive apical rod projection (magenta). Scale bars = 20 µm.

5.2.4. Development of olfactory rod cells is not affected by mutations in *adgrg6*

To examine if formation of olfactory rod cells is affected by early stop codon and missense mutations in *adgrg6*, I stained embryos from two mutant strains, *adgrg6*$^{fr24-/-}$ and *adgrg6*$^{tk256a-/-}$ respectively (Whitfield et al., 1996; Geng et al., 2013), with Alexa-phalloidin at 4 dpf. The resulting confocal images showed that olfactory rods were present in all homozygous mutant individuals in similar numbers, sizes, and distributions compared with phenotypically wild-type siblings (Figure 5.7A–A’’). There was no statistical difference in the number of olfactory rods per olfactory pit between *adgrg6*$^{fr24-/-}$ mutants (9.6 ± 2.4 [mean ± s.d.], *N* of olfactory pits = 8) and their wild-type siblings (10.3 ± 1.5 [mean ± s.d.], *N* = 3; Figure 5.7B). Moreover, no statistical difference was observed in the lengths of olfactory rods between *adgrg6*$^{fr24-/-}$ mutants (9.6 ± 2.1 [mean ± s.d.] µm, *n* of olfactory rods = 67) and their wild-type siblings (9.4 ± 1.4 [mean ± s.d.] µm, *n* = 26; Figure 5.7C), thus indicating that *adgrg6* function is not necessary for the formation of olfactory rod cells at the larval stage.

Curiously, MCCs, which are the ‘hexagonal’ cells to the right (lateral side) of the opening of the olfactory pits in Figure 5.7A–A’’ (see also Movie 5.1), appeared to be somewhat affected by the mutations in *adgrg6*. There were irregular ‘gaps’ in the lateral patches of MCCs in both *adgrg6*$^{fr24-/-}$ and *adgrg6*$^{tk256a-/-}$ mutant larvae (see arrows in Figure 5.7A’, A’’), suggesting some MCCs may be deformed or dysfunctional.

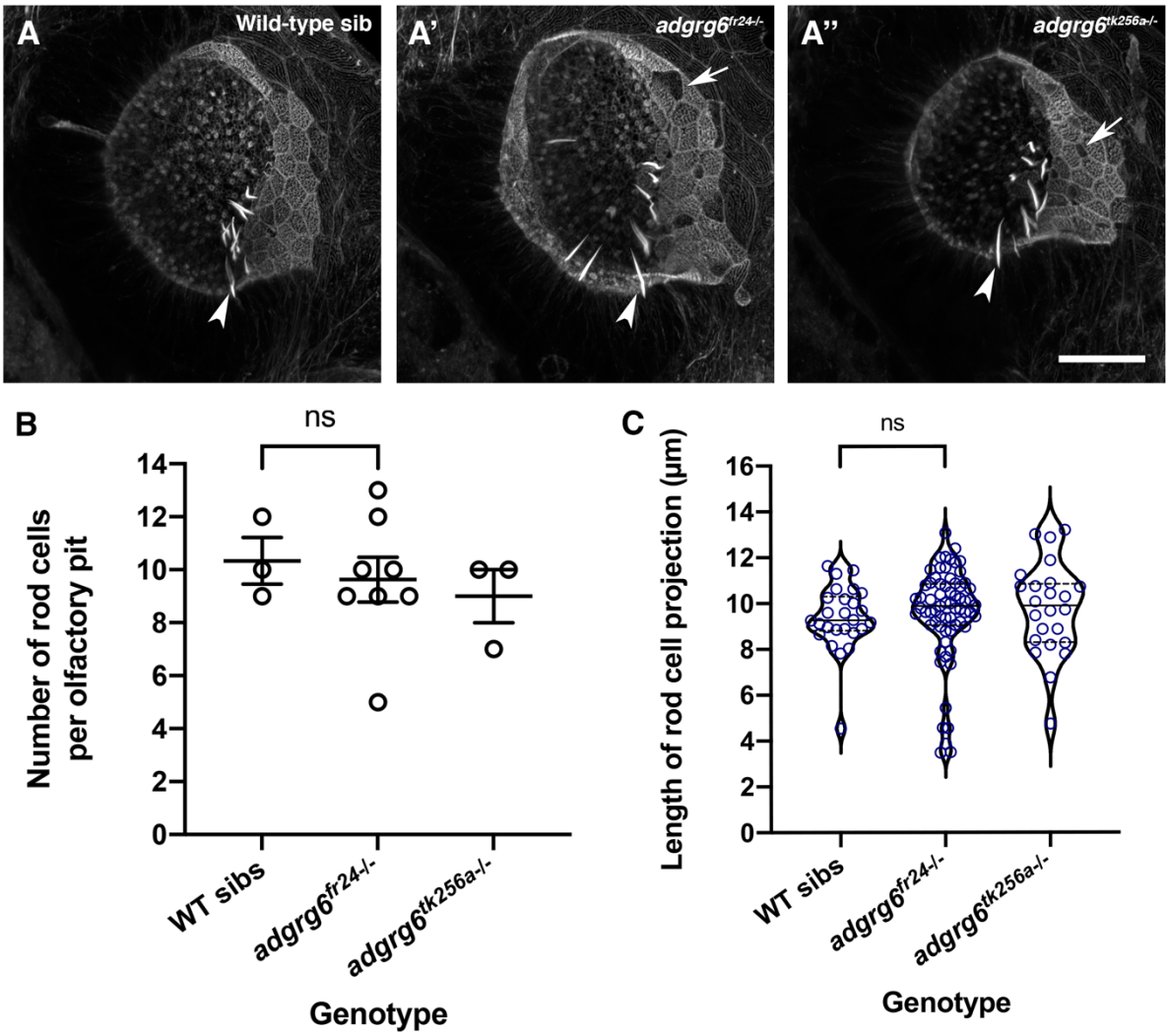

Figure 5.7. Formation of olfactory rod projections is unaffected by homozygous mutations in *adgrg6*.

(A–A'') Maximum intensity projections of Airyscan confocal images of olfactory pits stained with Alexa-phalloidin in a 4 dpf *adgrg6*^{fr24} phenotypically wild-type sibling **(A)**, *adgrg6*$^{fr24-/-}$ mutant (protein-truncating allele) **(A')**, and *adgrg6*$^{tk256a-/-}$ mutant (hypomorphic allele) **(A'')**. Anterior to the top, lateral to the right. Arrowheads mark example olfactory rods. Arrows mark example 'gaps' in the lateral patches of MCCs in *adgrg6*$^{fr24-/-}$ and *adgrg6*$^{tk256a-/-}$ mutant larvae. Scale bar = 20 µm. (See also Movie 5.1.) **(B)** Number of olfactory rods per olfactory pit in 4 dpf *adgrg6*^{fr24} phenotypically wild-type siblings (*N* of olfactory pits = 3), *adgrg6*$^{fr24-/-}$ mutants (*N* = 8), and *adgrg6*$^{tk256a-/-}$ mutants (*N* = 3). Bars indicate mean ± S.E.M. for each group. Welch's two-tailed *t*-test between wild-type siblings and *adgrg6*$^{fr24-/-}$; ns, not significant (*P* = 0.5831). **(C)** Lengths of olfactory rod cell projections in 4 dpf *adgrg6*^{fr24} phenotypically wild-type siblings (*n* of olfactory rods = 26), *adgrg6*$^{fr24-/-}$ mutants (*n* = 67), and *adgrg6*$^{tk256a-/-}$ mutants (*n* = 24). Violin plot; bars indicate the median and lower and upper quartiles for each group. Mann-Whitney *U* test between wild-type siblings and *adgrg6*$^{fr24-/-}$; ns, not significant (*P* = 0.1382).

5.2.5. Modulation of Adgrg6 receptor signalling with ligands and candidate agonists may trigger a response in olfactory rod cells

I next aimed to test if activation of the Adgrg6 signalling pathway could trigger olfactory rod cell activity. 6 dpf *Tg(actb2:Lifeact-RFP)* larvae were treated with collagen type IV, an Adgrg6 receptor ligand (Paavola et al., 2014), as well as the candidate Adgrg6 receptor pathway agonist compounds, carapin-8(9)-ene, deoxygedunin, ivermectin, apomorphine hydrochloride, and colforsin (see Table 2.3; Bradley et al., 2019; Diamantopoulou et al., 2019). Colforsin, a forskolin analogue, activates adenylyl cyclase and increases levels of cAMP in any cell. Colforsin-induced activity detected in olfactory rod cells may not be specific to the Adgrg6 signalling pathway, thus, it is used here as a positive control only. To assess cell activity following compound treatment, I performed multiplexed HCR RNA-FISH for expression of *cfos*, an immediate-early gene as a readout for neuronal activity (Krukoff, 1999; Choi et al., 2018; Shainer et al., 2023), and *adgrg6* as a marker for olfactory rod cells. I quantified the Manders' colocalisation coefficients for the proportion of *adgrg6* expression pixels that overlapped with *cfos* expression pixels for each treatment group and compared with the untreated control group (*N* of olfactory pits = 10; Figure 5.8B). Colocalisation of expression of the two genes would indicate stimulation in olfactory rod cells.

I observed a widespread increase in *cfos* expression in the OE following treatment with 25 µM colforsin as expected, and there was an increase in the Manders' colocalisation coefficient with a large Hedges' *g* effect size of 5.66 [95.0% confidence interval (CI) 4.12, 7.75] (*N* = 4; Figure 5.8A, E). Although there were no noticeable increases in *cfos* expression overall in the OE, there were slight increases in the Manders' colocalisation coefficients with medium Hedges' *g* effect sizes following treatments with 0.6 µg/ml collagen IV (1.89 [95.0% CI 0.71, 3.4], *N* = 4; Figure 5.8A, C) and 25 µM carapin-8(9)-ene (1.41 [95.0% CI 0.861, 1.98], *N* = 8; Figure 5.8A, D). The remaining treatment groups did not lead to any increase in Manders' colocalistion coefficients (Figure 5.8A). This result implies that some olfactory rod cells may be able to respond to chemical treatments with collagen IV or carapin-8(9)-ene, possibly via activation of the Adgrg6 receptor signalling pathway.

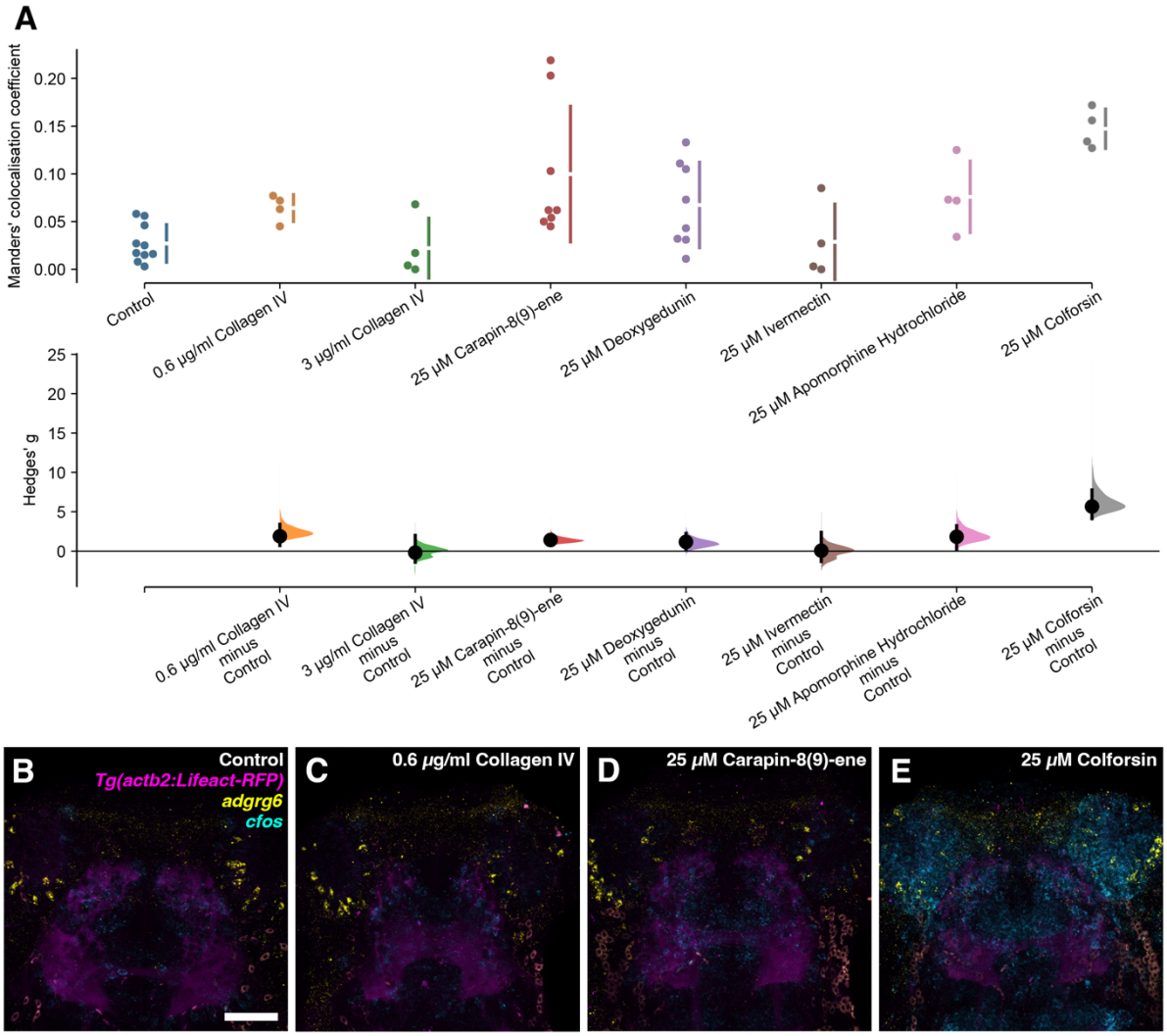

Figure 5.8. Olfactory rod cells may respond to chemical treatment with collagen IV, carapin-8(9)-ene, or colforsin.

(A) Cumming estimation plot showing the mean difference for seven comparisons against the shared control. The proportion of *adgrg6* HCR RNA-FISH signal pixels overlapping with *cfos* HCR RNA-FISH signal pixels for untreated control group (*N* of olfactory pits = 10), 0.6 µg/ml collagen IV (*N* = 4), 3 µg/ml collagen IV (*N* = 4), 25 µM carapin-8(9)-ene (*N* = 8), 25 µM deoxygedunin (*N* = 8), 25 µM ivermectin (*N* = 4), 25 µM apomorphine hydrochloride (*N* = 4), and 25 µM colforsin (*N* = 4) treatment groups, as represented by Manders' colocalisation coefficients, are plotted on the upper axis. Mean differences are plotted as bootstrap sampling distributions on the lower axis, and each mean difference is depicted as a dot. 95.0% CIs are indicated by the ends of the vertical error bars. **(B–E)** Maximum intensity projection of confocal image of merged *Tg(actb2:Lifeact-RFP)* signal (magenta), *adgrg6* HCR RNA-FISH signal (yellow), and *cfos* HCR RNA-FISH signal (cyan) in the head of a 6 dpf wild-type untreated control larva **(B)**, 0.6 µg/ml collagen IV-treated larva **(C)**, 25 µM carapin-8(9)-ene-treated larva **(D)**, and 25 µM colforsin-treated larva **(E)**; dorsal view, anterior to the top. Scale bar = 50 µm.

5.2.6. The zebrafish olfactory epithelium and olfactory rod cells respond to mechanical stimulation

To investigate the mechanosensitivity of the zebrafish OE, I delivered puffs of odourless E3 medium into the left-side olfactory pit of 6 dpf *Tg(actb2:Lifeact-RFP)* larvae, leaving the right-side olfactory pit as an unstimulated contralateral control (Figure 5.9A, B, Movie 5.2), and performed multiplexed HCR RNA-FISH for *cfos* with *adgrg6*. The resulting confocal images showed a stark increase in expression of *cfos* in the mechanostimulated left-side OE compared with the control right-side OE, represented by an increase in mean grey fluorescence value with a large Hedges' *g* effect size of 1.0 [95.0% CI 0.629, 1.5] (*N* of larvae = 4; Figure 5.9C–D). This unambiguously demonstrated that cells in the zebrafish OE, including many OSNs, can respond to mechanical stimuli in a widespread manner. Additionally, there was an increase in the co-expression of *adgrg6* and *cfos* in the mechanostimulated left-side OE compared with the control right-side OE. This was quantified by the Manders' colocalisation coefficient with a large Hedges' *g* of 0.876 [95.0% CI -0.0192, 3.15] (*n* of cells = 77; Figure 5.9E–F''), and denoted that olfactory rod cells can also respond to mechanical stimuli, as hypothesised.

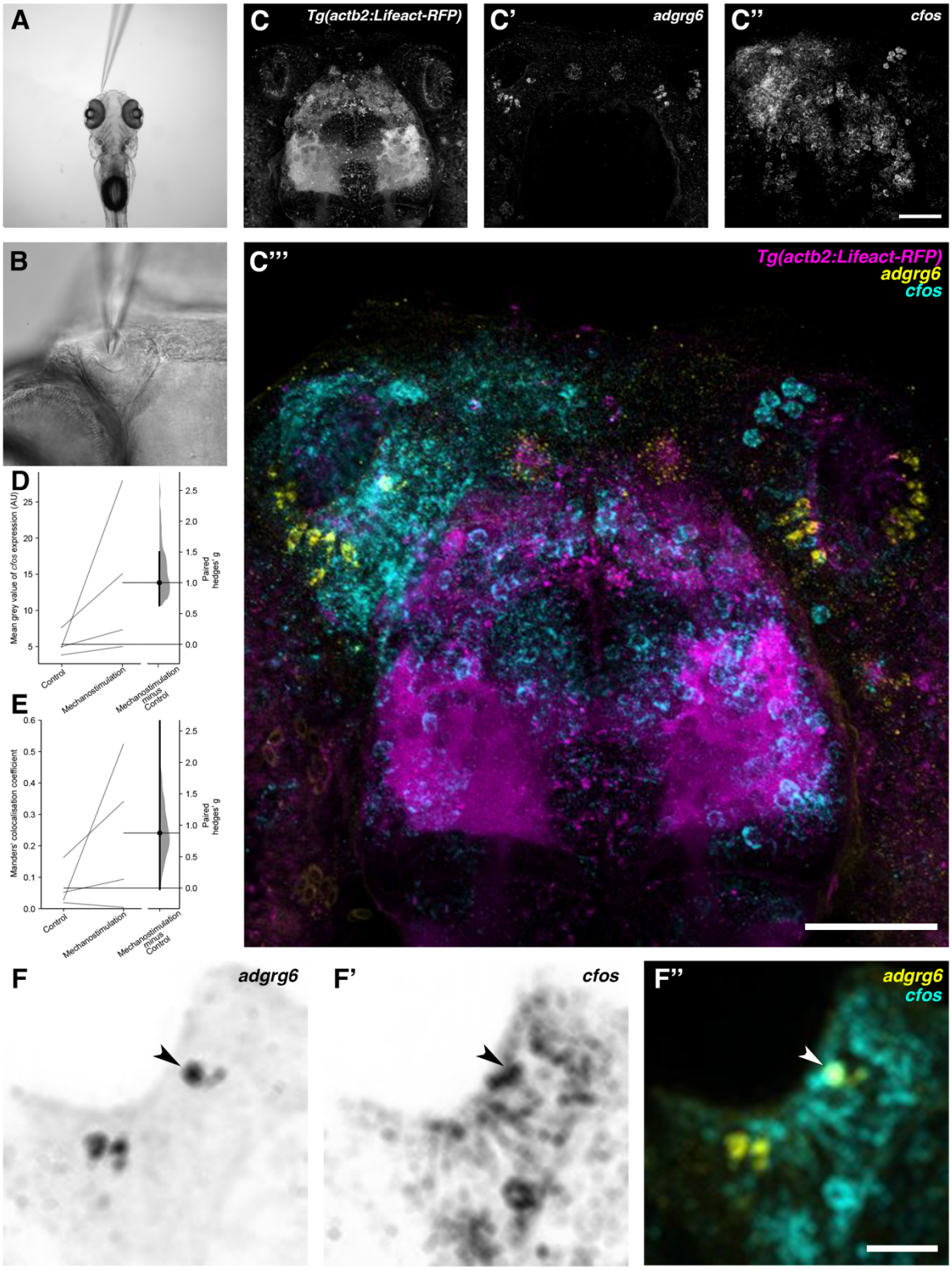

Figure 5.9. The zebrafish olfactory epithelium and olfactory rod cells respond to mechanical stimulation.

(A, B) The set-up for mechanical stimulus delivery into the left-side olfactory pit of 6 dpf *Tg(actb2:Lifeact-RFP)* larva, while leaving the right-side olfactory pit as an unstimulated contralateral control. Pipette shown in the

image is filled with odourless E3 medium and connected to a microinjector. (See Movie 5.2.) **(C–C’’’)** Maximum intensity projection of confocal image of *Tg(actb2:Lifeact-RFP)* signal **(C)**, *adgrg6* HCR RNA-FISH signal **(C’)**, *cfos* HCR RNA-FISH signal **(C’’)**, and merged signals **(C’’’)** in a 6 dpf wild-type larval head following mechanostimulation in the left-side OE; dorsal view, anterior to the top. Scale bars = 50 µm. **(D)** Gardner-Altman estimation plot showing the paired Hedges’ *g* between *cfos* HCR RNA-FISH signal in the mechanostimulated left-side OE and the contralateral control right-side OE (*N* of larvae = 4), as represented by the quantification of mean grey value (arbitrary units). Both groups are plotted on the left axis as a slopegraph with each paired set connected by a line. The paired mean difference is plotted on the right axis as a bootstrap sampling distribution and the mean difference is depicted as a dot. Paired two-tailed permutation *t*-test with estimation statistics; paired Hedges’ *g* = 1.0 [95.0% CI 0.629, 1.5], *P* = 0.0. 95.0% CI is indicated by the ends of the vertical error bar. **(E)** Gardner-Altman estimation plot showing the paired Hedges’ *g* between the proportion of *adgrg6* HCR RNA-FISH signal pixels overlapping with *cfos* HCR RNA-FISH signal pixels in the mechanostimulated left-side OE and the contralateral control right-side OE (*N* of larvae = 4, *n* of *adgrg6*-expressing cells = 77), as represented by the Manders’ colocalisation coefficient. Both groups are plotted on the left axis as a slopegraph with each paired set connected by a line. The paired mean difference is plotted on the right axis as a bootstrap sampling distribution and the mean difference is depicted as a dot. Paired two-tailed permutation *t*-test with estimation statistics; paired Hedges’ *g* = 0.876 [95.0% CI -0.0192, 3.15], *P* = 0.119. 95.0% CI is indicated by the ends of the vertical error bar. **(F–F’’)** Spatially averaged (radius: 3.0 pixels) maximum intensity projection of confocal image of *adgrg6* HCR RNA-FISH signal with greyscale values inverted **(F)**, *cfos* HCR RNA-FISH signal with greyscale values inverted **(F’)**, and merged signals **(F’’)** in the 6 dpf wild-type larva shown in **C–C’’’**, enlarged on the mechanostimulated left-side OE. Arrowheads mark an example of an *adgrg6*-expressing olfactory rod cell with strong co-expression of *cfos* following mechanostimulation. Scale bar = 20 µm.

5.2.7. A mutation in *adgrg6* does not appear to affect cilia beat frequency in high viscosity

As previously mentioned, one possible reason for mechanosensation in the zebrafish OE is to detect changes in fluid flow or viscosity to feedback into the control of motile cilia, and ultimately aid in odour perception. Here, I aimed to assess whether mechanosensory Adgrg6 receptors in olfactory rod cells play a role in the control of CBF in the OE in normal and high viscosity conditions. Olfactory pits of *adgrg6*$^{fr24\text{-}/\text{-}}$ mutants and phenotypically wild-type siblings were imaged at 137–150 Hz in E3 (1 cP; Movies 5.3, 5.5) and then in 4% methyl cellulose in E3 (30 cP; Movies 5.4, 5.6). The changes in CBF were subsequently quantified using a method described by Jeong et al. (2022).

From my analysis, the mean CBF in wild-type siblings at 1 cP was 18.0 ± 1.0 (s.d.) Hz (*N* of olfactory pits = 2; Figure 5.10A). Supporting reports from Ringers et al. (2023), increasing the viscosity of medium to 30 cP decreased the mean CBF to 13.3 ± 1.3 (s.d.) Hz (Figure 5.10B, E). In *adgrg6*$^{fr24-/-}$ mutants, the mean CBF at 1 cP was 21.6 ± 4.0 (s.d.) Hz (*N* = 3; Figure 5.10C), which had similarly decreased to 13.1 ± 2.0 (s.d.) Hz at 30 cP (Figure 5.10D, E). There was a larger range in CBF in *adgrg6*$^{fr24-/-}$ mutant larvae in normal viscosity compared with wild-type siblings, and the CBF also appeared more uniform across the OE, but there were no noticeable differences between the two genotypes in high viscosity from this preliminary imaging. Therefore, it is not yet clear what mechanosensory role Adgrg6 and olfactory rod cells may play in the OE, or how they may affect MCCs.

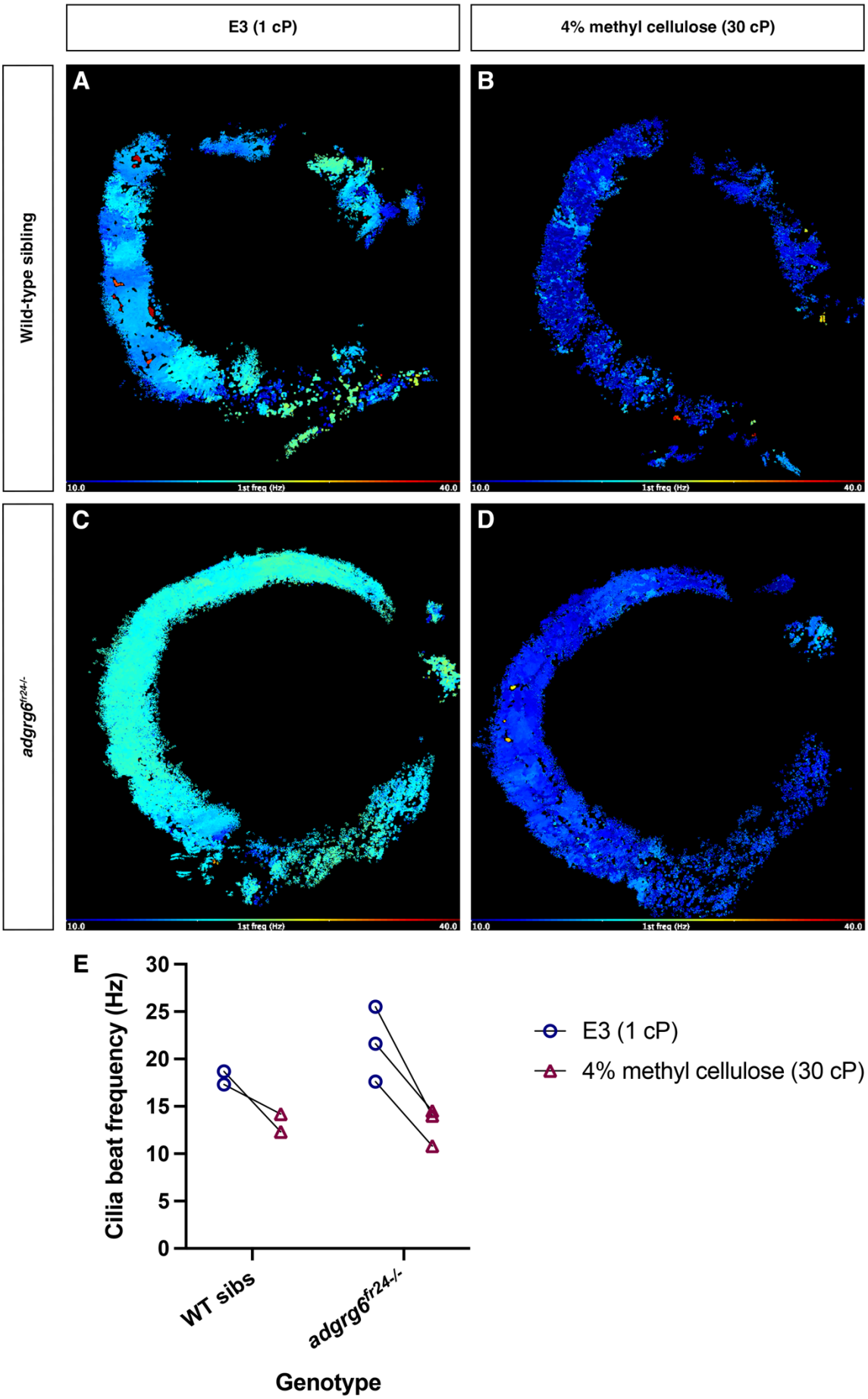
E3 (1 cP)
4% methyl cellulose (30 cP)
Wild-type sibling
adgrg6fr24-/-
A
B
C
D
10.0
1st freq (Hz)
40.0
E
Cilia beat frequency (Hz)
30
25
20
15
10
5
0
WT sibs
adgrg6fr24-/-
Genotype
E3 (1 cP)
4% methyl cellulose (30 cP)

Figure 5.10. Cilia beat frequencies in normal and high viscosity conditions do not appear to be affected in *adgrg6*$^{fr24-/-}$ zebrafish mutants (raw images taken by S. J. Jesuthasan, N. J. van Hateren, and T. T. Whitfield, analysis by K. Y. Cheung).

(A–D) Frequency maps showing peak CBF in each pixel of olfactory pits of a 4 dpf wild-type sibling in E3 (1 cP) **(A)** and in 4% methyl cellulose (30 cP) **(B)**, and 4 dpf *adgrg6*$^{fr24-/-}$ mutant larva in E3 (1 cP) **(C)** and in 4% methyl cellulose (30 cP) **(D)**. (See Movies 5.3–5.6.) **(E)** Grouped plot showing the decrease in CBF (Hz) in response to a high viscosity medium in wild-type siblings and in *adgrg6*$^{fr24-/-}$ mutant larvae. Connecting lines indicate the same olfactory pit. No statistical analyses were carried out due to the small sample size.

5.3. Discussion

I have identified a unique gene marker for olfactory rod cells, as combined data from DIG-ISH and HCR RNA-FISH demonstrated that they exclusively express *adgrg6* in the larval zebrafish OE. Expression pattern of the gene matched the apical and posterolateral distribution of the cells. Moreover, staining in dissected olfactory organs of adults also showed that olfactory rod cells are present in the non-sensory regions of the OE. Although the *adgrg6*-expressing cells in adults were rich in actin, not all *adgrg6*-positive cells contained an obvious rod projection. This was only evident for some cells, and may either indicate that the morphology of the apical projection changes during development and ageing, or it may reflect true heterogeneity in the *adgrg6*-positive cell population in the adult OE. It appeared that *adgrg6* gene is not necessary for the formation of olfactory rods in larvae; however, the role that Adgrg6 receptors play within olfactory rod cell function remains to be elucidated. Finally, my data corroborate previous findings that the zebrafish OE is a mechanosensory tissue. The reasons for mechanosensation in olfactory rod cells are speculated below.

5.3.1. Properties of Adgrg6 receptors and signalling pathway in olfactory rod cells

Despite their location in the so-called non-sensory regions of adult olfactory organs, it does not necessarily mean that olfactory rod cells are non-sensory, but only suggests that they do not express known OR genes. The majority of ORs and VRs belong to class A (rhodopsin-like) GPCRs which have variable sizes of NTFs and CTFs (reviewed in Fleischer et al., 2009; Cong et al., 2019). This differs from the typical large NTF characteristic of aGPCRs. Additionally, as

there is no evidence to suggest that Adgrg6 detects odorants, olfactory rod cells should not currently be classed as another type of OSN.

It is of interest that olfactory rod cells express an aGPCR with a proposed mechanoreceptive role, and that they possess a large oscillating actin-rich apical projection suitable for mechanosensation of the external environment. I had aimed to ascertain where within olfactory rod cells the Adgrg6 receptors are found; perhaps the receptors could be located on the apical rod projection where they bind to external ligands and aid with mechanosensation, or they could be located on the basal side of the cell body where they are in contact with other epithelial cells and bind to ECM components. I performed immunohistochemistry using a commercially available polyclonal antibody (see Materials and Methods section 2.3.2 for details); however, the results were uninterpretable due to a lot of unspecific binding of the antibody. Other methods, including the use of custom-produced antibodies or Ankyrons (next-generation stable recombinant target binding reagents; ProImmune), could instead be used in future experiments to determine the location of Adgrg6 receptors in olfactory rod cells.

It may be possible that olfactory rod cells could be activated by collagen IV and carapin-8(9)-ene via the Adgrg6 signalling pathway, but there were no significant increases in *cfos* expression levels, and these results are ambiguous. The candidate agonists listed in Table 2.3 were identified via high-throughput screens for their ability to rescue mutant phenotypes in hypomorphic *adgrg6* zebrafish mutants only (Diamantopoulou et al., 2019). It is currently unclear where within the signalling pathway these compounds act, or if they are specific to Adgrg6, nor has there been any evidence to suggest that they activate the signalling pathway in wild-type zebrafish. I did not test whether receptor activity via these compounds would additionally require mechanostimulation, for example, in a similar manner to laminin-211-mediated activation (Petersen et al., 2015). As this work is preliminary, aside from *cfos* transcription, I do not address the extent of how modulation of Adgrg6 receptor signalling via ligands or compounds influences olfactory rod cells. Screening the effects of candidate antagonists (compounds that can phenocopy *adgrg6* zebrafish mutants) and further observation of any olfactory phenotype in *adgrg6* mutants would be a more fruitful way to characterise Adgrg6 signalling in the OE in the future.

Results with the use of *cfos* as a readout for neuronal activity (Krukoff, 1999; Shainer et al., 2023) should be interpreted with caution, as activity will not always result in its transcription. Thus, little or no overlapping expression of *adgrg6* and *cfos* does not necessarily suggest that olfactory rod cells were not responding to the stimulus, but only indicates that *cfos* was not transcribed. However, a remarkable increase in *cfos* expression in the OE as a whole following mechanical stimulation undoubtedly demonstrated that the zebrafish OE is a mechanosensory tissue. Much like in the mammalian MOE, OSNs responded to mechanostimulation, and response was widespread. Mechanosensation in mammalian OSNs is dependent on G-protein-coupled ORs; although it is likely that ORs, TAARs, and VRs are present, it is not clear from my data which classes of receptors are responsible for this in zebrafish. For the case of olfactory rod cells, I hypothesise that the proposed mechanoreceptive aGPCR Adgrg6 has a role in mechanosensation.

5.3.2. Association of olfactory rod cells to multi-ciliated cells

I previously observed that olfactory rod cells are posterolaterally clustered in the olfactory pit, but the significance of this is not yet known. It would, however, be surprising if their specific location does not play a part in their function. Made particularly evident in the phalloidin stain images in Figure 5.7A–A'' (see also Movie 5.1), olfactory rod cells, located in the OSN-containing sensory zone of the larval olfactory pit, were consistently located near the border with the lateral cluster of MCCs. HCR RNA-FISH in adult olfactory organs revealed that *adgrg6*-expressing cells were located on the non-sensory lateral tips of rosette lamellae. The OE undergoes a drastic morphological change throughout development from larva to adult, during which it appears the olfactory rod cells migrate from the OSN-containing sensory region and integrate into the MCC-containing non-sensory region, thus retaining their proximity to MCCs. The relative location between the two cell types provides potential evidence that they could be related in function.

There was a serendipitous observation of 'gaps' in the lateral patches of MCCs in the OE of *adgrg6* mutant larvae. This suggests that a mutation in the *adgrg6* gene, and possible dysfunction of olfactory rod cells, may result in a reduction of MCCs or deformation of the cilia

carpet, but further observations are needed. Again, this raises the possibility that *adgrg6* and olfactory rod cell function directly influence MCCs.

The expression of a proposed mechanoreceptive aGPCR in olfactory rod cells, the morphology of the rod projection, the transcription of *cfos* following mechanostimulation, and their close association to MCCs hint at a candidate function for detecting ciliary-driven fluid flow. Thus, I began to investigate this by testing whether Adgrg6 has a role in detecting changes in viscosity to control CBF. From my preliminary data analysis, there was no notable change in CBF in normal or high viscosities between wild-type siblings and *adgrg6*$^{fr24-/-}$ mutants; however, the CBFs were variable and sample sizes were too small for statistical analyses. Further work should be done before drawing conclusions, such as analysis of the effect of water viscosity or flow rate on ciliary coherence across the cilia carpet, in *adgrg6* mutants or in larvae with laser-ablated olfactory rod projections.

5.3.3. *Adgrg6*-expressing microvillous cells in the mammalian main olfactory epithelium

Based on transcriptional profiling data in mice, it has been reported that *adgrg6* is expressed in microvillous cells (MVCs; Baxter et al., 2021). MVCs are a class of pear-shaped cells with a tuft of 'stiff' microvilli on their apical surface found in the mouse MOE, and express components of the taste transduction pathway such as gustducin and TrpM5 channels (Hansen and Finger, 2008; Lin et al., 2008a; Genovese and Tizzano, 2018). They themselves lack axons but are sparsely innervated by trigeminal nerve fibres and are widely considered to act as paraneurons (Fujita, 1989; Carr et al., 1991; Genovese and Tizzano, 2018). MVCs are reportedly almost molecularly and functionally identical to solitary chemosensory cells (SCCs), found in mouse nasal respiratory epithelia and vomeronasal organ ducts, which have sensory and inflammatory functions within the upper respiratory tract. They are known to respond to various chemicals, irritants, bacterial signalling molecules and high concentrations of odorants, and subsequently act via acetylcholine release to locally modulate surrounding cells and trigger protective reflexes such as sneezing (Finger et al., 2003; Gulbransen et al., 2008; Lin et al., 2008b; Tizzano et al., 2010, 2011; Saunders et al., 2014; Genovese and Tizzano, 2018).

As the MOE is directly exposed to the external environment, it acts as the first line of defence and a physical barrier against foreign pathogens entering the brain. It is therefore imperative that a defensive mechanism is in place within the MOE, as well as in the upper respiratory tract, to prevent neuronal damage. As such, it has been found that MVCs are enriched in many transcripts, such as *IL25* and *Il17rb*, coding for proteins with roles in infection, inflammation, and immunity. MVCs can be activated following viral infection, resulting in the triggering of mucociliary clearance by adjacent sustentacular (support) cells via the TrpM5 transduction pathway (Baxter et al., 2021). Furthermore, the importance and necessity of these cells in protecting and maintaining the physiological function of the olfactory system can be demonstrated in *Skn1a*$^{-/-}$ mutant mice, where loss of TrpM5-expressing MVCs causes impaired odour-mediated responses and behaviours (Lemons et al., 2017). Due to the versatile roles that Adgrg6 plays during the innate immune response and Schwann cell regeneration following peripheral nerve injury, Baxter et al. (2021) speculated that Adgrg6 in MVCs may contribute by initiating macrophage recruitment upon viral infection, thereby promoting neurogenesis and survival of OSNs. Although there may be many other potential functions of MVCs, it is yet to be discovered if their tuft of 'stiff' actin-rich apical projections could contribute to the detection of mechanical stimuli, such as airflow through the nasal cavity.

In addition to the mouse MOE, MVCs can also be found in other species, for example in the nasal cavities of the American alligator, *Alligator mississippiensis* (Hansen, 2007). In humans, TRPM5-positive MVCs are characterised as epithelial sensors that locally regulate immunity, while TRPM5-negative MVCs correspond to ionocytes that express cystic fibrosis transmembrane conductance regulator protein (CFTR; Ualiyeva et al., 2023). It is not yet known if MVCs exist in lower vertebrate models such as the zebrafish. Although there is no evidence of *trpm5* expression in the zebrafish OE, other transient receptor potential channel genes, including *trpm2* and *trpm4b*, are expressed there (Kastenhuber et al., 2013).

Olfactory rod cells in the zebrafish OE and MVCs in the mouse MOE both possess distinct actin-rich apical projections, albeit different from each other, and both specifically express *adgrg6* (Baxter et al., 2021; this work, unpublished). Expression of neuronal tubulin is detected in paraneurons (Iwanaga et al., 1982) and is also expected to be present in MVCs, which would be consistent with activity of the *tubb* promoter in olfactory rod cells. Despite one cell type

occurring in a water-living animal while the other in air-breathing animals, there appear to be numerous similarities. Perhaps olfactory rod cells may function similarly to MVCs, and participate in volume release for local modulation of surrounding cells (Genovese and Tizzano, 2018); this remains to be explored. There is now a scope for scrutinisation of zebrafish OE scRNA-seq data to analyse the transcriptome of olfactory rod cells and to compare it to the published MVC transcriptome (Baxter et al., 2021); ultimately, this would determine if they are homologous cell types and may elucidate cell functions.

5.3.4. Concluding remarks

To summarise, I have identified the olfactory cell type in zebrafish that expresses *adgrg6*. Now with a gene marker for olfactory rod cells, it opens various avenues for further characterisation of this rare cell type. Future work could include creating a new transgenic line under an *adgrg6* promoter to visualise only these cells in the OE, testing cell functions based on already established Adgrg6 receptor functions, assessing cell activity in *adgrg6* mutants, and scRNA-seq analysis. Expression of *adgrg6* in zebrafish olfactory rod cells gives rise to the idea that there may be a homologous *adgrg6*-expressing cell type with actin-rich apical specialisations present in the MOE of mammals.

Chapter 6. Transcriptomic analysis reveals potential ionoregulatory functions for olfactory rod cells

6.1. Introduction

6.1.1. Introduction to ionocytes

Ionocytes are non-neuronal mitochondrion-rich cells, predominantly located in kidneys, skin, mammalian lungs, and fish gills, which actively transport ions against their concentration gradients to control ion balance and maintain osmotic homeostasis (reviewed in Hwang and Lee, 2007; reviewed in Hwang and Chou, 2013). Ionocytes are split into four broad classes based on the expression of ion transport proteins and their functions: Na^+,-K^+-ATPase-rich (NaR) ionocytes which uptake calcium, H^+-ATPase-rich (HR) ionocytes which secrete protons, Na^+,-Cl^- co-transporter-expressing (NCC) ionocytes which uptake sodium and chloride, and K^+-secreting (KS) ionocytes which secrete potassium (reviewed in Hwang and Lee, 2007; reviewed in Hwang and Chou, 2013). Different types of ionocytes do not generally share a common typical morphology; for example, TRPM5-negative MVC ionocytes in the olfactory and respiratory epithelia of mice are rounded in shape (Ualiyeva et al., 2023), whereas zebrafish neuromast-associated (Nm) ionocytes are elongated (Peloggia et al., 2021). Both possess apical tufts of microvilli that extend into the external environment, but ionocytes are not normally known to contain a large actin-rich rod-like projection.

In mammals, ionocytes in the airways play a vital role in regulating airway fluid and mucous physiology, and a dysfunction in these cells can lead to cystic fibrosis phenotypes (discussed further in section 6.3.3; Montoro et al., 2018). In marine teleost fish, ionocytes in the kidneys and gills actively secrete excess ions absorbed from seawater. On the other hand, in freshwater teleosts such as zebrafish, ionocytes in the skin and gills actively absorb ions from the external environment, compensating for passive water gain (reviewed in Hwang and Lee, 2007; reviewed in Hwang and Chou, 2013). Ionocytes have a clear physiological importance in the olfactory and respiratory epithelia in mice and humans (Montoro et al., 2018; Ualiyeva et al., 2023), and in the gills of various freshwater and marine fish species (Ferrando, 2008;

Dymek et al., 2021). Ionocytes are known to be located in the zebrafish larval gills, skin, kidney, and lateral line neuromasts (reviewed in Hwang and Lee, 2007; reviewed in Hwang and Chou, 2013; Peloggia et al., 2021; Cazorla-Vázquez et al., 2023), but they have not been described in the OE.

6.1.2. Transcriptomic analysis of *adgrg6*-expressing cells

As *adgrg6* has been identified as a unique gene marker for olfactory rod cells in the larval OE, it opens the possibility for further characterisation of the cell properties by transcriptomic analysis. This would result in the compilation of a comprehensive list of differentially and non-differentially expressed genes in olfactory rod cells, which may provide further indication of the cell functions. Moreover, it would also allow for comparison with scRNA-seq datasets from other species to identify potential homologous cell types.

A scRNA-seq dataset generated from dissected adult zebrafish olfactory organs, published by Kraus et al. (2022), was processed, normalised, and analysed by our collaborator J. Peloggia (T. Piotrowski lab) in the aim of helping us identify markers of olfactory rod cells. After running my own Seurat analysis on the normalised dataset, I generated a uniform manifold approximation and projection (UMAP) model with 13 cell clusters (Figure 6.1A). Although some *adgrg6*-expressing cells were scattered throughout several clusters, the cluster that contained most *adgrg6*-expressing cells was identified as cluster 11 (Figure 6.1B–D). Genes expressed in this cluster included *actb2*, *elavl3*, *cldnb*, and *cldnh*, but not *ompa*, *ompb*, *trpc2a*, *trpc2b*, *foxj1a*, *foxj1b*, or *sox10* (Figure 6.2).

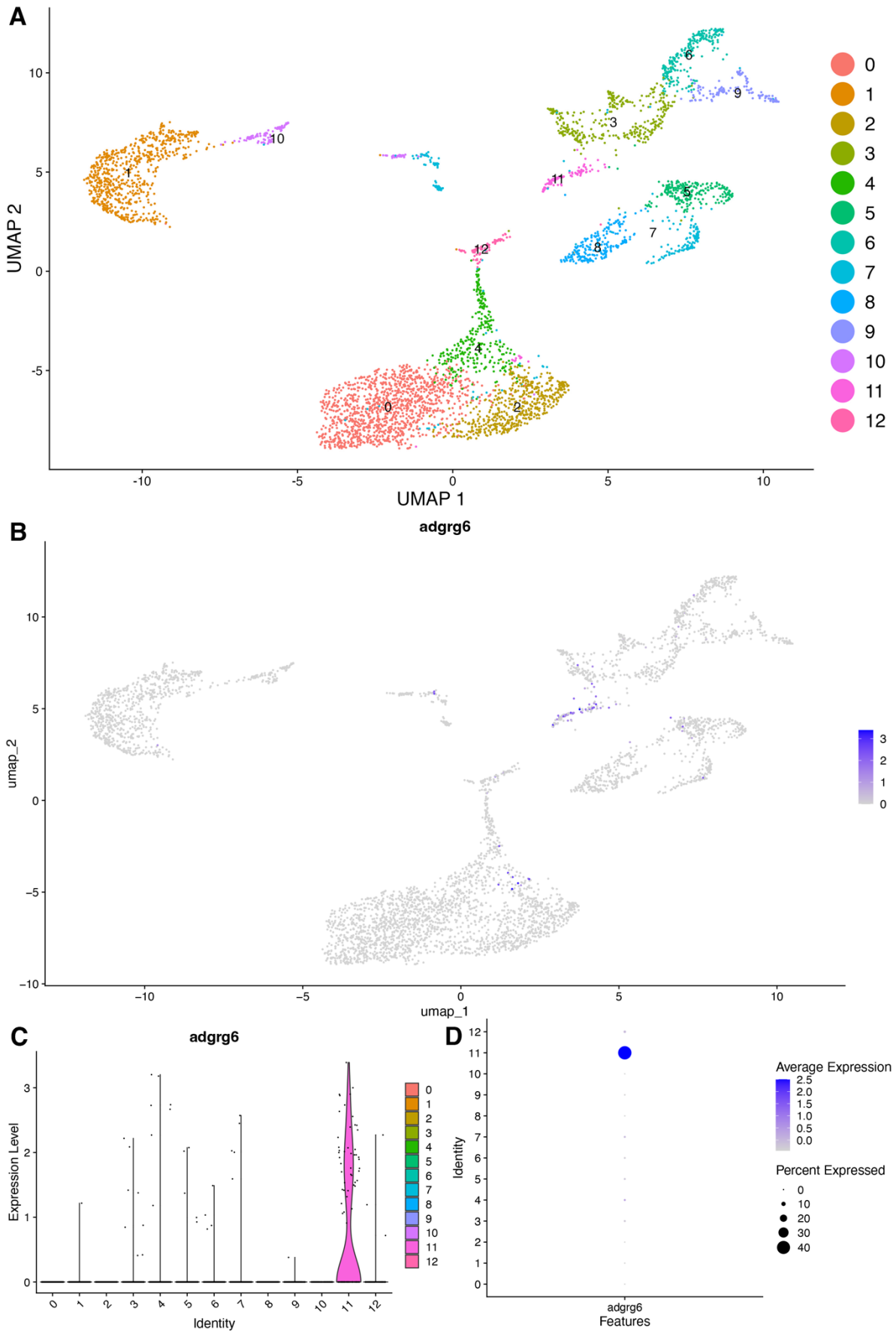
A
UMAP 2
UMAP 1
0
1
2
3
4
5
6
7
8
9
10
11
12
B
adgrg6
umap_2
umap_1
C
adgrg6
Expression Level
Identity
D
Identity
adgrg6
Features
Average Expression
Percent Expressed

Figure 6.1. Identification of an *adgrg6*-expressing cell cluster in scRNA-seq data from dissected adult zebrafish olfactory organs (raw data published in Kraus et al., 2022).

(A) A UMAP plot showing 13 unannotated cell clusters in the scRNA-seq data. **(B–D)** A feature plot **(B)**, violin plot **(C)**, and dot plot **(D)** showing the expression level of *adgrg6* in each cluster. Together, the plots show that cluster 11 is the cluster that contained the most *adgrg6*-expressing cells.

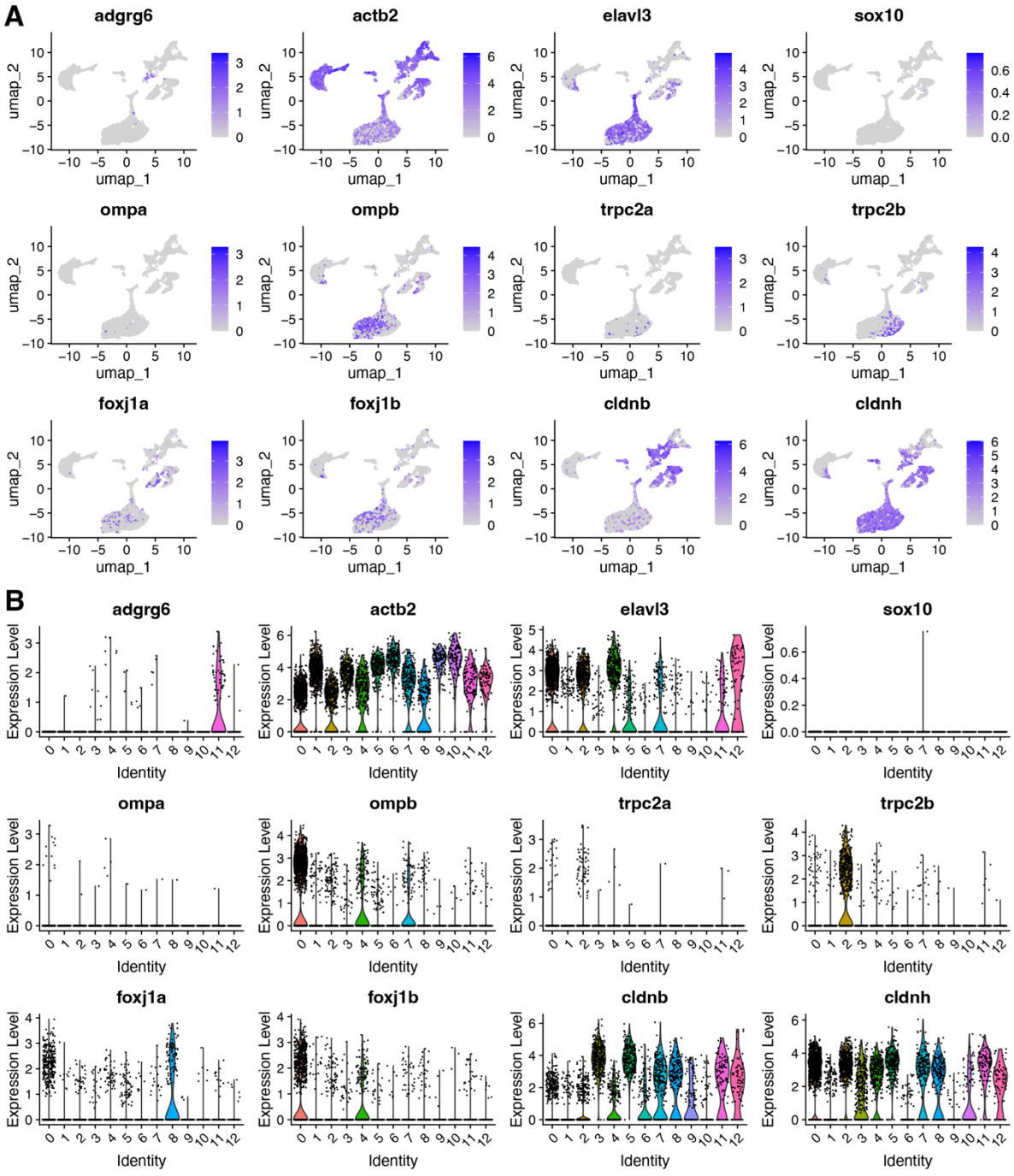

Figure 6.2. Expression of selected gene markers across different cell clusters in scRNA-seq data from dissected adult zebrafish olfactory organs (raw data published in Kraus et al., 2022).

Feature plots **(A)** and violin plots **(B)** showing the expression level of *adgrg6*, *actb2*, *elavl3*, *sox10*, *ompa*, *ompb*, *trpc2a*, *trpc2b*, *foxj1a*, *foxj1b*, *cldnb*, and *cldnh* in each cell cluster (gene markers selected based on previous transgene expression data).

Differential expression analysis between the *adgrg6*-expressing cell cluster and all other cell types yielded a list of 272 differentially expressed genes; the top 20 differentially expressed genes in this population are listed in Table 6.1 (see also Figure 6.3A). Within the top 20 differentially expressed genes were *trpv6*, *gcm2*, *foxi3b*, and *atp1a1a.3* (Figure 6.3), recognised by J. Peloggia as common markers of ionocytes due to their expression Nm ionocytes (Peloggia et al., 2021). *Trpv6*, *gcm2*, and *foxi3b*, are classical markers of, or involved in the differentiation of NaR ionocytes (Hsiao et al., 2007; Chang et al., 2009; Dai et al., 2014; Kumai et al., 2015; Cai et al., 2020), while *atp1a1a* genes code for the alpha 1 subunit of Na^+,-K^+-ATPase involved in sodium and potassium transport (Liao et al., 2009). Additionally, *ceacam1*, another strongly differentially expressed gene in *adgrg6*-expressing cells is a marker of HR ionocytes in the zebrafish epidermis (Kowalewski et al., 2021). This transcriptomic evidence of co-expression of *adgrg6* with common ionocyte-marker genes therefore raises the possibility that olfactory rod cells may be a type of ionoregulatory cell that acts by detecting ion composition in the external environment and pumping ions to maintain homeostasis.

Table 6.1. A list of the top 20 differentially expressed genes in the cluster containing *adgrg6*-expressing cells from a dissected adult zebrafish olfactory organ scRNA-seq dataset (raw data published in Kraus et al., 2022).

No.	Gene
1	*si:dkey-33i11.4*
2	*trpv6*
3	*tpte*
4	*mafbb*
5	*gcm2*
6	*lfng*
7	*ceacam1*
8	*sstr5*
9	*foxi3b*
10	*adgrg6*
11	*ppp1r3ab*
12	*notch1b*
13	*pvalb8*
14	*s100a11*
15	*atp1a1a.3*
16	*ftr99*
17	*pcdh17*
18	*sgk2a*
19	*mylka*
20	*tmprss13a*

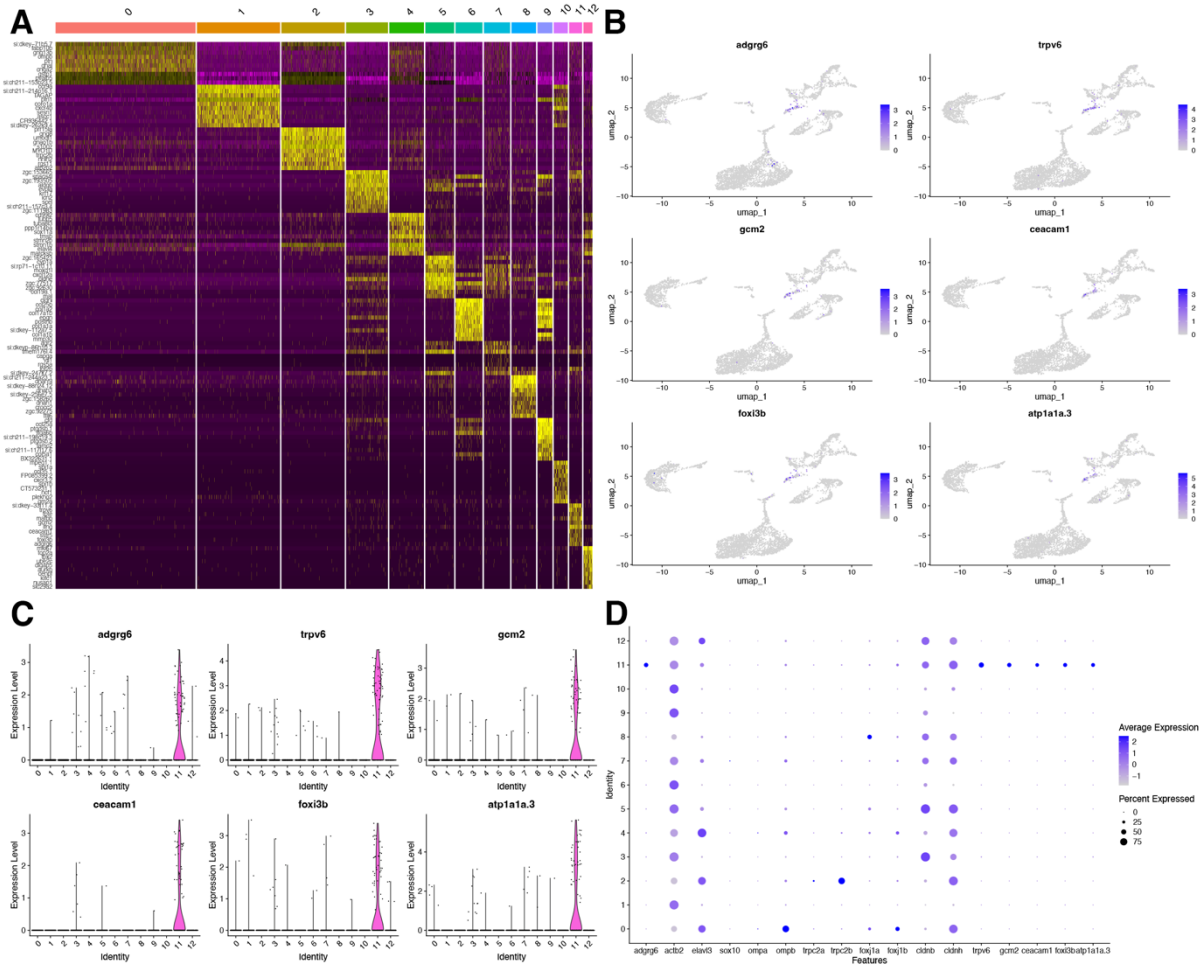

Figure 6.3. Differential expression of ionocyte-marker genes in the *adgrg6*-expressing cell cluster in scRNA-seq data from dissected adult zebrafish olfactory organs (raw data published in Kraus et al., 2022).

(A) A feature expression heatmap showing the top 10 differentially expressed genes in each cell cluster. **(B, C)** Feature plots **(B)** and violin plots **(C)** showing the expression level of *adgrg6* and ionocyte-marker genes *trpv6*, *gcm2*, *ceacam1*, *foxi3b*, and *atp1a1a.3* in each cell cluster. **(D)** A dot plot showing the expression level of *adgrg6* and selected gene markers, including ionocyte-marker genes *trpv6*, *gcm2*, *ceacam1*, *foxi3b*, and *atp1a1a.3*, in each cell cluster.

In this chapter, I aimed to begin to test the idea that olfactory rod cells are ionocytes, by investigating if they express ion transport proteins and by observing if they are affected in environments of different salinities.

6.2. Results

6.2.1. Na^+,-K^+-ATPase is expressed in a rare subset of olfactory rod cells

As an initial test to examine whether olfactory rod cells are a type of ionocyte, I performed a double stain on 5 dpf wild-type larvae with a monoclonal antibody against avian Na^+,-K^+-ATPase (α5 subunit) and Alexa-phalloidin. The resulting staining showed that Na^+,-K^+-ATPase-positive cells, presumably NaR ionocytes, were present in cranial neuromasts and in the OE (Figure 6.4A–A''). In the OE, NaR cells were predominantly located in two separate populations — an anteromedial population and a posterolateral population (Figure 6.4A'). Most of the NaR cells did not correspond to an Alexa-phalloidin labelled olfactory rod, and most of the olfactory rod cells were not labelled against Na^+,-K^+-ATPase; however, although it was not consistent across all larvae, a handful of olfactory rod cells did appear to be labelled (*N* of larvae = 5, *n* of cells = 4; Figure 6.4B–B''). This suggests that a rare subset of olfactory rod cells express sodium-potassium ion pumps and may be involved in ionoregulation.

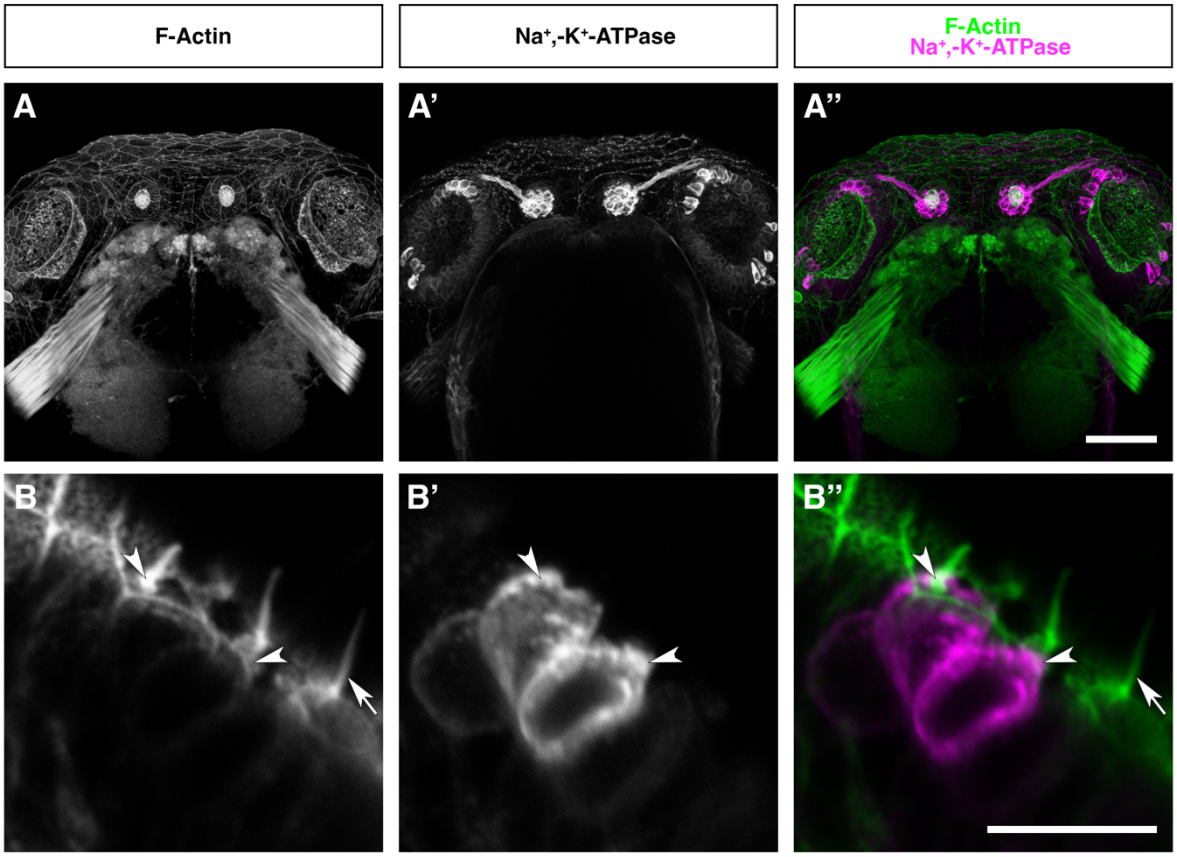

Figure 6.4. A rare subset of olfactory rod cells express Na^+,-K^+-ATPase.

(A–A'') Maximum intensity projection of confocal images of Alexa-phalloidin signal **(A)**, Na^+,-K^+-ATPase (α5 subunit) immunohistochemistry signal **(A')**, and merged signals **(A'')** in the head of a 5 dpf wild-type larva; dorsal view, anterior to the top. Scale bar = 50 µm. **(B–B'')** Enlargement of Alexa-phalloidin signal **(B)**, Na^+,-K^+-ATPase (α5 subunit) immunohistochemistry signal **(B')**, and merged signals **(B'')** in olfactory rod cells in the left OE from row **A**. Arrowheads mark Na^+,-K^+-ATPase-positive olfactory rod cells. Arrows mark a Na^+,-K^+-ATPase-negative olfactory rod cell. Scale bar = 10 µm.

6.2.2. Olfactory rod cell frequency is modulated in a low salinity environment

The frequency of Nm ionocytes is modulated by changes in the external environment. For example, decreasing the salinity of the medium that larvae are incubated in increases the average number of Nm ionocytes per neuromast, and vice versa (Peloggia et al., 2021). To test the effect of changes in salinity on the number of olfactory rod cells, *Tg(actb2:Lifeact-RFP)* larvae were incubated in either MilliQ water (low salinity) or 5× E3 medium (high salinity) at 3 dpf, and subsequently imaged at 5 dpf. The number of olfactory rods per olfactory pit in larvae incubated in high salinity (*N* of olfactory pits = 10) was variable, with a mean of 9.2 ± 4.0 (s.d.), but there was no statistical difference when compared with the control group (11.1 ± 2.4 [mean ± s.d.], *N* = 10). Contrasting with Nm ionocytes, the number of olfactory rods per olfactory pit in larvae incubated in low salinity (*N* = 10) had significantly decreased, with a mean of 4.7 ± 3.9 (s.d.) (Figure 6.5).

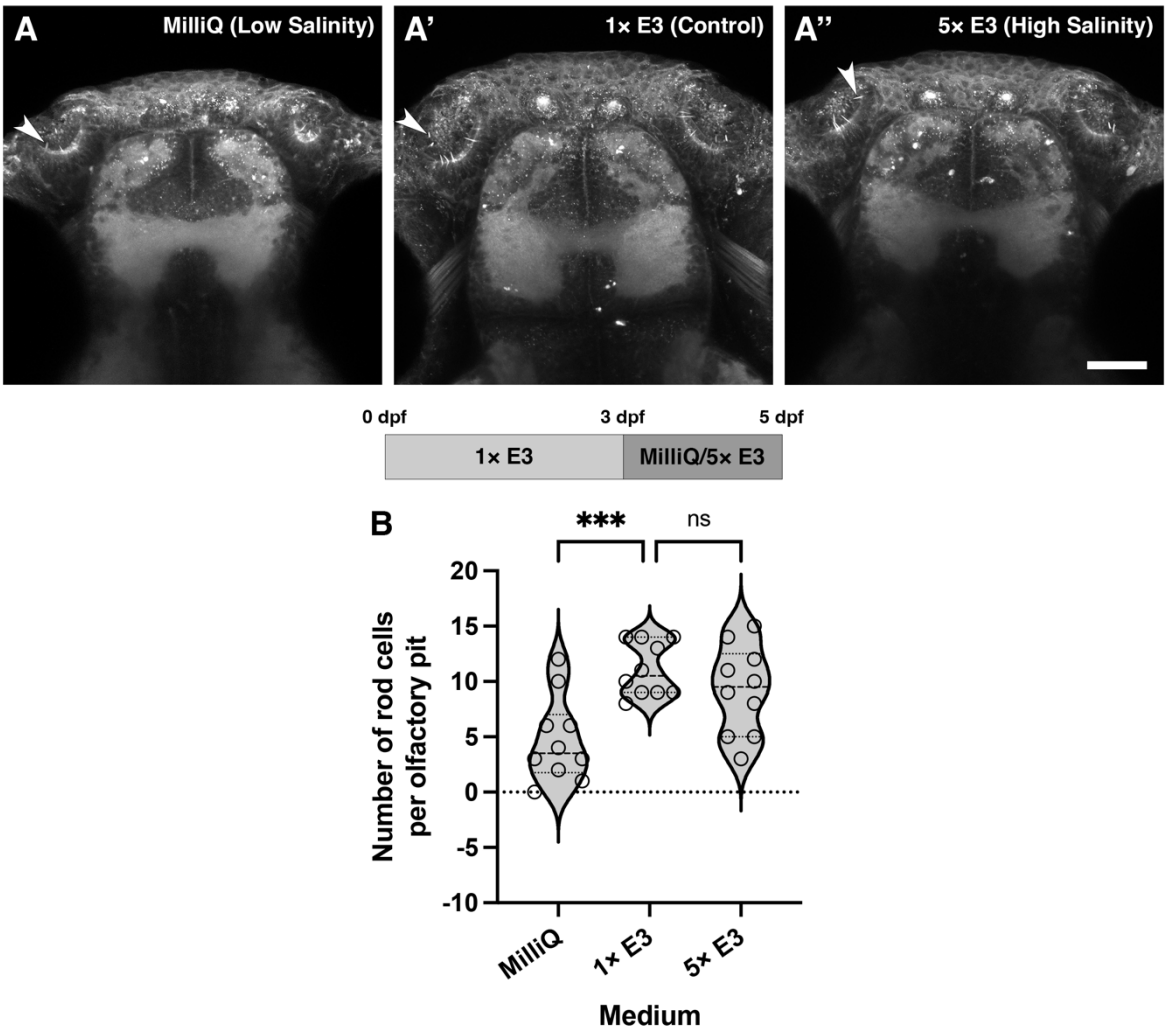

Figure 6.5. Olfactory rod cell numbers can be modulated by incubation of larvae in a low salinity medium. **(A–A'')** Maximum intensity projections confocal images of 5 dpf *Tg(actb2:Lifeact-RFP)* larvae after incubation in MilliQ (low salinity) from 3–5 dpf **(A)**, 1× E3 (control) from 0–5 dpf **(A')**, and 5× E3 (high salinity) from 3–5 dpf **(A'')**; dorsal view, anterior to the top. Arrowheads mark example olfactory rods. Scale bar = 50 µm. **(B)** Number of olfactory rod cell projections per olfactory pit in 5 dpf *Tg(actb2:Lifeact-RFP)* larvae after incubation in MilliQ from 3–5 dpf (*N* of olfactory pits = 10), 1× E3 (*N* = 10), and 5× E3 from 3–5 dpf (*N* = 10). Violin plot; bars indicate the median and lower and upper quartiles for each group. Brown-Forsythe and Welch ANOVA tests with Dunnett's T3 multiple comparisons test; 1× E3 versus MilliQ incubation, *** indicates *P* = 0.0009; 1× E3 versus 5× E3 incubation, ns, not significant (*P* = 0.3814).

6.3. Discussion

Based on the ideas generated from transcriptomic analysis, I started to explore whether olfactory rod cells may be a type of ionocyte in the zebrafish OE. Incubation of larvae in a different salinity medium led to a change in olfactory rod cell numbers, suggesting that the cells can detect and acclimate to changes in ion composition in the external environment. Only low salinity, and not high salinity, appeared to affect the numbers of olfactory rod cells; however, this may require further experimental repeats before a conclusion can be drawn as the data from larvae incubated in high salinity was variable. It is of interest that olfactory rod cells responded in an opposite manner to Nm ionocytes; Nm ionocytes, which express both HR and NaR ionocyte markers, increase in frequency in low salinity and vice versa (Peloggia et al., 2021), whereas olfactory rod cells decreased in number in low salinity. A possible explanation behind this is that the two cell types possess transport proteins that are involved in the transportation of different ions to maintain homeostasis, therefore a low salinity environment would have differing effects on each cell type.

Na^+,-K^+-ATPase expression was detected anteromedially and posterolaterally in the OE; apart from a small number of olfactory rod cells, it is not yet clear what other olfactory cell types express this protein. Here, I only tested for expression of Na^+,-K^+-ATPase in olfactory rod cells, thus, a critical next step would be to test for the expression of other ion transport proteins common in zebrafish ionocytes. For example, this includes H^+-ATPase, for proton secretion and sodium uptake, and Na^+,-Cl^- co-transporter (NCC), for sodium and chloride uptake (reviewed in Hwang and Lee, 2007; reviewed in Hwang and Chou, 2013). In line with this idea, *atp6v1aa*, which codes for H^+-ATPase subunit A (Horng et al., 2007), is differentially expressed in the *adgrg6*-expressing cell cluster in the Kraus et al. (2022) scRNA-seq dataset.

Further experiments could be done to see if changes in other environmental conditions, such as pH, would similarly lead to an acclimation of olfactory rod cell numbers. I previously treated zebrafish larvae with lipopolysaccharide (LPS), SARS-CoV-2 spike receptor binding domain protein, and cadmium chloride ($CdCl_2$) to test the effects of bacteria, viral components, or heavy metal toxicity in the environment respectively, but none had any effect on the cell numbers (data not shown).

6.3.1. Heterogeneity of olfactory rod cells

Several key pieces of evidence from my data so far suggest that olfactory rod cells may be heterogeneous. A subset of olfactory rod cells was labelled with the *Tg(sox10:Lifeact-mRFPruby)* transgene, a subset was retrogradely labelled by injection of DiD into the OB, and a subset of *adgrg6*-expressing cells in the adult OE possessed the distinct actin-rich rod-shaped apical projection which was not clear for all cells. I have now shown that only a small group of olfactory rod cells expressed Na^+,-K^+-ATPase. This points towards the idea that there are multiple classes of olfactory rod cells. Following this, I hypothesise that the olfactory rod cells negative for Na^+,-K^+-ATPase may express other ion transport proteins, and the different subclasses function together to detect different ions or parameters to maintain ionic homeostasis. The idea of heterogeneity can be explored with further transcriptomic analysis, by seeing if there are two or more populations of *adgrg6*-expressing cells in the OE with distinct transcriptomic profiles.

6.3.2. Transcriptomic profile of olfactory rod cells

Transcriptomic analysis revealed that cells in the *adgrg6*-expressing cluster expressed *actb2*, *elavl3*, *cldnb*, and *cldnh*, but not *ompa*, *ompb*, *trpc2a*, *trpc2b*, *foxj1a*, *foxj1b*, or *sox10*. With the exception of *sox10*, which as previously mentioned is a notoriously leaky promoter, this gene expression profile matched my transgene expression data for olfactory rod cells. However, it still remains to be confirmed by HCR RNA-FISH whether olfactory rod cells differentially co-express the ionocyte gene markers listed in Table 6.1. Exclusive co-expression of *adgrg6* with these genes in the OE would corroborate that the *adgrg6*-expressing cell cluster in the UMAP model from Kraus et al.'s (2022) scRNA-seq dataset was correctly identified as the cluster which contained most olfactory rod cells. This would ultimately lead to the opportunity for future analyses of the cell's whole transcriptome and comparison with transcriptomes of potential homologous cells in other species.

Interestingly, transcriptomic analysis has also recently revealed that HR and NaR ionocytes in the zebrafish, mouse, and human kidneys express *adgrg6*, *gcm2*, *and trpv6*. Here, the cells are speculated to play roles such as acid secretion, buffering blood and intracellular pH, and control of cytoplasmic calcium levels (Cazorla-Vázquez et al., 2023). Since there is an apparent need for *adgrg6*-expressing ionocytes in other organs of zebrafish and mammals, it would not be surprising to find that they are present in the olfactory organ as well.

6.3.3. Ionocytes in the olfactory system

Ionocytes have already been reported in the olfactory system of various fish species. A histological study in the *Raja clavata* OE revealed the presence of NaR ionocytes (light-stained cells), which were proposed to regulate ionic composition of olfactory mucous (Ferrando, 2008). Furthermore, a TEM and SEM study in marine sharks showed that there were variations in the densities of ionocytes between the OE of different species, which was speculated to be due to the different salinities of their respective habitat zones (Dymek et al., 2021). On the other hand, the same study found no ionocytes in the OE of freshwater batoids (Dymek et al., 2021), which is intriguing as here I propose the presence of ionocytes in the OE of a freshwater fish species.

It has been reported that a sparse subset of unclassified cells in the zebrafish OE detect sodium and chloride ions, and that the fish respond by reorientating themselves to navigate salt gradients in their freshwater habitat (Herrera et al., 2020); however, it is not yet known whether ion transport proteins such as Na^+,-K^+-ATPase are involved. Another candidate reason for the need for ionocytes in aquatic noses is to detect ion composition and in turn secrete/uptake ions or send chemical signals to neighbouring goblet cells to control the viscosity of mucous. The control of mucous ion composition and viscosity may directly influence the CBF of MCCs, thus enhancing mucociliary clearance and the perception of odours. Olfactory rod cells could be mechanosensory as previously proposed, in addition to potential ionoregulatory functions; the apical rod projection could detect changes in mucous viscosity, while mechanoreceptors in the basal membrane of the cell body could detect cell swelling or shrinking, both of which would be results of ionic changes. It is of interest that as well as being a common marker gene for ionocytes, *trpv6* codes for the mechanosensitive

calcium ion channel TRPV6, which can be activated in response to microvilli-mediated fluid flow and shear stress (Cha et al., 2013; Miura et al., 2015). Thus, *trpv6* could be involved in both mechanosensory and ionoregulatory functions in olfactory rod cells. These ideas remain to be tested, and could be validated in *adgrg6* zebrafish mutants, or in zebrafish with laser-ablated olfactory rods.

Ionocytes are reported to play an essential role in the OE of air-breathing terrestrial animals. As described previously, MVCs in the mammalian MOE express *adgrg6* (Baxter et al., 2021). It was later found that these are split into two subclasses: TRPM5-positive and TRPM5-negative MVCs (Ualiyeva et al., 2023). TRPM5-negative MVCs were discovered to be *foxi1*-positive ionocytes that strongly expressed transcripts for cystic fibrosis transmembrane conductance regulator in both mice (*Cftr*) and humans (*CFTR*; Ualiyeva et al., 2023). These cells shared common characteristics with pulmonary ionocytes, which when *foxi1* was knocked-out of, led to a loss of *Cftr* expression, a disruption in airway mucous, and cystic fibrosis phenotypes (Montoro et al., 2018). Ionocytes in the olfactory and respiratory epithelia therefore have major implications in disease.

6.3.4. Concluding remarks

Initial transcriptomic analysis has been valuable for bridging the gap between identification of a unique gene marker of olfactory rod cells, and identification of their potential functions. Although it remains to be confirmed whether olfactory rod cells express ionocyte gene markers, my preliminary data suggest that Na^+,-K^+-ATPase-expressing ionocytes, some of which are olfactory rod cells, are present in the zebrafish OE. Previous studies in multiple species imply the importance of having ionoregulatory cells in the nose and airways, thus, the identification of zebrafish olfactory ionocytes would have a widespread significance and provide new avenues for clinical research.

Chapter 7. Discussion

To summarise the findings presented in this thesis, I have characterised a rare cell type in the zebrafish OE, which morphologically and molecularly differs from known classes of sensory and non-sensory olfactory cells. Olfactory rod cells possess a unique actin-rich rod-shaped projection extending about 10 µm above the epithelial surface, which has a morphology consistent for a role in mechanosensation. The cell bodies are rounded in shape, positioned apically in the epithelium, and clustered posterolaterally in the olfactory pit close to lateral MCCs. Olfactory rod cells arise during early olfactory pit development, increase in numbers and size of apical projection during larval stages, and are present through to adulthood. Labelling in live larvae by Lifeact transgenes reveals that the rod projections can oscillate, possibly passively, as a result of surrounding motile cilia beating. Expression of calcium indicators driven by *elavl3* and neuronal *beta tubulin* promoters, and the presence of possible axons projecting to the OBs as revealed by retrograde tracing with DiD, suggest that they may be a class of sensory cell. *Adgrg6*, a human disease-implicated gene which codes for a putative mechanosensory aGPCR, is exclusively expressed in olfactory rod cells in the larval zebrafish OE, but the function of the gene does not appear to be essential for the development of the cell. Transcription of *cfos* in olfactory rod cells following mechanical stimulation indicates that the cells are mechanosensory. Finally, scRNA-seq analysis showed that *adgrg6*-expressing cells in the adult zebrafish OE also differentially express various gene markers for ionocytes. A rare subset of olfactory rod cells may indeed be ionocytes as they express a sodium-potassium ion transport protein, which may be consistent with the finding that olfactory rod cells appear to detect and acclimate to a low salinity environment. Based on my findings so far, I propose that olfactory rod cells are heterogeneous and multimodal, and have mechanosensory and ionoregulatory functions to control the viscosity of olfactory mucous, which in turn may influence cilia beat dynamics. Ultimately, by facilitating mucociliary clearance and odour perception, this would be a mechanism that enhances the physiological function of the olfactory system. Although characterisation of olfactory rod cells is not yet conclusive or exhaustive, the work done as part of this thesis has yielded significant discoveries on the properties of a rare and novel cell type.

7.1. Clinical relevance and impact of my work on olfactory rod cells

The vertebrate olfactory system can often be implicated in many infectious diseases (reviewed in Dando et al., 2014) and neurological disorders (reviewed in Whitlock, 2015). In wild animals, the loss of a functioning olfactory system may heavily impact their behaviour and ability to survive, while in humans, it may lead to a lower quality of life. A detailed understanding of the vertebrate olfactory system is important from cellular, developmental, and physiological perspectives, and for its clinical relevance. The identification of zebrafish olfactory rod cells offers new opportunities to explore the biology of these cells in a genetically tractable model organism, and thus to understand their contribution to the multimodal sensory functions of the vertebrate OE.

Adgrg6 is a human disease-implicated gene, mutations in which can cause arthrogyrposis multiplex congenita (Ravenscroft et al., 2015), and are also implicated in intellectual disabilities (Hosseini et al., 2019), musculoskeletal defects (Ravenscroft et al., 2015; reviewed in Baxendale et al., 2021), and cancers (Maiga et al., 2016). Zebrafish are already widely utilised for studying the functions and receptor signalling pathways of Adgrg6, particularly with respect to inner ear morphogenesis and PNS maturation (reviewed in Baxendale et al., 2021). Although the expression of *adgrg6* in the developing zebrafish OE was reported over a decade ago (Geng et al., 2013), the identification of the olfactory cell type which expresses the gene now offers a new perspective for future studies. It is currently unclear whether mutations in *adgrg6* cause any defects in olfactory rod cells or in the neurophysiology of the olfactory system, but it is expected that the work done in this thesis will have a clinical relevance.

The proposed idea that olfactory rod cells contribute to a mechanism for controlling cilia beat dynamics in olfactory MCCs via mechanosensory and/or ionoregulatory functions would be significant. It would be a mechanism that enhances clearing of bacteria, viruses, and other irritants from the olfactory system, while drawing in odorants and flushing them out again. Simply put, the cells would therefore be contributing to defending the central nervous system (CNS) from infections while facilitating olfaction. More broadly, this proposed mechanism may

also provide an understanding on how various regions of the human body, such as the airway, spinal cord, and reproductive tract control the beat dynamics of their motile cilia.

A similar cell type to the olfactory rod cell, the TRPM5-negative MVC ionocyte, has been reported in the olfactory and respiratory epithelia in mice and humans. These cells are shown to be critical in regulating airway mucous and are implicated in cystic fibrosis phenotypes (Montoro et al., 2018; Ualiyeva et al., 2023). Although airway diseases are not completely replicable in aquatic animals, the study of olfactory rod cells in a more accessible model organism nonetheless gives valuable insight on the genes and cellular signalling pathways that may be compromised in such diseases.

7.2. Future work

The story of olfactory rod cells has only just begun. The ongoing development and innovation of techniques in biomedical research expands the scope and opportunity for further cell characterisation. In terms of functional characterisation, it will be important to determine how different salinities affect mucosal viscosity and cilia beat dynamics in the zebrafish OE. Future work should address whether a dysfunction in olfactory rod cells, through either a mutation in *adgrg6* or laser ablation of the olfactory rod, would affect those parameters or hinder the physiological function of the olfactory system. In the context of transcriptomic characterisation, the next step would be confirming the gene expression profile of olfactory rod cells and comparing it with the transcriptome of potential homologous cells. Identification of homologous cell types would ultimately broaden the horizon and impact of research on olfactory rod cells.

7.3. Concluding remarks

In this thesis, I combined various staining, genetic, and imaging techniques to characterise the morphology, development, and gene expression of zebrafish olfactory rod cells. I began to explore the multimodal functions of the cells, and evidence hints at mechanosensory and ionoregulatory roles. Although clinical applications of this work may be a long way away, the

impact of this research contributes to shaping our current knowledge and understanding of the olfactory system neurophysiology, and provides a solid groundwork and starting point for future studies.

Appendix 1. Movie legends

Movie 3.1. Olfactory rods are labelled in the olfactory epithelia of live zebrafish by the *Tg(actb2:Lifeact-RFP)* transgene (published in Cheung et al., 2021).

3D rendering of a confocal image of a 4 dpf *Tg(actb2:Lifeact-RFP)*;*Tg(elavl3:H2B-GCaMPs)* double-transgenic larval olfactory pit; anterior to the top. Olfactory rods are labelled in magenta; neuronal nuclei are labelled in green.

Movie 3.2. Olfactory rods labelled with Lifeact-RFP in the olfactory epithelia of live zebrafish larvae oscillate (published in Cheung et al., 2021).

Fast-capture time series confocal imaging (5.98 frames per second, fps) of olfactory rods in a 6 dpf *Tg(actb2:Lifeact-RFP)* larva; anterior to the top, lateral to the left. Playback speed of the movie is 6 fps. Scale bar = 10 µm.

Movie 3.3. Olfactory rods labelled with Lifeact-mRFPruby in the olfactory epithelia of live zebrafish larvae oscillate (published in Cheung et al., 2021).

Fast-capture time series light-sheet imaging (50.04 fps) of a 5 dpf *Tg(sox10:Lifeact-mRFPruby)* larval olfactory pit; anterior to the top left, lateral to the top right. Beating olfactory cilia are visible in brightfield (greyscale), and oscillating olfactory rods are labelled by Lifeact-mRFPruby (magenta). Playback speed of the movie is 7 fps. Scale bar = 20 µm.

Movie 3.4. Olfactory rods labelled with Lifeact-mRFPruby are stable structures in the larval zebrafish olfactory epithelium from 78 hpf to 120 hpf.

Light-sheet time-lapse movie of the developing olfactory pit of a *Tg(sox10:Lifeact-mRFPruby)* larva from 78 hpf to 120 hpf; anterior to the top, lateral to the right. *Z*-stack images were acquired at an interval of 10 minutes. Scale bar = 20 µm.

Movie 5.1. Olfactory rod cells are located beside the lateral cluster of multi-ciliated cells.
3D rendering of a confocal image of an Alexa-phalloidin stained 4 dpf wild-type sibling larval olfactory pit; anterior to the top. The movie shows olfactory rods located in the OSN-containing sensory zone of the olfactory pit near the border with the lateral cluster of MCCs ('hexagonal' cells).

Movie 5.2. Delivery of a mechanical stimulus into the larval olfactory epithelium.
The set-up for mechanical stimulus delivery into the left-side olfactory pit of 6 dpf *Tg(actb2:Lifeact-RFP)* larva, while leaving the right-side olfactory pit as an unstimulated contralateral control. The pipette, connected to a microinjector, delivered odourless E3 medium over a 60-second period.

Movie 5.3. Olfactory cilia beating in a wild-type sibling in normal viscosity (recording taken by S. J. Jesuthasan, N. J. van Hateren, and T. T. Whitfield, analysis and video processing by K. Y. Cheung).
Spinning disk imaging (150 fps) imaging of MCC motile cilia beating in the olfactory pit of a 4 dpf wild-type sibling in E3 (1 cP). The CBF measured here was 18.7 Hz. Playback speed of the movie is 150 fps. Scale bar = 20 µm.

Movie 5.4. Olfactory cilia beating in a wild-type sibling in high viscosity (recording taken by S. J. Jesuthasan, N. J. van Hateren, and T. T. Whitfield, analysis and video processing by K. Y. Cheung).
Spinning disk imaging (150 fps) imaging of MCC motile cilia beating in the olfactory pit of a 4 dpf wild-type sibling in 4% methyl cellulose in E3 (30 cP). The CBF here was 12.3 Hz. Playback speed of the movie is 150 fps. Scale bar = 20 µm.

Movie 5.5. Olfactory cilia beating in an *adgrg6*$^{fr24-/-}$ mutant larva in normal viscosity (recording taken by S. J. Jesuthasan, N. J. van Hateren, and T. T. Whitfield, analysis and video processing by K. Y. Cheung).
Spinning disk imaging (150 fps) imaging of MCC motile cilia beating in the olfactory pit of a 4 dpf *adgrg6*$^{fr24-/-}$ mutant larva in E3 (1 cP). The CBF measured here was 21.6 Hz. Playback speed of the movie is 150 fps. Scale bar = 20 µm.

Movie 5.6. Olfactory cilia beating in an *adgrg6*$^{fr24-/-}$ mutant larva in high viscosity (recording taken by S. J. Jesuthasan, N. J. van Hateren, and T. T. Whitfield, analysis and video processing by K. Y. Cheung).

Spinning disk imaging (150 fps) imaging of MCC motile cilia beating in the olfactory pit of a 4 dpf *adgrg6*$^{fr24-/-}$ mutant larva in 4% methyl cellulose in E3 (30 cP). The CBF measured here was 14.5 Hz. Playback speed of the movie is 150 fps. Scale bar = 20 µm.

Appendix 2. Cheung, K. Y., Jesuthasan, S. J., Baxendale, S., van Hateren, N. J., Marzo, M., Hill, C. J., Whitfield, T. T. (2021). Olfactory rod cells: a rare cell type in the larval zebrafish olfactory epithelium with a large actin-rich apical projection. *Front. Physiol.* 12, 626080. doi: 10.3389/fphys.2021.626080

Appendix 3. Script for Seurat analysis of single-cell RNA sequencing (scRNA-seq) data

```
zebrafish_osn <- readRDS("~/Desktop/Zebrafish Olfactory scRNA-seq
Plots/zebrafish_osn.rds")
View(zebrafish_osn)

install.packages("SeuratObject")
library(dplyr)
library(Seurat)
library(patchwork)
library(SeuratObject)
library(sp)

# Standard pre-processing workflow
# QC and selecting cells for further analysis

# The [[ operator can add columns to object metadata. This is a great place to stash QC stats
zebrafish_osn[["percent.mt"]] <- PercentageFeatureSet(zebrafish_osn, pattern = "^MT-")

# Visualize QC metrics as a violin plot
VlnPlot(zebrafish_osn, features = c("nFeature_RNA", "nCount_RNA", "percent.mt"), ncol = 3)

# FeatureScatter is typically used to visualize feature-feature relationships, but can be used
for anything calculated by the object, i.e. columns in object metadata, PC scores etc.
plot1 <- FeatureScatter(zebrafish_osn, feature1 = "nCount_RNA", feature2 = "percent.mt")
plot2 <- FeatureScatter(zebrafish_osn, feature1 = "nCount_RNA", feature2 =
"nFeature_RNA")
plot1 + plot2
```

```
zebrafish_osn <- subset(zebrafish_osn, subset = nFeature_RNA > 200 & nFeature_RNA < 2500 & percent.mt < 5)

# Normalizing the data
zebrafish_osn <- NormalizeData(zebrafish_osn, normalization.method = "LogNormalize", scale.factor = 10000)
zebrafish_osn <- NormalizeData(zebrafish_osn)

# Identification of highly variable features (feature selection)
zebrafish_osn <- FindVariableFeatures(zebrafish_osn, selection.method = "vst", nfeatures = 2000)

# Identify the 10 most highly variable genes
top10 <- head(VariableFeatures(zebrafish_osn), 10)

# Plot variable features with and without labels
plot1 <- VariableFeaturePlot(zebrafish_osn)
plot2 <- LabelPoints(plot = plot1, points = top10, repel = TRUE)
plot1 + plot2

# Scaling the data
all.genes <- rownames(zebrafish_osn)
zebrafish_osn <- ScaleData(zebrafish_osn, features = all.genes)

# Perform linear dimensional reduction
zebrafish_osn <- RunPCA(zebrafish_osn, features = VariableFeatures(object = zebrafish_osn))

# Examine and visualize PCA results a few different ways
print(zebrafish_osn[["pca"]], dims = 1:5, nfeatures = 5)
VizDimLoadings(zebrafish_osn, dims = 1:2, reduction = "pca")
DimPlot(zebrafish_osn, reduction = "pca") + NoLegend()
DimHeatmap(zebrafish_osn, dims = 1, cells = 500, balanced = TRUE)
```

```
DimHeatmap(zebrafish_osn, dims = 1:15, cells = 500, balanced = TRUE)

# Determine the ‘dimensionality’ of the dataset
ElbowPlot(zebrafish_osn)

# Cluster the cells
zebrafish_osn <- FindNeighbors(zebrafish_osn, dims = 1:10)
zebrafish_osn <- FindClusters(zebrafish_osn, resolution = 0.5)

# Look at cluster IDs of the first 5 cells
head(Idents(zebrafish_osn), 5)

# Run non-linear dimensional reduction (UMAP/tSNE)
zebrafish_osn <- RunUMAP(zebrafish_osn, dims = 1:10)

# Note that you can set `label = TRUE` or use the LabelClusters function to help label
individual clusters
DimPlot(zebrafish_osn, reduction = "umap")

#Finding differentially expressed features (cluster biomarkers)

# Find all markers of cluster 11
cluster11.markers <- FindMarkers(zebrafish_osn, ident.1 = 11)
head(cluster11.markers, n = 20)

# Find markers for every cluster compared to all remaining cells, report only the positive
ones
zebrafish_osn.markers <- FindAllMarkers(zebrafish_osn, only.pos = TRUE)
zebrafish_osn.markers %>%
  group_by(cluster) %>%
  dplyr::filter(avg_log2FC > 1)
```

```
cluster11.markers <- FindMarkers(zebrafish_osn, ident.1 = 11, logfc.threshold = 0.25,
test.use = "roc", only.pos = TRUE)

View(cluster11.markers)

VlnPlot(zebrafish_osn, features = c("adgrg6"))
VlnPlot(zebrafish_osn, features = c("adgrg6", "actb2", "elavl3", "sox10", "ompa", "ompb",
"trpc2a", "trpc2b", "foxj1a", "foxj1b", "cldnb", "cldnh"))

FeaturePlot(zebrafish_osn, features = c("adgrg6"))
FeaturePlot(zebrafish_osn, features = c("adgrg6", "actb2", "elavl3", "sox10","ompa",
"ompb", "trpc2a", "trpc2b", "foxj1a", "foxj1b", "cldnb", "cldnh"))

RidgePlot(zebrafish_osn, features = c("adgrg6"))
RidgePlot(zebrafish_osn, features = c("adgrg6", "actb2", "elavl3", "sox10","ompa", "ompb",
"trpc2a", "trpc2b", "foxj1a", "foxj1b", "cldnb", "cldnh"))

DotPlot(zebrafish_osn, features = c("adgrg6"))
DotPlot(zebrafish_osn, features = c("adgrg6", "actb2", "elavl3", "sox10","ompa", "ompb",
"trpc2a", "trpc2b", "foxj1a", "foxj1b", "cldnb", "cldnh"))

zebrafish_osn.markers %>%
  group_by(cluster) %>%
  dplyr::filter(avg_log2FC > 1) %>%
  slice_head(n = 10) %>%
  ungroup() -> top10
DoHeatmap(zebrafish_osn, features = top10$gene) + NoLegend()

# Visualize co-expression of two features simultaneously
FeaturePlot(zebrafish_osn, features = c("adgrg6", "ceacam1"), blend = TRUE)
FeaturePlot(zebrafish_osn, features = c("adgrg6", "trpv6"), blend = TRUE)
FeaturePlot(zebrafish_osn, features = c("adgrg6", "foxi3b"), blend = TRUE)
```

```
FeaturePlot(zebrafish_osn, features = c("adgrg6", "gcm2"), blend = TRUE)
FeaturePlot(zebrafish_osn, features = c("adgrg6", "atp1a1a.3"), blend = TRUE)

# Assigning cell type identity to clusters
new.cluster.ids <- c("0", "1", "2", "3", "4", "5", "6", "7", "8", "9", "10", "Olfactory rod cells",
"12")
names(new.cluster.ids) <- levels(zebrafish_osn)
zebrafish_osn <- RenameIdents(zebrafish_osn, new.cluster.ids)
DimPlot(zebrafish_osn, reduction = "umap", label = TRUE, pt.size = 0.5) + NoLegend()

library(ggplot2)
plot <- DimPlot(zebrafish_osn, reduction = "umap", label = TRUE, label.size = 4.5) +
xlab("UMAP 1") + ylab("UMAP 2") +
  theme(axis.title = element_text(size = 18), legend.text = element_text(size = 18)) +
guides(colour = guide_legend(override.aes = list(size = 10)))
ggsave(filename = "~/Desktop/Zebrafish Olfactory scRNA-seq
Plots/zebrafish_osn_umap.jpg", height = 7, width = 12, plot = plot, quality = 50)

saveRDS(zebrafish_osn, file = "~/Desktop/Zebrafish Olfactory scRNA-seq
Plots/zebrafish_osn_seurat.rds")
```

Bibliography

Ache, B. W., and Young, J. M. (2005). Olfaction: Diverse species, conserved principles. *Neuron* 48, 417–430. doi:10.1016/j.neuron.2005.10.022.

Agetsuma, M., Aizawa, H., Aoki, T., Nakayama, R., Takahoko, M., Goto, M., et al. (2010). The habenula is crucial for experience-dependent modification of fear responses in zebrafish. *Nat. Neurosci.* 13, 1354–1356. doi:10.1038/nn.2654.

Aguillon, R., Batut, J., Subramanian, A., Madelaine, R., Dufourcq, P., Schilling, T. F., et al. (2018). Cell-type heterogeneity in the early zebrafish olfactory epithelium is generated from progenitors within preplacodal ectoderm. *Elife* 7, e32041. doi:10.7554/eLife.32041.

Aguillon, R., Madelaine, R., Aguirrebengoa, M., Guturu, H., Link, S., Dufourcq, P., et al. (2020). Morphogenesis is transcriptionally coupled to neurogenesis during peripheral olfactory organ development. *Development* 147, dev192971. doi:10.1242/dev.192971.

Ahuja, G., Nia, S. B., Zapilko, V., Shiriagin, V., Kowatschew, D., Oka, Y., et al. (2014). Kappe neurons, a novel population of olfactory sensory neurons. *Sci. Rep.* 4, 4037. doi:10.1038/srep04037.

Aleström, P., D'Angelo, L., Midtlyng, P. J., Schorderet, D. F., Schulte-Merker, S., Sohm, F., et al. (2019). Zebrafish: Housing and husbandry recommendations. *Lab. Anim.* 0, 1–12. doi:10.1177/0023677219869037.

Alioto, T. S., and Ngai, J. (2005). The odorant receptor repertoire of teleost fish. *BMC Genomics* 6, 173. doi:10.1186/1471-2164-6-173.

Araç, D., Aust, G., Calebiro, D., Engel, F. B., Formstone, C., Goffinet, A., et al. (2012). Dissecting signaling and functions of adhesion G protein-coupled receptors. *Ann. N. Y. Acad. Sci.* 1276, 1–25. doi:10.1111/j.1749-6632.2012.06820.x.

Axel, R. (1995). The molecular logic of smell. *Sci. Am.* 273, 154–159. doi:10.1038/scientificamerican1095-154.

Bannister, L. H. (1965). The fine structure of the olfactory surface of teleostean fishes. *Q. J. Microsc. Sci.* 106, 333–342.

Bannister, L. H. (1966). Is *Rhabdospora thelohani* (Laguesse) a sporozoan parasite or a tissue cell of lower vertebrates? *Parasitology* 56, 633–638. doi:10.1017/S0031182000071651.

Baraban, M., Gordillo Pi, C., Bonnet, I., Gilles, J.-F., Lejeune, C., Cabrera, M., et al. (2023). Actomyosin contractility in olfactory placode neurons opens the skin epithelium to form the zebrafish nostril. *Dev. Cell* 58, 1–15. doi:10.1016/j.devcel.2023.02.001.

Barr-Gillespie, P.-G. (2015). Assembly of hair bundles, an amazing problem for cell biology. *Mol. Biol. Cell* 26, 2727–2732. doi:10.1091/mbc.E14-04-0940.

Baxendale, S., Asad, A., Shahidan, N. O., Wiggin, G. R., and Whitfield, T. T. (2021). The adhesion GPCR Adgrg6 (Gpr126): Insights from the zebrafish model. *Genesis* 59, e23417. doi:10.1002/dvg.23417.

Baxter, B. D., Larson, E. D., Merle, L., Feinstein, P., Polese, A. G., Bubak, A. N., et al. (2021). Transcriptional profiling reveals potential involvement of microvillous TRPM5-expressing cells in viral infection of the olfactory epithelium. *BMC Genomics* 22, 224. doi:10.1186/s12864-021-07528-y.

Bayramli, X., Kocagöz, Y., Sakizli, U., and Fuss, S. H. (2017). Patterned arrangements of olfactory receptor gene expression in zebrafish are established by radial movement of specified olfactory sensory neurons. *Sci. Rep.* 7, 5572. doi:10.1038/s41598-017-06041-1.

Behrndt, M., Salbreux, G., Campinho, P., Hauschild, R., Oswald, F., Roensch, J., et al. (2012). Forces driving epithelial spreading in zebrafish gastrulation. *Science (80-.).* 338, 257–260. doi:10.1126/science.1224143.

Bettini, S., Milani, L., Lazzari, M., Maurizii, M. G., and Franceschini, V. (2017). Crypt cell markers in the olfactory organ of *Poecilia reticulata*: analysis and comparison with the fish model *Danio rerio*. *Brain Struct. Funct.* 222, 3063–3074. doi:10.1007/s00429-017-1386-2.

Bhatia-Dey, N., and Heinbockel, T. (2021). The olfactory system as marker of neurodegeneration in aging, neurological and neuropsychiatric disorders. *Int. J. Environ. Res. Public Health* 18, 6976. doi:10.3390/ijerph18136976.

Bibliowicz, J., Alié, A., Espinasa, L., Yoshizawa, M., Blin, M., Hinaux, H., et al. (2013). Differences in chemosensory response between eyed and eyeless *Astyanax mexicanus* of the Rio Subterráneo cave. *Evodevo* 4, 25. doi:10.1186/2041-9139-4-25.

Biechl, D., Tietje, K., Gerlach, G., and Wullimann, M. F. (2016). Crypt cells are involved in kin recognition in larval zebrafish. *Sci. Rep.* 6, 24590. doi:10.1038/srep24590.

Böhm, U. L., Prendergast, A., Djenoune, L., Figueiredo, S. N., Gomez, J., Stokes, C., et al. (2016). CSF-contacting neurons regulate locomotion by relaying mechanical stimuli to spinal circuits. *Nat. Commun.* 7, 10866. doi:10.1038/ncomms10866.

Bolte, S., and Cordelières, F. P. (2006). A guided tour into subcellular colocalization analysis in light microscopy. *J. Microsc.* 224, 213–232. doi:10.1111/j.1365-2818.2006.01706.x.

Bradley, E. C., Cunningham, R. L., Wilde, C., Morgan, R. K., Klug, E. A., Letcher, S. M., et al. (2019). *In vivo* identification of small molecules mediating Gpr126/Adgrg6 signaling during Schwann cell development. *Ann. N. Y. Acad. Sci.* 1456, 44–63. doi:10.1111/nyas.14233.

Brann, D. H., Tsukahara, T., Weinreb, C., Lipovsek, M., Van den Berge, K., Gong, B., et al. (2020). Non-neuronal expression of SARS-CoV-2 entry genes in the olfactory system suggests mechanisms underlying COVID-19-associated anosmia. *Sci. Adv.* 6, eabc5801. doi:10.1126/sciadv.abc5801.

Brann, J. H., and Firestein, S. J. (2014). A lifetime of neurogenesis in the olfactory system. *Front. Neurosci.* 8, 182. doi:10.3389/fnins.2014.00182.

Breipohl, W., Bijvank, G. J., and Zippel, H. P. (1973). Rastermikroskopische untersuchungen der olfaktorischen rezeptoren im riechepithel des goldfisches (*Carassius auratus*). *Zeitschrift für Zellforsch. und Mikroskopische Anat.* 138, 439–454. doi:10.1007/BF00307104.

Brinkmann, A., and Schild, D. (2016). One special glomerulus in the olfactory bulb of *Xenopus laevis* tadpoles integrates a broad range of amino acids and mechanical stimuli. *J. Neurosci.* 36, 10978–10989. doi:10.1523/JNEUROSCI.4631-15.2016.

Buchanan, T. W., Tranel, D., and Adolphs, R. (2003). A specific role for the human amygdala in olfactory memory. *Learn. Mem.* 10, 319–325. doi:10.1101/lm.62303.

Buck, L., and Axel, R. (1991). A novel multigene family may encode odorant receptors: a molecular basis for odor recognition. *Cell* 65, 175–187. doi:10.1016/0092-8674(91)90418-X.

Butler, A., Hoffman, P., Smibert, P., Papalexi, E., and Satija, R. (2018). Integrating single-cell transcriptomic data across different conditions, technologies, and species. *Nat. Biotechnol.* 36, 411–420. doi:10.1038/nbt.4096.

Byrd, C. A., and Brunjes, P. C. (1995). Organization of the olfactory system in the adult zebrafish: histological, immunohistochemical, and quantitative analysis. *J. Comp. Neurol.* 358, 247–259. doi:10.1002/cne.903580207.

Cai, R., Liu, X., Zhang, R., Hofmann, L., Zheng, W., Amin, M. R., et al. (2020). Autoinhibition of TRPV6 channel and regulation by PIP2. *iScience* 23, 101444. doi:10.1016/j.isci.2020.101444.

Calvo-Ochoa, E., and Byrd-Jacobs, C. A. (2019). The olfactory system of zebrafish as a model for the study of neurotoxicity and injury: Implications for neuroplasticity and disease. *Int. J. Mol. Sci.* 20, 1639. doi:10.3390/ijms20071639.

Calvo-Ochoa, E., Byrd-Jacobs, C. A., and Fuss, S. H. (2021). Diving into the streams and waves of constitutive and regenerative olfactory neurogenesis: insights from zebrafish. *Cell Tissue Res.* 383, 227–253. doi:10.1007/s00441-020-03334-2.

Carney, T. J., Dutton, K. A., Greenhill, E., Delfino-Machín, M., Dufourcq, P., Blader, P., et al. (2006). A direct role for Sox10 in specification of neural crest-derived sensory neurons. *Development* 133, 4619–4630. doi:10.1242/dev.02668.

Carr, V. M., Farbman, A. I., Colletti, L. M., and Morgan, J. I. (1991). Identification of a new non-neuronal cell type in rat olfactory epithelium. *Neuroscience* 45, 433–449. doi:10.1016/0306-4522(91)90239-K.

Cartwright, J. H. E., Piro, O., and Tuval, I. (2019). Chemosensing versus mechanosensing in nodal and Kupffer's vesicle cilia and in other left-right organizer organs. *Philos. Trans. R. Soc. Lond. B. Biol. Sci.* 375, 20190566. doi:10.1098/rstb.2019.0566.

Cazorla-Vázquez, S., Kösters, P., Bertz, S., Pfister, F., Daniel, C., Dedden, M., et al. (2023). Adhesion GPCR Gpr126 (Adgrg6) expression profiling in zebrafish, mouse, and human kidney. *Cells* 12, 1988. doi:10.3390/cells12151988.

Cha, S.-K., Kim, J.-H., and Huang, C.-L. (2013). Flow-induced activation of TRPV5 and TRPV6 channels stimulates Ca^{2+}-activated K^+ channel causing membrane hyperpolarization. *Biochim. Biophys. Acta - Mol. Cell Res.* 1833, 3046–3053. doi:10.1016/j.bbamcr.2013.08.017.

Chang, W.-J., Horng, J.-L., Yan, J.-J., Hsiao, C.-D., and Hwang, P.-P. (2009). The transcription factor, glial cell missing 2, is involved in differentiation and functional regulation of H+-ATPase-rich cells in zebrafish (Danio rerio). *Am. J. Physiol. - Regul. Integr. Comp. Physiol.* 296, 1192–1201. doi:10.1152/ajpregu.90973.2008.

Cheung, K. Y., Jesuthasan, S. J., Baxendale, S., van Hateren, N. J., Marzo, M., Hill, C. J., et al. (2021). Olfactory rod cells: a rare cell type in the larval zebrafish olfactory epithelium with a large actin-rich apical projection. *Front. Physiol.* 12, 626080. doi:10.3389/fphys.2021.626080.

Chia, J. S. M., Wall, E. S., Wee, C. L., Rowland, T. A. J., Cheng, R.-K., Cheow, K., et al. (2019). Bacteria evoke alarm behaviour in zebrafish. *Nat. Commun.* 10, 3831. doi:10.1038/s41467-019-11608-9.

Choi, H. M. T., Beck, V. A., and Pierce, N. A. (2014). Next-generation *in situ* hybridization chain reaction: Higher gain, lower cost, greater durability. *ACS Nano* 8, 4284–4294. doi:10.1021/nn405717p.

Choi, H. M. T., Calvert, C. R., Husain, N., Huss, D., Barsi, J. C., Deverman, B. E., et al. (2016). Mapping a multiplexed zoo of mRNA expression. *Development* 143, 3632–3637. doi:10.1242/dev.140137.

Choi, H. M. T., Chang, J. Y., Trinh, L. A., Padilla, J. E., Fraser, S. E., and Pierce, N. A. (2010). Programmable *in situ* amplification for multiplexed imaging of mRNA expression. *Nat. Biotechnol.* 28, 1208–1212. doi:10.1038/nbt.1692.

Choi, H. M. T., Schwarzkopf, M., Fornace, M. E., Acharya, A., Artavanis, G., Stegmaier, J., et al. (2018). Third-generation *in situ* hybridization chain reaction: multiplexed, quantitative, sensitive, versatile, robust. *Development* 145, dev165753. doi:10.1242/dev.165753.

Choi, S. S. A., Chan, H. H., Chan, C. M., Wang, X., Webb, S. E., Leung, K. W., et al. (2022). Neuromasts and olfactory organs of zebrafish larvae represent possible sites of SARS-CoV-2 pseudovirus host cell entry. *J. Virol.* 96, e01418-22. doi:doi/10.1128/jvi.01418-22.

Chou, S.-W., Hwang, P., Gomez, G., Fernando, C. A., West, M. C., Pollock, L. M., et al. (2011). Fascin 2b is a component of stereocilia that lengthens actin-based protrusions. *PLoS One* 6, e14807. doi:10.1371/journal.pone.0014807.

Cong, X., Zheng, Q., Ren, W., Chéron, J.-B., Fiorucci, S., Wen, T., et al. (2019). Zebrafish olfactory receptors ORAs differentially detect bile acids and bile salts. *J. Biol. Chem.* 294, 6762–6771. doi:10.1074/jbc.RA118.006483.

Connelly, T., Yu, Y., Grosmaitre, X., Wang, J., Santarelli, L. C., Savigner, A., et al. (2015). G protein-coupled odorant receptors underlie mechanosensitivity in mammalian olfactory sensory neurons. *Proc. Natl. Acad. Sci. U. S. A.* 112, 590–595. doi:10.1073/pnas.1418515112.

Costa, K. C. M., Brigante, T. A. V., Fernandes, G. G., Scomparin, D. S., Scarante, F. F., de Oliveira, D. P., et al. (2021). Zebrafish as a translational model: An experimental alternative to study the mechanisms involved in anosmia and possible neurodegenerative aspects of COVID-19? *eNeuro* 8, ENEURO.0027-21.2021. doi:10.1523/ENEURO.0027-21.2021.

Dai, W., Bai, Y., Hebda, L., Zhong, X., Liu, J., Kao, J., et al. (2014). Calcium deficiency-induced and TRP channel-regulated IGF1R-PI3K-Akt signaling regulates abnormal epithelial cell proliferation. *Cell Death Differ.* 21, 568–581. doi:10.1038/cdd.2013.177.

Dana, H., Mohar, B., Sun, Y., Narayan, S., Gordus, A., Hasseman, J. P., et al. (2016). Sensitive red protein calcium indicators for imaging neural activity. *Elife* 5, e12727. doi:10.7554/eLife.12727.

Dando, S. J., Mackay-Sim, A., Norton, R., Currie, B. J., St. John, J. A., Ekberg, J. A. K., et al. (2014). Pathogens penetrating the central nervous system: infection pathways and the cellular and molecular mechanisms of invasion. *Clin. Microbiol. Rev.* 27, 691–726. doi:10.1128/CMR.00118-13.

Datta, N. C., and Bandopadhyay, S. K. (1997). Ultrastructure of cell types of the olfactory epithelium in a catfish, *Heteropneustes fossilis* (Bloch). *J. Biosci.* 22, 233–245. doi:10.1007/BF02704736.

Demirler, M. C., Sakizli, U., Bali, B., Kocagöz, Y., Eski, S. E., Ergönen, A., et al. (2019). Purinergic signalling selectively modulates maintenance but not repair neurogenesis in the zebrafish olfactory epithelium. *FEBS J.* 287, 2699–2722. doi:10.1111/febs.15170.

DePasquale, J. A. (2020). Tropomyosin and alpha-actinin in teleost rodlet cells. *Acta Zool.* 00, 1–10. doi:10.1111/azo.12344.

Desban, L., Prendergast, A., Roussel, J., Rosello, M., Geny, D., Wyart, C., et al. (2019). Regulation of the apical extension morphogenesis tunes the mechanosensory response of microvilliated neurons. *PLoS Biol.* 17, e3000235. doi:10.1371/journal.pbio.3000235.

Dezfuli, B. S., Capuano, S., Simoni, E., Previati, M., and Giari, L. (2007). Rodlet cells and the sensory systems in zebrafish (*Danio rerio*). *Anat. Rec.* 290, 367–374. doi:10.1002/ar.20507.

Diamantopoulou, E., Baxendale, S., de la Vega de León, A., Asad, A., Holdsworth, C. J., Abbas, L., et al. (2019). Identification of compounds that rescue otic and myelination defects in the zebrafish *adgrg6* (*gpr126*) mutant. *Elife* 8, e44889. doi:10.7554/eLife.44889.

Djenoune, L., Khabou, H., Joubert, F., Quan, F. B., Figueiredo, S. N., Bodineau, L., et al. (2014). Investigation of spinal cerebrospinal fluid-contacting neurons expressing PKD2L1: evidence for a conserved system from fish to primates. *Front. Neuroanat.* 8, 26. doi:10.3389/fnana.2014.00026.

Djenoune, L., Mahamdeh, M., Truong, T. V., Nguyen, C. T., Fraser, S. E., Brueckner, M., et al. (2023). Cilia function as calcium-mediated mechanosensors that instruct left-right asymmetry. *Science (80-.).* 379, 71–78. doi:10.1126/science.abq7317.

Douguet, D., and Honoré, E. (2019). Mammalian mechanoelectrical transduction: Structure and function of force-gated ion channels. *Cell* 179, 340–354. doi:10.1016/j.cell.2019.08.049.

Duggan, C. D., DeMaria, S., Baudhuin, A., Stafford, D., and Ngai, J. (2008). *Foxg1* is required for development of the vertebrate olfactory system. *J. Neurosci.* 28, 5229–5239. doi:10.1523/JNEUROSCI.1134-08.2008.

Dummer, A., Poelma, C., DeRuiter, M. C., Goumans, M.-J. T. H., and Hierck, B. P. (2016). Measuring the primary cilium length: improved method for unbiased high-throughput analysis. *Cilia* 5, 7. doi:10.1186/s13630-016-0028-2.

Dunn, T. W., Mu, Y., Narayan, S., Randlett, O., Naumann, E. A., Yang, C.-T., et al. (2016). Brain-wide mapping of neural activity controlling zebrafish exploratory locomotion. *Elife* 5, e12741. doi:10.7554/eLife.12741.

Dutton, K. A., Pauliny, A., Lopes, S. S., Elworthy, S., Carney, T. J., Rauch, J., et al. (2001). Zebrafish colourless encodes *sox10* and specifies non-ectomesenchymal neural crest fates. *Development* 128, 4113–4125.

Dymek, J., Muñoz, P., Mayo-Hernández, E., Kuciel, M., and Żuwała, K. (2021). Comparative analysis of the olfactory organs in selected species of marine sharks and freshwater batoids. *Zool. Anz.* 294, 50–61. doi:10.1016/j.jcz.2021.07.013.

Dynes, J. L., and Ngai, J. (1998). Pathfinding of olfactory neuron axons to stereotyped glomerular targets revealed by dynamic imaging in living zebrafish embryos. *Neuron* 20, 1081–1091. doi:10.1016/S0896-6273(00)80490-0.

Elsaesser, R., and Paysan, J. (2007). The sense of smell, its signalling pathways, and the dichotomy of cilia and microvilli in olfactory sensory cells. *BMC Neurosci.* 8, S1. doi:10.1186/1471-2202-8-S3-S1.

Esterberg, R., Hailey, D. W., Coffin, A. B., Raible, D. W., and Rubel, E. W. (2013). Disruption of intracellular calcium regulation is integral to aminoglycoside-induced hair cell death. *J. Neurosci.* 33, 7513–7525. doi:10.1523/JNEUROSCI.4559-12.2013.

Esterberg, R., Linbo, T., Pickett, S. B., Wu, P., Ou, H. C., Rubel, E. W., et al. (2016). Mitochondrial calcium uptake underlies ROS generation during aminoglycoside-induced hair cell death. *J. Clin. Invest.* 126, 3556–3566. doi:10.1172/JCI84939.

Farnsworth, D. R., Saunders, L. M., and Miller, A. C. (2020). A single-cell transcriptome atlas for zebrafish development. *Dev. Biol.* 459, 100–108. doi:10.1016/j.ydbio.2019.11.008.

Ferrando, S. (2008). Ionocytes in the olfactory epithelium of developing *Raja clavata*. *Ital. J. Zool.* 75, 233–236. doi:10.1080/11250000801934120.

Finger, T. E., Böttger, B., Hansen, A., Anderson, K. T., Alimohammadi, H., and Silver, W. L. (2003). Solitary chemoreceptor cells in the nasal cavity serve as sentinels of respiration. *Proc. Natl. Acad. Sci. U. S. A.* 100, 8981–8986. doi:10.1073/pnas.1531172100.

Firestein, S. (2001). How the olfactory system makes sense of scents. *Nature* 413, 211–218. doi:10.1038/35093026.

Fleischer, J., Breer, H., and Strotmann, J. (2009). Mammalian olfactory receptors. *Front. Cell. Neurosci.* 3, 9. doi:10.3389/neuro.03.009.2009.

Fujita, T. (1989). Present status of paraneuron concept. *Arch. Histol. Cytol.* 52, 1–8. doi:10.1679/aohc.52.Suppl_1.

Geng, F.-S., Abbas, L., Baxendale, S., Holdsworth, C. J., Swanson, A. G., Slanchev, K., et al. (2013). Semicircular canal morphogenesis in the zebrafish inner ear requires the function of *gpr126* (*lauscher*), an adhesion class G protein-coupled receptor gene. *Development* 140, 4362–4374. doi:10.1242/dev.098061.

Genovese, F., and Tizzano, M. (2018). Microvillous cells in the olfactory epithelium express elements of the solitary chemosensory cell transduction signaling cascade. *PLoS One* 13, e0202754. doi:10.1371/journal.pone.0202754.

Gillespie, P. G., and Müller, U. (2009). Mechanotransduction by hair cells: models, molecules, and mechanisms. *Cell* 139, 33–44. doi:10.1016/j.cell.2009.09.010.

Gloriam, D. E. I., Bjarnadóttir, T. K., Yan, Y.-L., Postlethwait, J. H., Schiöth, H. B., and Fredriksson, R. (2005). The repertoire of trace amine G-protein-coupled receptors: Large expansion in zebrafish. *Mol. Phylogenet. Evol.* 35, 470–482. doi:10.1016/j.ympev.2004.12.003.

Grosmaitre, X., Santarelli, L. C., Tan, J., Luo, M., and Ma, M. (2007). Dual functions of mammalian olfactory sensory neurons as odor detectors and mechanical sensors. *Nat. Neurosci.* 10, 348–354. doi:10.1038/nn1856.

Gulbransen, B. D., Clapp, T. R., Finger, T. E., and Kinnamon, S. C. (2008). Nasal solitary chemoreceptor cell responses to bitter and trigeminal stimulants in vitro. *J. Neurophysiol.* 99, 2929–2937. doi:10.1152/jn.00066.2008.

Gupta, K., Mohanty, S. K., Mittal, A., Kalra, S., Kumar, S., Mishra, T., et al. (2020). The cellular basis of loss of smell in 2019-nCoV-infected individuals. *Brief. Bioinform.* 00, 1–9. doi:10.1093/bib/bbaa168.

Haas, P., and Gilmour, D. (2006). Chemokine signaling mediates self-organizing tissue migration in the zebrafish lateral line. *Dev. Cell* 10, 673–680. doi:10.1016/j.devcel.2006.02.019.

Hansen, A. (2007). Olfactory and solitary chemosensory cells: two different chemosensory systems in the nasal cavity of the American alligator, *Alligator mississippiensis*. *BMC Neurosci.* 8, 64. doi:10.1186/1471-2202-8-64.

Hansen, A., and Finger, T. E. (2008). Is TrpM5 a reliable marker for chemosensory cells? Multiple types of microvillous cells in the main olfactory epithelium of mice. *BMC Neurosci.* 9, 115. doi:10.1186/1471-2202-9-115.

Hansen, A., Reutter, K., and Zeiske, E. (2002). Taste bud development in the zebrafish, *Danio rerio*. *Dev. Dyn.* 223, 483–496. doi:10.1002/dvdy.10074.

Hansen, A., and Zeiske, E. (1993). Development of the olfactory organ in the zebrafish, *Brachydanio rerio*. *J. Comp. Neurol.* 333, 289–300. doi:10.1002/cne.903330213.

Hansen, A., and Zeiske, E. (1998). The peripheral olfactory organ of the zebrafish, *Danio rerio*: an ultrastructural study. *Chem. Senses* 23, 39–48. doi:10.1093/chemse/23.1.39.

Hansen, A., and Zielinski, B. S. (2005). Diversity in the olfactory epithelium of bony fishes: Development, lamellar arrangement, sensory neuron cell types and transduction components. *J. Neurocytol.* 34, 183–208. doi:10.1007/s11068-005-8353-1.

Hao, Y., Hao, S., Andersen-Nissen, E., Mauck III, W. M., Zheng, S., Butler, A., et al. (2021). Integrated analysis of multimodal single-cell data. *Cell* 184, 3573–3587. doi:10.1016/j.cell.2021.04.048.

Hao, Y., Stuart, T., Kowalski, M. H., Choudhary, S., Hoffman, P., Hartman, A., et al. (2023). Dictionary learning for integrative, multimodal and scalable single-cell analysis. *Nat. Biotechnol.* doi:10.1038/s41587-023-01767-y.

Harris, J. A., Cheng, A. G., Cunningham, L. L., MacDonald, G., Raible, D. W., and Rubel, E. W. (2003). Neomycin-induced hair cell death and rapid regeneration in the lateral line of zebrafish (*Danio rerio*). *JARO - J. Assoc. Res. Otolaryngol.* 4, 219–234. doi:10.1007/s10162-002-3022-x.

Heath, J., and Holifield, B. (1991). Actin alone in lamellipodia. *Nature* 352, 107–108. doi:10.1038/352107a0.

Hernádi, L. (1993). Fine structural characterization of the olfactory epithelium and its response to divalent cations Cd^{2+} in the fish Alburnus alburnus (Teleostei, Cyprinidae): a scanning and transmission electron microscopic study. *Neurobiology* 1, 11–31.

Herrera, K. J., Panier, T., Guggiana-Nilo, D., and Engert, F. (2020). Larval zebrafish use olfactory detection of sodium and chloride to avoid salt water. *Curr. Biol.* 31, 1–12. doi:10.1016/j.cub.2020.11.051.

Hildebrand, D. G. C., Cicconet, M., Torres, R. M., Choi, W., Quan, T. M., Moon, J., et al. (2017). Whole-brain serial-section electron microscopy in larval zebrafish. *Nature* 545, 345–349. doi:10.1038/nature22356.

Ho, J., Tumkaya, T., Aryal, S., Choi, H., and Claridge-Chang, A. (2019). Moving beyond *P* values: data analysis with estimation graphics. *Nat. Methods* 16, 565–566. doi:10.1038/s41592-019-0470-3.

Höfer, D., and Drenckhahn, D. (1999). Localisation of actin, villin, fimbrin, ezrin and ankyrin in rat taste receptor cells. *Histochem. Cell Biol.* 112, 79–86. doi:10.1007/s004180050394.

Horng, J.-L., Lin, L.-Y., Huang, C.-J., Katoh, F., Kaneko, T., and Hwang, P.-P. (2007). Knockdown of V-ATPase subunit A (*atp6v1a*) impairs acid secretion and ion balance in zebrafish (*Danio rerio*). *Am. J. Physiol. - Regul. Integr. Comp. Physiol.* 292, 2068–2076. doi:10.1152/ajpregu.00578.2006.

Hosseini, M., Fattahi, Z., Abedini, S. S., Hu, H., Ropers, H. H., Kalscheuer, V. M., et al. (2019). *GPR126*: A novel candidate gene implicated in autosomal recessive intellectual disability. *Am. J. Med. Genet. Part A* 179, 13–19. doi:10.1002/ajmg.a.40531.

Howe, K., Clark, M. D., Torroja, C. F., Torrance, J., Berthelot, C., Muffato, M., et al. (2013). The zebrafish reference genome sequence and its relationship to the human genome. *Nature* 496, 498–503. doi:10.1038/nature12111.

Hsiao, C.-D., You, M.-S., Guh, Y.-J., Ma, M., Jiang, Y.-J., and Hwang, P.-P. (2007). A positive regulatory loop between *foxi3a* and *foxi3b* is essential for specification and differentiation of zebrafish epidermal ionocytes. *PLoS One* 2, e302. doi:10.1371/journal.pone.0000302.

Hwang, P.-P., and Chou, M.-Y. (2013). Zebrafish as an animal model to study ion homeostasis. *Pflugers Arch. Eur. J. Physiol.* 465, 1233–1247. doi:10.1007/s00424-013-1269-1.

Hwang, P.-P., and Lee, T.-H. (2007). New insights into fish ion regulation and mitochondrion-rich cells. *Comp. Biochem. Physiol. - A Mol. Integr. Physiol.* 148, 479–497. doi:10.1016/j.cbpa.2007.06.416.

Ichikawa, M., and Ueda, K. (1977). Fine structure of the olfactory epithelium in the goldfish, Carassius auratus. *Cell Tissue Res.* 183, 445–455. doi:10.1007/bf00225659.

Imai, T., Sakano, H., and Vosshall, L. B. (2010). Topographic mapping — the olfactory system. *Cold Spring Harb. Perspect. Biol.* 2, a001776.

Inaba, Y., Chauhan, V., van Loon, A. P., Choudhury, L. S., and Sagasti, A. (2020). Keratins and plakin family cytolinker proteins control the length of epithelial microridge protrusions. *Elife* 9, e58149. doi:10.7554/eLife.58149.

Iqbal, T., and Byrd-Jacobs, C. (2010). Rapid degeneration and regeneration of the zebrafish olfactory epithelium after Triton X-100 application. *Chem. Senses* 35, 351–361. doi:10.1093/chemse/bjq019.

Irion, U., Krauss, J., and Nüsslein-Volhard, C. (2014). Precise and efficient genome editing in zebrafish using the CRISPR/Cas9 system. *Development* 141, 4827–4830. doi:10.1242/dev.115584.

Iwanaga, T., Fujita, T., and Ito, S. (1982). Immunohistochemical staining of enteroendocrine paraneurons with anti-brain tubulin antiserum. *Biomed. Res.* 3, 99–101. doi:10.2220/biomedres.3.99.

Iwata, R., Kiyonari, H., and Imai, T. (2017). Mechanosensory-based phase coding of odor identity in the olfactory bulb. *Neuron* 96, 1139–1152. doi:10.1016/j.neuron.2017.11.008.

Jeong, I., Hansen, J. N., Wachten, D., and Jurisch-Yaksi, N. (2022). Measurement of ciliary beating and fluid flow in the zebrafish adult telencephalon. *STAR Protoc.* 3, 101542. doi:10.1016/j.xpro.2022.101542.

Jessen, J. R., Willett, C. E., and Lin, S. (1999). Artificial chromosome transgenesis reveals long-distance negative regulation of *rag1* in zebrafish. *Nat. Genet.* 23, 15–16. doi:10.1038/12609.

Kastenhuber, E., Gesemann, M., Mickoleit, M., and Neuhauss, S. C. F. (2013). Phylogenetic analysis and expression of zebrafish transient receptor potential melastatin family genes. *Dev. Dyn.* 242, 1236–1249. doi:10.1002/dvdy.24020.

Kawakami, K., Abe, G., Asada, T., Asakawa, K., Fukuda, R., Ito, A., et al. (2010). zTrap: zebrafish gene trap and enhancer trap database. *BMC Dev. Biol.* 10, 105. doi:10.1186/1471-213X-10-105.

Kermen, F., Franco, L. M., Wyatt, C., and Yaksi, E. (2013). Neural circuits mediating olfactory-driven behavior in fish. *Front. Neural Circuits* 7, 62. doi:10.3389/fncir.2013.00062.

Kimmel, C. B., Ballard, W. W., Kimmel, S. R., Ullmann, B., and Schilling, T. F. (1995). Stages of embryonic development of the zebrafish. *Dev. Dyn.* 203, 253–310. doi:10.1002/aja.1002030302.

Koide, T., Miyasaka, N., Morimoto, K., Asakawa, K., Urasaki, A., Kawakami, K., et al. (2009). Olfactory neural circuitry for attraction to amino acids revealed by transposon-mediated gene trap approach in zebrafish. *Proc. Natl. Acad. Sci. U. S. A.* 106, 9884–9889. doi:10.1073/pnas.0900470106.

Kotecha, A. M., Corrêa, A. D. C., Fisher, K. M., and Rushworth, J. V. (2018). Olfactory dysfunction as a global biomarker for sniffing out Alzheimer's disease: A meta-analysis. *Biosensors* 8, 41. doi:10.3390/bios8020041.

Kotrschal, K., Krautgartner, W.-D., and Hansen, A. (1997). Ontogeny of the solitary chemosensory cells in the zebrafish, *Danio rerio*. *Chem. Senses* 22, 111–118. doi:10.1093/chemse/22.2.111.

Kowalewski, J., Paris, T., Gonzalez, C., Lelièvre, E., Valencia, L. C., Boutrois, M., et al. (2021). Characterization of a member of the CEACAM protein family as a novel marker of proton pump-rich ionocytes on the zebrafish epidermis. *PLoS One* 16, e0254533. doi:10.1371/journal.pone.0254533.

Kraus, A., Casadei, E., Huertas, M., Ye, C., Bradfute, S., Boudinot, P., et al. (2020). A zebrafish model for COVID-19 recapitulates olfactory and cardiovascular pathophysiologies caused by SARS-CoV-2. *bioRxiv*. doi:10.1101/2020.11.06.368191.

Kraus, A., Huertas, M., Ellis, L., Boudinot, P., Levraud, J.-P., and Salinas, I. (2022). Intranasal delivery of SARS-CoV-2 spike protein is sufficient to cause olfactory damage, inflammation and olfactory dysfunction in zebrafish. *Brain. Behav. Immun.* 102, 341–359. doi:10.1016/j.bbi.2022.03.006.

Krause, G., Winkler, L., Mueller, S. L., Haseloff, R. F., Piontek, J., and Blasig, I. E. (2008). Structure and function of claudins. *Biochim. Biophys. Acta - Biomembr.* 1778, 631–645. doi:10.1016/j.bbamem.2007.10.018.

Krishnan, J., and Rohner, N. (2017). Cavefish and the basis for eye loss. *Philos. Trans. R. Soc. B Biol. Sci.* 372, 20150487. doi:10.1098/rstb.2015.0487.

Krishnan, S., Mathuru, A. S., Kibat, C., Rahman, M., Lupton, C. E., Stewart, J., et al. (2014). The right dorsal habenula limits attraction to an odor in zebrafish. *Curr. Biol.* 24, 1167–1175. doi:10.1016/j.cub.2014.03.073.

Krukoff, T. L. (1999). "c-fos expression as a marker of functional activity in the brain," in *Cell Neurobiology Techniques*, eds. A. A. Boulton, G. B. Baker, and A. N. Bateson (Humana Press), 213–230. doi:10.1385/0-89603-510-7:213.

Küffer, A., Lakkaraju, A. K. K., Mogha, A., Petersen, S. C., Airich, K., Doucerain, C., et al. (2016). The prion protein is an agonistic ligand of the G protein-coupled receptor Adgrg6. *Nature* 536, 464–468. doi:10.1038/nature19312.

Kumai, Y., Kwong, R. W. M., and Perry, S. F. (2015). A role for transcription factor glial cell missing 2 in Ca^{2+} homeostasis in zebrafish, *Danio rerio*. *Pflugers Arch. Eur. J. Physiol.* 467, 753–765. doi:10.1007/s00424-014-1544-9.

Kwong, R. W. M., and Perry, S. F. (2013). The tight junction protein claudin-b regulates epithelial permeability and sodium handling in larval zebrafish, *Danio rerio*. *Am. J. Physiol. - Regul. Integr. Comp. Physiol.* 304, 504–513. doi:10.1152/ajpregu.00385.2012.

Lakhina, V., Marcaccio, C. L., Shao, X., Lush, M. E., Jain, R. A., Fujimoto, E., et al. (2012). Netrin/DCC signaling guides olfactory sensory axons to their correct location in the olfactory bulb. *J. Neurosci.* 32, 4440–4456. doi:10.1523/JNEUROSCI.4442-11.2012.

Lee, A., Mathuru, A. S., Teh, C., Kibat, C., Korzh, V., Penney, T. B., et al. (2010). The habenula prevents helpless behavior in larval zebrafish. *Curr. Biol.* 20, 2211–2216. doi:10.1016/j.cub.2010.11.025.

Lemons, K., Fu, Z., Aoudé, I., Ogura, T., Sun, J., Chang, J., et al. (2017). Lack of TRPM5-expressing microvillous cells in mouse main olfactory epithelium leads to impaired odor-evoked responses and olfactory-guided behavior in a challenging chemical environment. *eNeuro* 4, e0135. doi:10.1523/ENEURO.0135-17.2017.

Leon, K., Cunningham, R. L., Riback, J. A., Feldman, E., Li, J., Sosnick, T. R., et al. (2020). Structural basis for adhesion G protein-coupled receptor Gpr126 function. *Nat. Commun.* 11, 194. doi:10.1038/s41467-019-14040-1.

Liao, B.-K., Chen, R.-D., and Hwang, P.-P. (2009). Expression regulation of Na^+-K^+-ATPase α1-subunit subtypes in zebrafish gill ionocytes. *Am. J. Physiol. - Regul. Integr. Comp. Physiol.* 296, 1897–1906. doi:10.1152/ajpregu.00029.2009.

Liberles, S. D., and Buck, L. B. (2006). A second class of chemosensory receptors in the olfactory epithelium. *Nature* 442, 645–650. doi:10.1038/nature05066.

Lin, H.-H., Ng, K.-F., Chen, T.-C., and Tseng, W.-Y. (2022). Ligands and beyond: Mechanosensitive adhesion GPCRs. *Pharmaceuticals* 15, 219. doi:10.3390/ph15020219.

Lin, W., Ezekwe Jr, E. A. D., Zhao, Z., Liman, E. R., and Restrepo, D. (2008a). TRPM5-expressing microvillous cells in the main olfactory epithelium. *BMC Neurosci.* 9, 114. doi:10.1186/1471-2202-9-114.

Lin, W., Ogura, T., Margolskee, R. F., Finger, T. E., and Restrepo, D. (2008b). TRPM5-expressing solitary chemosensory cells respond to odorous irritants. *J. Neurophysiol.* 99, 1451–1460. doi:10.1152/jn.01195.2007.

Lin, X., Zhou, Q., Zhao, C., Lin, G., Xu, J., and Wen, Z. (2019). An ectoderm-derived myeloid-like cell population functions as antigen transporters for Langerhans cells in zebrafish epidermis. *Dev. Cell* 49, 605–617. doi:10.1016/j.devcel.2019.03.028.

Lister, J. A., Robertson, C. P., Lepage, T., Johnson, S. L., and Raible, D. W. (1999). *nacre* encodes a zebrafish microphthalmia-related protein that regulates neural-crest-derived pigment cell fate. *Development* 126, 3757–3767. doi:doi.org/10.1242/dev.126.17.3757.

Lizano, E., Hayes, J. L., and Willard, F. S. (2021). A synthetic method to assay adhesion-family G-protein coupled receptors. Determination of the G-protein coupling profile of ADGRG6(GPR126). *Biochem. Biophys. Res. Commun.* 534, 317–322. doi:10.1016/j.bbrc.2020.11.086.

Loomis, P. A., Zheng, L., Sekerková, G., Changyaleket, B., Mugnaini, E., and Bartles, J. R. (2003). Espin cross-links cause the elongation of microvillus-type parallel actin bundles in vivo. *J. Cell Biol.* 163, 1045–1055. doi:10.1083/jcb.200309093.

Lu, J., Liu, R., Miao, A., Chen, X., Xiao, W., Wang, Y., et al. (2020). The role of cldnh during the early retinal development in zebrafish. *Exp. Eye Res.* 200, 108207. doi:10.1016/j.exer.2020.108207.

Madelaine, R., Garric, L., and Blader, P. (2011). Partially redundant proneural function reveals the importance of timing during zebrafish olfactory neurogenesis. *Development* 138, 4753–4762. doi:10.1242/dev.066563.

Maier, E. C., Saxena, A., Alsina, B., Bronner, M. E., and Whitfield, T. T. (2014). Sensational placodes: Neurogenesis in the otic and olfactory systems. *Dev. Biol.* 389, 50–67. doi:10.1016/j.ydbio.2014.01.023.

Maiga, A., Lemieux, S., Pabst, C., Lavallée, V. P., Bouvier, M., Sauvageau, G., et al. (2016). Transcriptome analysis of G protein-coupled receptors in distinct genetic subgroups of acute myeloid leukemia: identification of potential disease-specific targets. *Blood Cancer J.* 6, e431. doi:10.1038/bcj.2016.36.

Marin, C., Vilas, D., Langdon, C., Alobid, I., López-Chacón, M., Haehner, A., et al. (2018). Olfactory dysfunction in neurodegenerative diseases. *Curr. Allergy Asthma Rep.* 18, 42. doi:10.1097/RMR.0000000000000271.

Mathuru, A. S., Kibat, C., Cheong, W. F., Shui, G., Wenk, M. R., Friedrich, R. W., et al. (2012). Chondroitin fragments are odorants that trigger fear behavior in fish. *Curr. Biol.* 22, 538–544. doi:10.1016/j.cub.2012.01.061.

Menco, B. P. M., and Jackson, J. E. (1997). Cells resembling hair cells in developing rat olfactory and nasal respiratory epithelia. *Tissue Cell* 29, 707–713. doi:10.1016/S0040-8166(97)80046-8.

Mitgau, J., Franke, J., Schinner, C., Stephan, G., Berndt, S., Placantonakis, D. G., et al. (2022). The N terminus of adhesion G protein–coupled receptor GPR126/ADGRG6 as allosteric force integrator. *Front. Cell Dev. Biol.* 10, 873278. doi:10.3389/fcell.2022.873278.

Miura, S., Sato, K., Kato-Negishi, M., Teshima, T., and Takeuchi, S. (2015). Fluid shear triggers microvilli formation via mechanosensitive activation of TRPV6. *Nat. Commun.* 6, 8871. doi:10.1038/ncomms9871.

Miyasaka, N., Sato, Y., Yeo, S.-Y., Hutson, L. D., Chien, C.-B., Okamoto, H., et al. (2005). Robo2 is required for establishment of a precise glomerular map in the zebrafish olfactory system. *Development* 132, 1283–1293. doi:10.1242/dev.01698.

Miyasaka, N., Wanner, A. A., Li, J., Mack-Bucher, J., Genoud, C., Yoshihara, Y., et al. (2013). Functional development of the olfactory system in zebrafish. *Mech. Dev.* 130, 336–346. doi:10.1016/j.mod.2012.09.001.

Mogha, A., Benesh, A. E., Patra, C., Engel, F. B., Schöneberg, T., Liebscher, I., et al. (2013). Gpr126 functions in Schwann cells to control differentiation and myelination via G-protein activation. *J. Neurosci.* 33, 17976–17985. doi:10.1523/JNEUROSCI.1809-13.2013.

Mogha, A., Harty, B. L., Carlin, D., Joseph, J., Sanchez, N. E., Suter, U., et al. (2016). Gpr126/Adgrg6 has Schwann cell autonomous and nonautonomous functions in peripheral nerve injury and repair. *J. Neurosci.* 36, 12351–12367. doi:10.1523/JNEUROSCI.3854-15.2016.

Mongera, A., Singh, A. P., Levesque, M. P., Chen, Y. Y., Konstantinidis, P., and Nüsslein-Volhard, C. (2013). Genetic lineage labeling in zebrafish uncovers novel neural crest contributions to the head, including gill pillar cells. *Development* 140, 916–925. doi:10.1242/dev.091066.

Monk, K. R., Naylor, S. G., Glenn, T. D., Mercurio, S., Perlin, J. R., Dominguez, C., et al. (2009). A G protein-coupled receptor is essential for Schwann cells to initiate myelination. *Science (80-.).* 325, 1402–1405. doi:10.1126/science.1173474.

Monk, K. R., Oshima, K., Jörs, S., Heller, S., and Talbot, W. S. (2011). Gpr126 is essential for peripheral nerve development and myelination in mammals. *Development* 138, 2673–2680. doi:10.1242/dev.062224.

Montoro, D. T., Haber, A. L., Biton, M., Vinarsky, V., Lin, B., Birket, S. E., et al. (2018). A revised airway epithelial hierarchy includes CFTR-expressing ionocytes. *Nature* 560, 319–324. doi:10.1038/s41586-018-0393-7.

Moran, D. T., Rowley III, J. C., Aiken, G. R., and Jafek, B. W. (1992). Ultrastructural neurobiology of the olfactory mucosa of the brown trout, *Salmo trutta*. *Microsc. Res. Tech.* 23, 28–48. doi:10.1002/jemt.1070230104.

Morrison, C. M., and Odense, P. H. (1978). Distribution and morphology of the rodlet cell in fish. *J. Fish. Board Canada* 35, 101–116. doi:10.1139/f78-014.

Mosimann, C., Puller, A.-C., Lawson, K. L., Tschopp, P., Amsterdam, A., and Zon, L. I. (2013). Site-directed zebrafish transgenesis into single landing sites with the phiC31 integrase system. *Dev. Dyn.* 242, 949–963. doi:10.1002/dvdy.23989.

Muller, J. F., and Marc, R. E. (1984). Three distinct morphological classes of receptors in fish olfactory organs. *J. Comp. Neurol.* 222, 482–495. doi:10.1002/cne.902220403.

Musa, G., Cazorla-Vázquez, S., van Amerongen, M. J., Stemmler, M. P., Eckstein, M., Hartmann, A., et al. (2019). *Gpr126* (*Adgrg6*) is expressed in cell types known to be exposed to mechanical stimuli. *Ann. N. Y. Acad. Sci.* 1456, 96–108. doi:10.1111/nyas.14135.

Nüsslein-Volhard, C., and Dahm, R. (2002). *Zebrafish: A Practical Approach*. Oxford: Oxford University Press.

Olivares, J., and Schmachtenberg, O. (2019). An update on anatomy and function of the teleost olfactory system. *PeerJ* 7, e7808. doi:10.7717/peerj.7808.

Paavola, K. J., Sidik, H., Zuchero, J. B., Eckart, M., and Talbot, W. S. (2014). Type IV collagen is an activating ligand for the adhesion G protein-coupled receptor GPR126. *Sci. Signal.* 7, ra76. doi:10.1126/scisignal.2005347.

Parisi, V., Guerrera, M. C., Abbate, F., Garcia-Suarez, O., Viña, E., Vega, J. A., et al. (2014). Immunohistochemical characterization of the crypt neurons in the olfactory epithelium of adult zebrafish. *Ann. Anat.* 196, 178–182. doi:10.1016/j.aanat.2014.01.004.

Peloggia, J., Münch, D., Meneses-Giles, P., Romero-Carvajal, A., Lush, M. E., Lawson, N. D., et al. (2021). Adaptive cell invasion maintains lateral line organ homeostasis in response to environmental changes. *Dev. Cell* 56, 1296–1312. doi:10.1016/j.devcel.2021.03.027.

Petersen, S. C., Luo, R., Liebscher, I., Giera, S., Jeong, S. J., Mogha, A., et al. (2015). The adhesion GPCR GPR126 has distinct, domain-dependent functions in Schwann cell development mediated by interaction with Laminin-211. *Neuron* 85, 755–769. doi:10.1016/j.neuron.2014.12.057.

Pickett, S. B., Thomas, E. D., Sebe, J. Y., Linbo, T., Esterberg, R., Hailey, D. W., et al. (2018). Cumulative mitochondrial activity correlates with ototoxin susceptibility in zebrafish mechanosensory hair cells. *Elife* 7, e38062. doi:10.7554/eLife.38062.

Pinto, C. S., Khandekar, A., Bhavna, R., Kiesel, P., Pigino, G., and Sonawane, M. (2019). Microridges are apical epithelial projections formed of F-actin networks that organize the glycan layer. *Sci. Rep.* 9, 12191. doi:10.1038/s41598-019-48400-0.

Rajan, S. G., and Saxena, A. (2022). Scents from the past: Lineage history and terminal identity in the olfactory system. *Nat. Sci.*, e20220037. doi:10.1002/ntls.20220037.

Ramírez-Weber, F.-A., and Kornberg, T. B. (1999). Cytonemes: cellular processes that project to the principal signaling center in *Drosophila* imaginal discs. *Cell* 97, 599–607. doi:10.1016/S0092-8674(00)80771-0.

Randlett, O., Wee, C. L., Naumann, E. A., Nnaemeka, O., Schoppik, D., Fitzgerald, J. E., et al. (2015). Whole-brain activity mapping onto a zebrafish brain atlas. *Nat. Methods* 12, 1039–1046. doi:10.1038/nmeth.3581.

Ravenscroft, G., Nolent, F., Rajagopalan, S., Meireles, A. M., Paavola, K. J., Gaillard, D., et al. (2015). Mutations of *GPR126* are responsible for severe arthrogryposis multiplex congenita. *Am. J. Hum. Genet.* 96, 955–961. doi:10.1016/j.ajhg.2015.04.014.

Rayamajhi, D., Ege, M., Ukhanov, K., Ringers, C., Zhang, Y., Jeong, I., et al. (2023). Foxj1 controls olfactory ciliogenesis and differentiation program of the olfactory sensory neurons. *bioRxiv*. doi:10.1101/2023.05.10.540158.

Reid, L., Meyrick, B., Antony, V. B., Chang, L. Y., Crapo, J. D., and Reynolds, H. Y. (2005). The mysterious pulmonary brush cell: A cell in search of a function. *Am. J. Respir. Crit. Care Med.* 172, 136–139. doi:10.1164/rccm.200502-203WS.

Reiten, I., Uslu, F. E., Fore, S., Pelgrims, R., Ringers, C., Diaz Verdugo, C., et al. (2017). Motile-cilia-mediated flow improves sensitivity and temporal resolution of olfactory computations. *Curr. Biol.* 27, 166–174. doi:10.1016/j.cub.2016.11.036.

Rhein, L. D., Cagan, R. H., Orkand, P. M., and Dolack, M. K. (1981). Surface specializations of the olfactory epithelium of rainbow trout, *Salmo gairdneri*. *Tissue Cell* 13, 577–587. doi:10.1016/0040-8166(81)90028-8.

Rinaldi, A. (2007). The scent of life. The exquisite complexity of the sense of smell in animals and humans. *EMBO Rep.* 8, 629–633. doi:10.1038/sj.embor.7401029.

Ringers, C., Bialonski, S., Ege, M., Solovev, A., Hansen, J. N., Jeong, I., et al. (2023). Novel analytical tools reveal that local synchronization of cilia coincides with tissue-scale metachronal waves in zebrafish multiciliated epithelia. *Elife* 12, e77701. doi:10.7554/eLife.77701.

Ringers, C., Olstad, E. W., and Jurisch-Yaksi, N. (2019). The role of motile cilia in the development and physiology of the nervous system. *Philos. Trans. R. Soc. Lond. B. Biol. Sci.* 375, 20190156. doi:10.1098/rstb.2019.0156.

Sánchez-Alcañiz, J. A., and Benton, R. (2017). Multisensory neural integration of chemical and mechanical signals. *BioEssays* 39, 1700060. doi:10.1002/bies.201700060.

Satija, R., Farrell, J. A., Gennert, D., Schier, A. F., and Regev, A. (2015). Spatial reconstruction of single-cell gene expression data. *Nat. Biotechnol.* 33, 495–502. doi:10.1038/nbt.3192.

Sato, Y., Miyasaka, N., and Yoshihara, Y. (2005). Mutually exclusive glomerular innervation by two distinct types of olfactory sensory neurons revealed in transgenic zebrafish. *J. Neurosci.* 25, 4889–4897. doi:10.1523/JNEUROSCI.0679-05.2005.

Saunders, C. J., Christensen, M., Finger, T. E., and Tizzano, M. (2014). Cholinergic neurotransmission links solitary chemosensory cells to nasal inflammation. *Proc. Natl. Acad. Sci. U. S. A.* 111, 6075–6080. doi:10.1073/pnas.1402251111.

Saxena, A., Peng, B. N., and Bronner, M. E. (2013). Sox10-dependent neural crest origin of olfactory microvillous neurons in zebrafish. *Elife* 2, e00336. doi:10.7554/eLife.00336.

Schindelin, J., Arganda-Carreras, I., Frise, E., Kaynig, V., Longair, M., Pietzsch, T., et al. (2012). Fiji: an open-source platform for biological-image analysis. *Nat. Methods* 9, 676–682. doi:10.1038/nmeth.2019.

Schmid, B., Schindelin, J., Cardona, A., Longair, M., and Heisenberg, M. (2010). A high-level 3D visualization API for Java and ImageJ. *BMC Bioinformatics* 11, 274. doi:10.1186/1471-2105-11-274.

Schneider, C., O'Leary, C. E., and Locksley, R. M. (2019). Regulation of immune responses by tuft cells. *Nat. Rev. Immunol.* 19, 584–593. doi:10.1038/s41577-019-0176-x.

Schulte, E. (1972). Untersuchungen an der regio olfactoria des aals, *Anguilla anguilla* L. *Zeitschrift für Zellforsch. und Mikroskopische Anat.* 125, 210–228. doi:10.1007/BF00306790.

Schwander, M., Kachar, B., and Müller, U. (2010). The cell biology of hearing. *J. Cell Biol.* 190, 9–20. doi:10.1083/jcb.201001138.

Sekerková, G., Zheng, L., Loomis, P. A., Changyaleket, B., Whitlon, D. S., Mugnaini, E., et al. (2004). Espins are multifunctional actin cytoskeletal regulatory proteins in the microvilli of chemosensory and mechanosensory cells. *J. Neurosci.* 24, 5445–5456. doi:10.1523/JNEUROSCI.1279-04.2004.

Sekerková, G., Zheng, L., Loomis, P. A., Mugnaini, E., and Bartles, J. R. (2006). Espins and the actin cytoskeleton of hair cell stereocilia and sensory cell microvilli. *Cell. Mol. Life Sci.* 63, 2329–2341. doi:10.1007/s00018-006-6148-x.

Sepahi, A., Kraus, A., Casadei, E., Johnston, C. A., Galindo-Villegas, J., Kelly, C., et al. (2019). Olfactory sensory neurons mediate ultrarapid antiviral immune responses in a TrkA-dependent manner. *Proc. Natl. Acad. Sci. U. S. A.* 116, 12428–12436. doi:10.1073/pnas.1900083116.

Shainer, I., Kuehn, E., Laurell, E., Al Kassar, M., Mokayes, N., Sherman, S., et al. (2023). A single-cell resolution gene expression atlas of the larval zebrafish brain. *Sci. Adv.* 9, eade9909. doi:10.1126/sciadv.ade9909.

Shigetani, Y., Wakamatsu, Y., Tachibana, T., and Okabe, M. (2016). Conversion of neural plate explants to pre-placodal ectoderm-like tissue in vitro. *Biochem. Biophys. Res. Commun.* 477, 807–813. doi:10.1016/j.bbrc.2016.06.139.

Sola, C., Giulianini, P. G., and Ferrero, E. A. (1993). Ultrastructural characterization of the olfactory organ in glass eels, *Anguilla anguilla* (Osteichthyes, Anguilliformes). *Ital. J. Zool.* 60, 253–261. doi:10.1080/11250009309355820.

Son, G., Jahanshahi, A., Yoo, S.-J., Boonstra, J. T., Hopkins, D. A., Steinbusch, H. W. M., et al. (2021). Olfactory neuropathology in Alzheimer's disease: a sign of ongoing neurodegeneration. *BMB Rep.* 54, 295–304. doi:10.5483/BMBRep.2021.54.6.055.

Sternberg, J. R., Prendergast, A. E., Brosse, L., Cantaut-Belarif, Y., Thouvenin, O., Orts-Del'Immagine, A., et al. (2018). Pkd2l1 is required for mechanoception in cerebrospinal fluid-contacting neurons and maintenance of spine curvature. *Nat. Commun.* 9, 3804. doi:10.1038/s41467-018-06225-x.

Stuart, T., Butler, A., Hoffman, P., Hafemeister, C., Papalexi, E., Mauck III, W. M., et al. (2019). Comprehensive integration of single-cell data. *Cell* 177, 1888–1902. doi:10.1016/j.cell.2019.05.031.

Su, C.-Y., Menuz, K., and Carlson, J. R. (2009). Olfactory perception: Receptors, cells, and circuits. *Cell* 139, 45–59. doi:10.1016/j.cell.2009.09.015.

Tang, W., and Bronner, M. E. (2020). Neural crest lineage analysis: from past to future trajectory. *Development* 147, dev193193. doi:10.1242/dev.193193.

Theriot, J. A., and Mitchison, T. J. (1991). Actin microfilament dynamics in locomoting cells. *Nature* 352, 126–131. doi:10.1038/352126a0.

Thisse, C., and Thisse, B. (2008). High-resolution in situ hybridization to whole-mount zebrafish embryos. *Nat. Protoc.* 3, 59–69. doi:10.1038/nprot.2007.514.

Tian, T., Zhao, L., Zhao, X., Zhang, M., and Meng, A. (2009). A zebrafish gene trap line expresses GFP recapturing expression pattern of *foxj1b*. *J. Genet. Genomics* 36, 581–589. doi:10.1016/S1673-8527(08)60150-2.

Tilney, L. G., Derosier, D. J., and Mulroy, M. J. (1980). The organization of actin filaments in the stereocilia of cochlear hair cells. *J. Cell Biol.* 86, 244–259. doi:10.1083/jcb.86.1.244.

Tiraboschi, E., Leonardelli, L., Segata, G., and Haase, A. (2021). Parallel processing of olfactory and mechanosensory information in the honey bee antennal lobe. *Front. Physiol.* 12, 790453. doi:10.3389/fphys.2021.790453.

Tizzano, M., Cristofoletti, M., Sbarbati, A., and Finger, T. E. (2011). Expression of taste receptors in solitary chemosensory cells of rodent airways. *BMC Pulm. Med.* 11, 3. doi:10.1186/1471-2466-11-3.

Tizzano, M., Gulbransen, B. D., Vandenbeuch, A., Clapp, T. R., Herman, J. P., Sibhatu, H. M., et al. (2010). Nasal chemosensory cells use bitter taste signaling to detect irritants and bacterial signals. *Proc. Natl. Acad. Sci. U. S. A.* 107, 3210–3215. doi:10.1073/pnas.0911934107.

Tuckman, H., Kim, J., Rangan, A., Lei, H., and Patel, M. (2021). Dynamics of sensory integration of olfactory and mechanical stimuli within the response patterns of moth antennal lobe neurons. *J. Theor. Biol.* 509, 110510. doi:10.1016/j.jtbi.2020.110510.

Ualiyeva, S., Lemire, E., Wong, C., Boyd, A., Avilés, E. C., Minichetti, D. G., et al. (2023). TRPM5^{+} microvillous tuft cells regulate neuroepithelial intrinsic olfactory stem cell proliferation. *bioRxiv*. doi:doi.org/10.1101/2022.09.26.509561.

Wakisaka, N., Miyasaka, N., Koide, T., Masuda, M., Hiraki-Kajiyama, T., and Yoshihara, Y. (2017). An adenosine receptor for olfaction in fish. *Curr. Biol.* 27, 1437–1447. doi:10.1016/j.cub.2017.04.014.

Wang, W.-D., Melville, D. B., Montero-Balaguer, M., Hatzopoulos, A. K., and Knapik, E. W. (2011). Tfap2a and Foxd3 regulate early steps in the development of the neural crest progenitor population. *Dev. Biol.* 360, 173–185. doi:10.1016/j.ydbio.2011.09.019.

Waryani, B., Zhao, Y., Zhang, C., Abbasi, A. R., Ferrando, S., Dai, R., et al. (2015). Surface architecture of the olfactory epithelium of two Chinese cave loaches (Cypriniformes: Nemacheilidae: *Oreonectes*). *Ital. J. Zool.* 82, 179–185. doi:10.1080/11250003.2015.1018851.

Waryani, B., Zhao, Y., Zhang, C., Dai, R., and Abbasi, A. R. (2013). Anatomical studies of the olfactory epithelium of two cave fishes *Sinocyclocheilus jii* and *S. furcodorsalis* (Cypriniformes: Cyprinidae) from China. *Pak. J. Zool.* 45, 1091–1101. doi:10.1080/11250003.2015.1018851.

Waterman, R. E., and Bell, D. H. (1984). Epithelial fusion during early semicircular canal formation in the embryonic zebrafish, *Brachydanio rerio*. *Anat. Rec.* 210, 101–114. doi:10.1002/ar.1092100113.

Whitfield, T. T., Granato, M., Van Eeden, F. J. M., Schach, U., Brand, M., Furutani-Seiki, M., et al. (1996). Mutations affecting development of the zebrafish inner ear and lateral line. *Development* 123, 241–254. doi:10.1242/dev.123.1.241.

Whitlock, K. E. (2015). The loss of scents: do defects in olfactory sensory neuron development underlie human disease? *Birth Defects Res. Part C - Embryo Today Rev.* 105, 114–125. doi:10.1002/bdrc.21094.

Whitlock, K. E., Smith, K. M., Kim, H., and Harden, M. V. (2005). A role *foxd3* and *sox10* in the differentiation of gonadotropin-releasing hormone (GnRH) cells in the zebrafish *Danio rerio*. *Development* 132, 5491–5502. doi:10.1242/dev.02158.

Whitlock, K. E., and Westerfield, M. (1998). A transient population of neurons pioneers the olfactory pathway in the zebrafish. *J. Neurosci.* 18, 8919–8927. doi:10.1523/jneurosci.18-21-08919.1998.

Whitlock, K. E., and Westerfield, M. (2000). The olfactory placodes of the zebrafish form by convergence of cellular fields at the edge of the neural plate. *Development* 127, 3645–3653.

Whitlock, K. E., Wolf, C. D., and Boyce, M. L. (2003). Gonadotropin-releasing hormone (GnRH) cells arise from cranial neural crest and adenohypophyseal regions of the neural plate in the zebrafish, *Danio rerio*. *Dev. Biol.* 257, 140–152. doi:10.1016/S0012-1606(03)00039-3.

Winder, S. J., and Ayscough, K. R. (2005). Actin-binding proteins. *J. Cell Sci.* 118, 651–654. doi:10.1242/jcs.01670.

Xiao, T., Roeser, T., Staub, W., and Baier, H. (2005). A GFP-based genetic screen reveals mutations that disrupt the architecture of the zebrafish retinotectal projection. *Development* 132, 2955–2967. doi:10.1242/dev.01861.

Xydakis, M. S., Albers, M. W., Holbrook, E. H., Lyon, D. M., Shih, R. Y., Frasnelli, J. A., et al. (2021). Post-viral effects of COVID-19 in the olfactory system and their implications. *Lancet Neurol.* 20, 753–761. doi:10.1016/S1474-4422(21)00182-4.

Yamamoto, M., and Ueda, K. (1978). Comparative morphology of fish olfactory epithelium — IV. *Bull. Japanese Soc. Sci. Fish.* 44, 1207–1212. doi:10.2331/suisan.44.1207.

Zachar, P. C., and Jonz, M. G. (2012). Confocal imaging of Merkel-like basal cells in the taste buds of zebrafish. *Acta Histochem.* 114, 101–115. doi:10.1016/j.acthis.2011.03.006.

Zhang, X.-Y., Huang, Z.-Q., Ning, T., Xiang, X.-H., Li, C.-Q., Chen, S.-Y., et al. (2018). Microscopic and submicroscopic gradient variation of olfactory systems among six *Sinocyclocheilus* species living in different environments. *Zool. Soc. Japan* 35, 411–420. doi:10.2108/zs170126.